PREDICTION METHODOLOGY FOR THE HEAT REJECTION FROM TURBOCHARGED OR NATURALLY ASPIRED AUTOMOBILE ENGINES

by

OVERTON L. PARISH IV, B.S.M.E., M.S.M.E.

A DISSERTATION

IN

MECHANICAL ENGINEERING

Submitted to the Graduate Faculty
of Texas Tech University in
Partial Fulfillment of
the Requirements for
the Degree of

DOCTOR OF PHILOSOPHY

Approved

Chairperson of the Committee

Accepted

Dean of the Graduate School

May, 2003

ACKNOWLEDGMENTS

I thank the following for their contributions to my dissertation: Ford Motor Company for their generous support for automotive research at Texas Tech University; Jack Williams and Mark Burns of Ford Motor Company for their insight into vehicle, engine, and heat rejection systems; Texas Tech University for their dedication to research and the faculty; the mechanical engineering department for their support of graduate research; Dr. Walter Oler for all the support, help, thoughtful insight and systematic approach; my doctorial committee for their support and creativity contributing to the analysis and understanding of automotive engineering, thermodynamic systems, and heat transfer; ThermoTek, Inc. for employment, flexibility, support and experience opportunities; Heywood for the most comprehensive text on a specific subject that I have ever seen; Jennifer Schmidt for her prompt and accurate editing; our parents--Linn and Terry Parish and D'Nard and Beth Arthur--for all the support; our kids Catherine and Isabella Parish for being so patient and special; and my bride, Deidre Parish, for her compassion and love.

TABLE OF CONTENTS

ABSTRACT

The objective of this research is to accurately predict the heat rejection of naturally aspired spark ignition (SI) engines and turbocharged compression ignition (CI) engines. This prediction method will be added to TTU-Cool, a software package developed at Texas Tech University for Ford Motor Company. The objective of TTU-Cool is to give the aerodynamics division at Ford a tool to predict, with minimal up front data, the cooling performance of a proposed automotive cooling system. The minimal data includes the road load requirements as well as engine size and number of cylinders.

Historically, Ford has used a least squares fit of the above data to approximate the heat rejection. The proposed methodology replaces the approximation with a physics-based approach to determining the heat rejection. The thermal model significantly expands the capabilities of TTU-Cool. SI and CI engine data are analyzed and correlated into a useful tool for new automobile concepts.

LIST OF FIGURES

LIST OF SYMBOLS

Alphabet

amep	Auxiliary Mean Effective Pressure (kPa)
A	Area (m^2), Air Mass (kg_a)
bmep	Brake Mean Effective Pressure (kPa)
B	Bore (m)
C	Specific Heat (kJ/kgK), Constant
D	Diameter (m)
fmep	Friction Mean Effective Pressure (kPa)
F	Fuel Mass (kg_f)
H	Heat Transfer Coefficient (W/m^2K)
imep	Indicated Mean Effective Pressure (kPa)
K	Thermal Conductivity (W/mK)
l	Length (m)
m	mass (kg)
n	Engine Speed (rpm)
N	Number
Nu	Nusselt Number
pmep	Pumping Mean Effective Pressure (kPa)
P	Pressure (kPa), Power (kW)
Pr	Prandtl Number
Q	Heat, (kJ)
r	Ratio
rfmep	Rubbing Friction Mean Effective Pressure (kPa)
R	Ideal Gas Constant (kJ/kgK), Radius (m)
Re	Reynolds Number
T	Temperature, K
V	Velocity (m/s), Volume (m^3)

W	Work (kJ)

Greek Symbols

γ	Ratio of Specific Heats
Δ	Change
ε	Heat Exchanger Effectiveness
η	Efficiency
ϕ	Fuel Equivalence Ratio
μ	Viscosity, (Ns/m^2)
ρ	Density (kg/m^3)
σ	Stefan-Boltzman Constant for Radiation
υ	Specific Volume (m^3/kg)

Subscripts

1-7	Stations of Thermodynamic Cycle
a	Air, Actual, Adiabatic
b	Brake
c	Compression, coolant
compressor	Compressor
cyl	Cylinder
coolant	Coolant
D	Displacement
e	Combusted Gas of Air and Fuel
f	Fuel, Flame
g	Combustion gas
in	Flows Into a System
LH	Lower Heating Value
Net	Net
o	Ambient, Stagnant Conditions
out	Flows Out of a System

p	Pressure, Prime Mover
r	Radiation, Ratio
ref	Reference
rf	Rubbing Friction
s	Stoichiometric
v	Volume
w	Wall

Superscripts

-	Average
*	Stoichiometric

CHAPTER I
INTRODUCTION

Proper design of the vehicle cooling system requires accurate knowledge of the engine heat rejected to coolant. Unfortunately, this data is frequently unavailable during the early stages of vehicle design, as there is often no engine hardware available for experimental testing. This problem is exacerbated under the shrinking duration of the design cycle, which dictates that a calibrated power train will not be available until six months before the first prototypes are to be completed on any given program. Analytical tools are needed to close this gap and provide the necessary information. The current method, the Lahvic regression in Ford's CVSP (Corporate Vehicle Simulation Program), is known to overestimate the thermal loads (Lahvic, 1986). A new model is necessary to more accurately and completely estimate heat rejection from both naturally aspired spark ignition (SI) and turbocharged compression ignition (CI) engines.

The goal, therefore, of this new, physics-based methodology is to estimate coolant heat rejection for an arbitrary, naturally aspirated gasoline and turbocharged Diesel engine with reasonable accuracy. This method is based on dynamometer tests of 11 naturally aspired gasoline Ford engines (4, 6, and 8 cylinders; 2.0L through 6.8L displacements) and four turbocharged Diesel Ford engines (6 and 8 cylinders; 2.7L through 7.3L displacements). However, if experimental data is available for a specific engine, the correlation coefficients in the model can be explicitly optimized for the given engine. In that case, the correlation accuracy is within the uncertainty of the experimental data.

The target users for this methodology are cooling system designers who require knowledge of engine heat rejection to coolant to properly size radiators, fans, and vehicle front-end openings. It allows design engineers to conduct upfront robustness studies of the cooling system and analytical investigations into target setting. The method can also be used to improve confidence in CAE modeling of front-end geometry and increase productivity of experimental testing of vehicle cooling systems.

The naturally aspired spark ignition engine heat rejection method is available in an Excel workbook called ttu_Heat. Turbocharged CI engine heat rejection method will be incorporated into this workbook in the near future. By default, heat rejection predictions for the SI engines utilize the standard correlation coefficients based on the data from the 11 engines. Optionally, the user can generate a unique correlation for a specific engine. Plots of a heat rejection map, power and heat transfer correlation results, and a correlation error summary support the calculations. Also included in ttu_Heat is a worksheet to facilitate unit conversions from dynamometer data files to the SI data needed for the correlation. All of the calculation worksheets are protected except for the user data entry areas. The workbook as a whole is not protected, which allows users to collect calculation results and build additional worksheets and plots to meet individual needs.

In addition to the above-mentioned Excel worksheet, this prediction method will be added to TTU-Cool, a software package developed at Texas Tech University for Ford Motor Company. The objective of TTU-Cool is to give the aerodynamics division at Ford a tool to predict the cooling requirements of a proposed automotive configuration with minimal data. The minimal data includes the road load requirements, engine size, and number of cylinders.

The Diesel engine has several unusual, additional features that must be included in the analysis. These additional features include the stronger presence of radiation due to elevated temperatures as compared to the gasoline cycle, and the addition of a turbocharger (Heywood, 1988).

The addition of the physics-based method for estimating engine heat rejection for both naturally aspired SI and Diesel CI engines will significantly expand the capabilities of TTU-Cool and has been requested by Ford Motor Company. SI and CI engine data were analyzed and correlated into a useful tool for new automobile concepts.

CHAPTER II
BACKGROUND AND LITERATURE SURVEY

In the current chapter, the background and basic information for naturally aspired spark ignition (SI) engines and turbocharged compression ignition (CI) engines are discussed. The literature survey reveals several major areas relevant to heat transfer from automotive engines. Turbocharging and intercooling, automotive heat transfer, computer simulations for the automotive performance prediction and "adiabatic" engine performance are all included in the literature review. By far, most of the recent research for the compression ignition engines has been in the area of "adiabatic" engine performance. Adiabatic engine literature is relevant to the current research because turbocharging is an important accessory in "adiabatic engines." Additionally, the area of pollution research for CI Diesel engines is huge. Although there is a large amount of recent literature concerning the reduction of pollutants from SI and CI engines, the topic is not critically related to the current research objectives and will only be briefly summarized herein.

Internal combustion engines capture energy released by combustion of hydrocarbon based fuel and air mixture reactants. The main products of combustion are the heat of combustion, nitrogen, carbon dioxide, and water. Other products are typically considered pollutants and include partially or unburned fuel, carbon monoxide, nitric oxide, nitrogen dioxide, and particles. The heat of combustion is the primary variable needed from the combustion process. For octane, the heat of combustion is 44,000 kJ/kg, which is the lower heating value of the fuel. For Diesel fuel, the heat of combustion is 43,000 kJ/kg, which again is the lower heating value of the fuel.

2.1 Spark Ignition Engine

Nikolaus Otto invented the spark ignition (SI) engine in 1876. Figure 2.1 is a photograph of a modern SI engine.

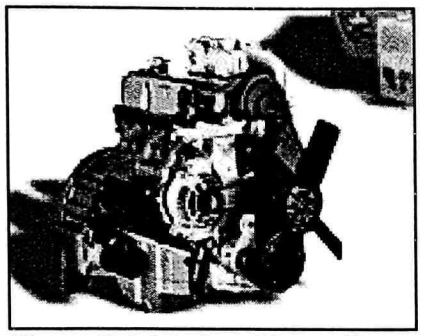

Figure 2.1 Modern Naturally Aspirated Spark Ignition Engine (Ford, 2003).

Since its introduction, the SI engine has become the most widely used prime mover in the automotive industry. The SI engine is a four-stroke engine. The term "four-stroke" relates to the cycle that the engine must traverse. These four strokes of the piston are the intake, compression, combustion, and exhaust. Each of these processes occurs only once every other rotation of the engine crankshaft. Alternatively, the power output from a given cylinder only occurs every other rotation.

The experimentally evaluated variation of cylinder pressure with respect to cylinder volume for a four-stroke SI engine (Heywood, 1988) is illustrated in Figure 2.2.

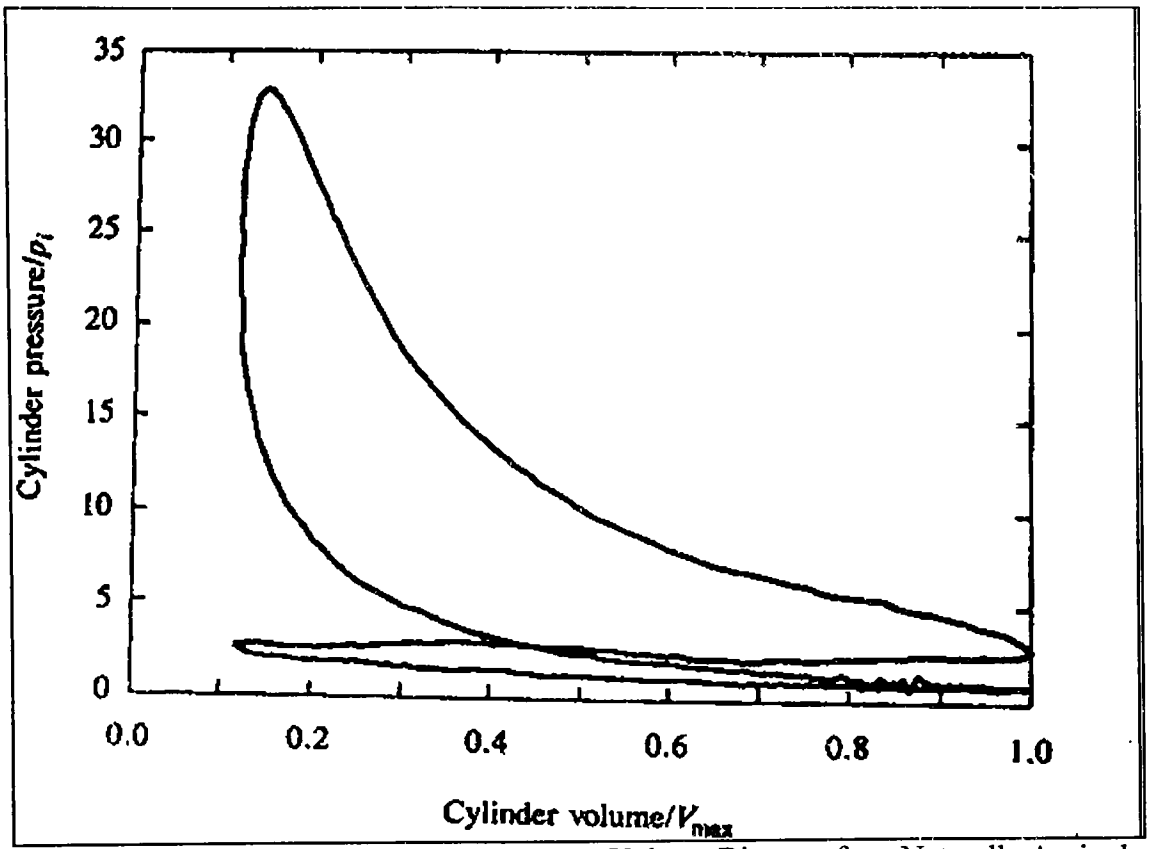

Figure 2.2 Actual Normalized Pressure versus Volume Diagram for a Naturally Aspired Spark Ignition Engine (Heywood, 1988).

The lower portion of Figure 2.2 shows the intake and exhaust portion of the cycle. The actual process, shown in Figure 2.2, followed by the air and fuel within the cylinder is modeled with a closed system following the ideal Otto cycle as illustrated in Figure 2.3.

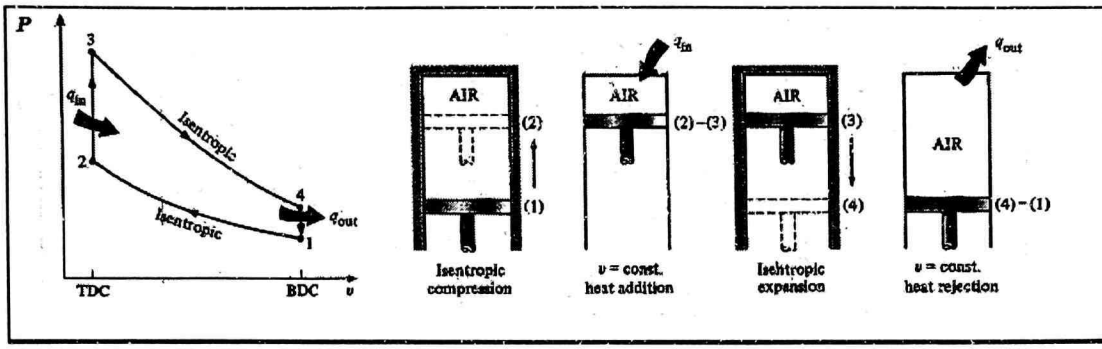

Figure 2.3 Pressures versus Specific Volume for the Ideal SI Engine Cycle (Cengel 1989).

Comparing Figures 2.3 and 2.2, shows that the ideal SI cycle is remarkably accurate in process, although inefficiencies must be included to obtain quantitative results. In the ideal cycle, a constant volume heat transfer represents the combustion process. The exhaust and intake processes are modeled with a single constant volume heat rejection process. The compression and expansion processes are treated as isentropic. This ideal SI engine cycle is well documented in the literature and nearly every modern thermodynamic text. From Figure 2.3, the following ideal processes can be identified. In the ideal cycle for a naturally aspired SI engine, the cycle begins with an isentropic compression of the charge air. The compression ratio, r, defined as

$$r = \frac{V_1}{V_2} = \frac{V_4}{V_3} \tag{2.1}$$

typically varies between 8 to 12. Note that stagnation states are assumed unless otherwise specified. The corresponding temperature and specific volume ratios based on an isentropic process are

$$\left(\frac{\upsilon_1}{\upsilon_2}\right)^{\gamma} = \left(\frac{T_2}{T_1}\right)^{\left[\frac{\gamma}{\gamma-1}\right]} = \frac{P_2}{P_1}. \tag{2.2}$$

The corresponding isentropic power to drive the compression can be calculated by

$$-\dot{W}_{c,in} = \dot{m}_a c_v T_1 (r^{\gamma-1} - 1). \tag{2.3}$$

The heat input from the fuel combustion occurs between States 2 and 3. In the ideal cycle, the combustion occurs at constant specific volume. SI engines are designed to have an air-fuel ratio very close to the ideal stoichiometric value of 14.6. Using the first law of thermodynamics, the temperature at State 3 can be calculated

$$T_3 = T_2 + \frac{Q_{LH}}{A/F\, c_v}. \tag{2.4}$$

The ideal gas law and the air cycle standard can then be used to calculate the pressure at State 3:

$$P_3 = \frac{R_a T_3}{\upsilon_3}. \tag{2.5}$$

From States 3 to 4, the power to drive the compression and the net output power are found using isentropic expansion relations. The specific volume at State 4 is the same as the starting specific volume at State 1:

$$v_4 = v_1. \tag{2.6}$$

With the assumption of an isentropic expansion, the temperature and pressure at State 4:

$$\left(\frac{v_3}{v_4}\right)^{\gamma} = \left(\frac{T_4}{T_3}\right)^{\left[\frac{\gamma_e}{\gamma_e - 1}\right]} = \frac{P_4}{P_3}. \tag{2.7}$$

The power output from States 3 to 4 are calculated using the first law of thermodynamics as

$$\dot{W}_{p,out} = \dot{m}_a \left(1 + \frac{1}{A/F} \right) c_v (T_3 - T_4). \tag{2.8}$$

The net power is the difference between the expansion and the compression power as defined in Equation 2.8 and 2.3, respectively.

The net power thus defined is referred to as the "indicated power" or the power indicated by the integral $\oint p\, dV$ for the complete cycle in one cylinder. The "brake power" is the power available at the output shaft of the engine. The brake power is reduced from the indicated power by frictional losses within the engine, pumping losses in the induction and exhaust systems, and by the accessory power requirements such as the fuel, oil and water pumps, and the alternator. The net of these losses or the difference between the indicated and brake power is defined as the "frictional power."

The thermal efficiency for a work producing cycle is

$$\eta_{th} = \frac{W_{net}}{Q_{in}}. \tag{2.9}$$

Referring to Figure 2.3, the thermal efficiency can be expanded to

$$\eta_{th} = \frac{W_{34} - W_{12}}{Q_{23}} = \frac{mC_v[(T_3 - T_4) - (T_2 - T_1)]}{mC_v(T_3 - T_2)} = 1 - \frac{T_1\left(T_4/T_1 - 1\right)}{T_2\left(T_3/T_2 - 1\right)}. \tag{2.10}$$

For the isentropic compression and expansion processes between the same minimum and maximum volumes,

$$\frac{T_2}{T_1} = \frac{T_3}{T_4} = r^{\gamma - 1} \tag{2.11}$$

where r is defined in Equation 2.1. Additionally, from the ideal cycle the following can be shown

$$\frac{T_4}{T_1} = \frac{T_3}{T_2}. \tag{2.12}$$

Substituting Equations 2.11 and 2.12 into Equation 2.10 yields

$$\eta_{th} = 1 - \frac{1}{r^{\gamma-1}}. \tag{2.13}$$

Thus, it is apparent that the maximum thermal efficiency for the ideal Otto cycle is a function of only the compression ratio and the ratio of the specific heats for the air-fuel mixture. For typical SI engines, compression ratios are generally between 8 and 12. Taking the ratio of specific heats at 1.3 as a representative average for the combusted air-fuel mixture yields maximum thermal efficiencies of 0.5 to 0.6 with the higher efficiency occurring at the highest compression ratio.

Utilization of compression ratios above 12 results in premature ignition of the air-fuel mixture at the high temperatures and pressures at the end of the compression stroke. This behavior, commonly known as "engine knock," results in unacceptable damage to the engine and therefore places an upper limit on the useful compression ratio.

The air induction rate is quantified in terms of the volumetric efficiency, which is the ratio of the airflow rate to the engine volume displacement rate,

$$\eta_V = \frac{\dot{m}_a}{\rho_a \, n/2 \, V_D}. \tag{2.10}$$

The volumetric efficiency is a non-dimensional expression of the mass flow rate through the engine and is directly dependent on throttle position.

Assuming 100% fuel combustion, the fuel conversion efficiency,

$$\eta_f = \frac{W_{net}}{m_f Q_{LH}} \tag{2.14}$$

is equivalent to the thermal efficiency with the same dependence on compression ratio and specific heat ratio. The net power output from an engine is equal to the net work output from a single cycle times the rate of work producing cycles, i.e.,

$$P_{net} = \frac{n}{2} W_{net} = \frac{n}{2} \eta_f m_f Q_{LH} . \tag{2.15}$$

The fuel mass per cycle may be written as

$$m_f = \frac{m_a}{A/F} = \frac{\eta_v \rho_a V_d}{A/F} . \tag{2.16}$$

Substituting Equation 2.16 into Equation 2.15,

$$P_{net} = \frac{n}{2} \eta_f \left(\frac{\eta_v \rho_a V_d}{A/F} \right) Q_{LH} \tag{2.17}$$

After normalizing the indicated power by dividing by engine speed and volume, the indicated mean effective pressure is defined as

$$imep = \frac{P_{net}}{\frac{n}{2} V_d} = \eta_f \eta_v \frac{\rho_a Q_{LH}}{A/F} . \tag{2.18}$$

The *imep* is the pressure required in a constant pressure expansion of the displaced volume to produce the same net work as the ideal cycle. The practical significance of the

imep is that it provides a normalized measure of engine power for which the effects of engine displacement and speed are removed.

In the application of Equation 2.18 to SI engines, $\eta_f, \rho_a, and\ Q_{LH}$ are effectively constants determined by the engine compression ratio and the air-fuel properties. Furthermore, the air-fuel ratio is maintained at approximately the stoichiometric value of 14.6.

The variable element in Equation 2.18 or the mechanism for power control of a SI engine is the volumetric efficiency. Its value is determined by the fixed and variable elements of the air induction system. The fixed elements include the air induction system while the principle variable element is the operator controlled throttle plate. Typical values for volumetric efficiency are 0.2 (throttle closed) to 0.85 (throttle wide open).

From another perspective,

$$\frac{\eta_v \rho_a}{A/F} \tag{2.19}$$

is effectively a non-dimensional characterization of the fuel flow rate. The product of that quotient with the lower heating value of the fuel gives an indication of the available fuel energy and is defined as the available mean effective pressure

$$Amep = \frac{\eta_v \rho_a Q_{LH}}{A/F} \tag{2.20}$$

and

$$imep = \eta_f \ Amep\,. \tag{2.21}$$

From Equation 2.21, *imep* is expected to be linear with respect to *Amep* with a slope equal to η_f. Graphically, this behavior can be shown in Figure 2.4

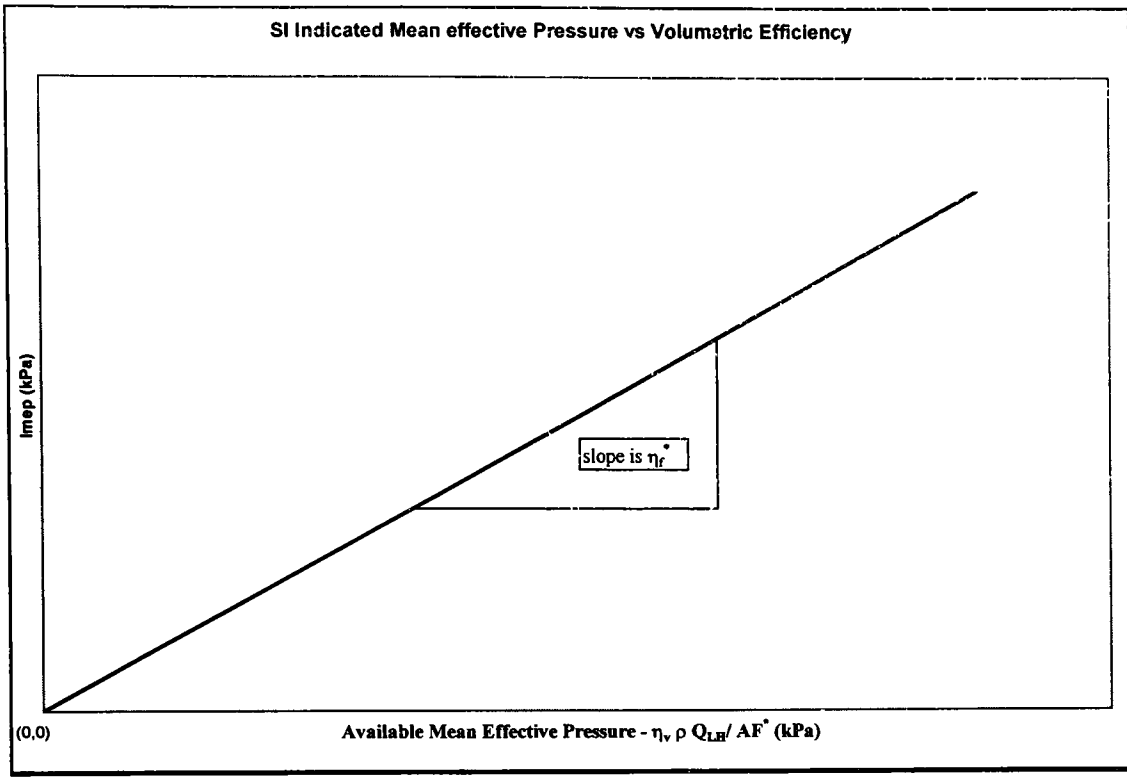

Figure 2.4 Indicated Mean Effective Pressure versus Available Mean Effective Pressure.

This behavior is demonstrated with actual engine data in the next chapter. As mentioned previously, the maximum volumetric efficiency in a naturally aspired SI engine is approximately 0.85. This limit effectively puts an upper bound on the imep and the power output for a given engine at a particular speed. However, this limit can be exceeded by mechanically compressing the cylinder air-fuel charge through supercharging or turbocharging.

2.2 Turbocharging and Intercooling

The difference between supercharging and turbocharging is the power source for the engine inflow compressor. The engine crankshaft drives superchargers whereas turbochargers utilize a turbine in the hot exhaust stream to provide the necessary power. There is a limit to the power increase achieved by turbocharging or supercharging. By compressing the air-fuel charge to the cylinder, there is higher pressure and temperature

at the beginning and end of the compression stroke. Inflow compression ratios must be limited to avoid premature ignition or knock in the SI engine. The problem is somewhat alleviated by providing charge air-cooling between the compressor and the intake manifold with an "intercooler". Intercoolers are air-to-air or air-to-coolant heat exchangers. A turbocharger is more commonly used with the compression ignition (CI) engine. The CI engine is discussed in detail in the next section. Figure 2.5 is a picture of a modern turbocharger.

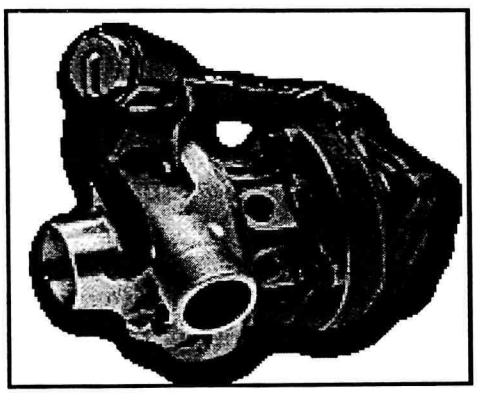

Figure 2.5 Garrett GT-15-25 Turbocharger (GT15-25, n.d.).

Merrion (1993) provides insight into the turbocharging process. The process consists of compressing the intake air to an internal combustion engine utilizing the energy in the exhaust gas stream to run a turbine that is directly connected to the compressor feeding air into the engine. The schematic, shown in Figure 2.6, is a physical and thermodynamic sketch of a turbocharger.

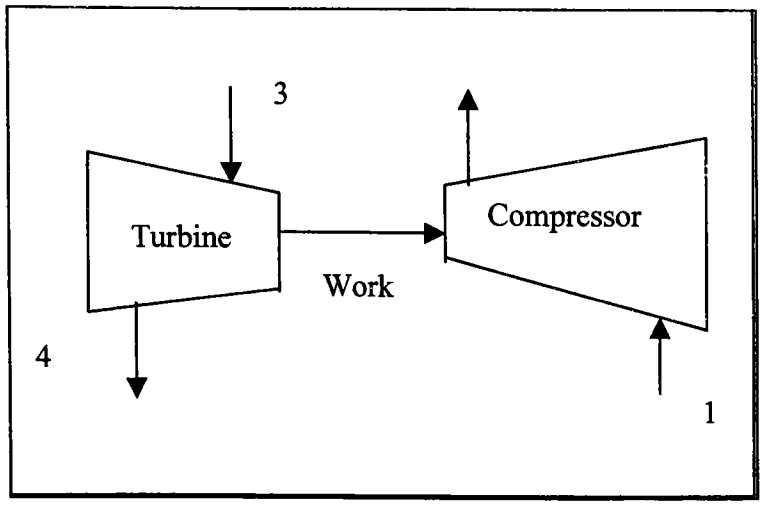

Figure 2.6 Thermodynamic Representation of a Turbocharger.

Turbocharging is the preferred method of supercharging because the energy required to drive the compressor is extracted from the exhaust gas waste stream. This is opposed to pure supercharging where power is bled off the output shaft or the electrical system. Turbochargers operate at high speeds, typically ranging from 15,000 to 100,000 rpm, dictating that most turbochargers are radial flow devices, especially in automotive applications. The high speeds require the turbocharger to be well balanced, made of materials that can handle the high centrifugal forces that are generated, and able to avoid blade resonance. The common operating boost pressure ratio is two or three-to-one when used with the CI engine. Turbocharging is even more attractive for vehicles that commonly operate at high altitudes due to the replacement of much needed volumetric efficiency.

In CI engines, the pressure increase due to the turbocharger is typically limited by mechanical stresses in the engine. In SI engines, the pressure increase due to turbocharging is typically limited by pre-ignition of the air-fuel mixture as previously discussed. Limiting the pressure increase at high engine volumetric efficiencies must be employed. There are three main methods to limit the turbocharger pressure ratio: sizing, exhaust stream bypass or wastegating, and variable geometry. The first and most simple method is to undersize the turbocharger turbine such that the limiting pressure cannot be

reached. The drawback to this method is that the boost at nominal driving conditions is minimal and insignificant.

The next level in over-boost protection is wastegating, which is currently the most common method. It is implemented by bypassing some of the exhaust gas around the turbine to limit the power supplied to the compressor. Wastegating increases the complexity of the turbocharger and does not utilize all of the energy available from the exhaust gasses. The most efficient and complicated method of over-boost protection is variable geometry turbochargers. These typically consist of varying either the nozzle or the vanes of the turbine.

Merrion (1993) describes two distinct philosophies in the design of turbochargers. Constant pressure turbochargers use the exhaust manifold to absorb blow-down pressure pulses. By absorbing these pulses, the flow is constant. Therefore, constant pressure turbochargers are more conducive to high turbine efficiencies. There is, however, a relatively high backpressure on the engine, requiring additional exhaust pumping during the exhaust stroke. Pulsed flow turbochargers represent the second philosophy in turbocharger design. They use the kinetic energy of pulses from the cylinders. The non-uniform flow and pressure reduces turbine efficiency. However, with a properly designed system, reduced efficiency in the turbine can be offset by lower backpressure on the engine. This type of design uses divided turbine housings to take advantage of individual cylinder pulses, thereby increasing the cost of this type of turbocharger.

Recalling the representation of the turbocharger in Figure 2.6, Station 1 is the ambient condition. Station 2 is the compressed air or mixture that is injected into the engine. Station 3 is the exhaust from the engine. Station 4 exits the turbine back to atmosphere. From a thermodynamic analysis, assuming negligible heat loss and elevation change and ideal gases, the compressor power, $\dot{W}_{compressor}$, can be shown as

$$-\dot{W}_{compressor} = \frac{\dot{m}_1 C_{p,1} T_{o,1}}{\eta_C}\left[\left(\frac{p_2}{p_{o,1}}\right)^{\left(\frac{\gamma-1}{\gamma}\right)} - 1\right] \tag{2.22}$$

From a similar thermodynamic analysis, the turbine power, $\dot{W}_{turbine}$, can be shown as

$$\dot{W}_{turbine} = \dot{m}_e C_{p,e} T_{o,3} \eta_T \left[1 - \left(\frac{p_4}{p_{o,3}}\right)^{\left(\frac{\gamma_e-1}{\gamma_e}\right)}\right]. \tag{2.23}$$

In addition to the thermodynamic analysis, experimental measurements and dimensional analysis are used to relate the parameters. Turbomachinery dimensional analysis typically employs the following important variables:

$$\dot{m}, \eta, \Delta T_0 = f\left(p_{o,in}, p_{o,out}, T_{0,in}, N, D, R, \gamma, \mu\right), \tag{2.24}$$

From experience, it has been observed that the Reynolds number and the ratio of the specific heats have little effect on the performance of turbomachinery. These can typically be eliminated from the analysis. Therefore, the following dimensionless groups (Heywood, 1988) are formed:

$$\frac{\dot{m}\sqrt{RT_{o,in}}}{p_{o,in}D^2}, \eta, \frac{\Delta T_o}{T_{o,in}} = f\left(\frac{ND}{\sqrt{RT_{o,in}}}, \frac{p_{o,out}}{p_{o,in}}\right). \tag{2.25}$$

The turbine flow range is largely fixed by the ratio of turbine flow area to the radial distance of the shaft centerline to the centroid of the inlet area (A/R ratio). The A/R ratio, illustrated in Figure 2.7, has a strong influence on the performance of the turbocharger; however, it has not been included in the dimensional analysis to the author's knowledge.

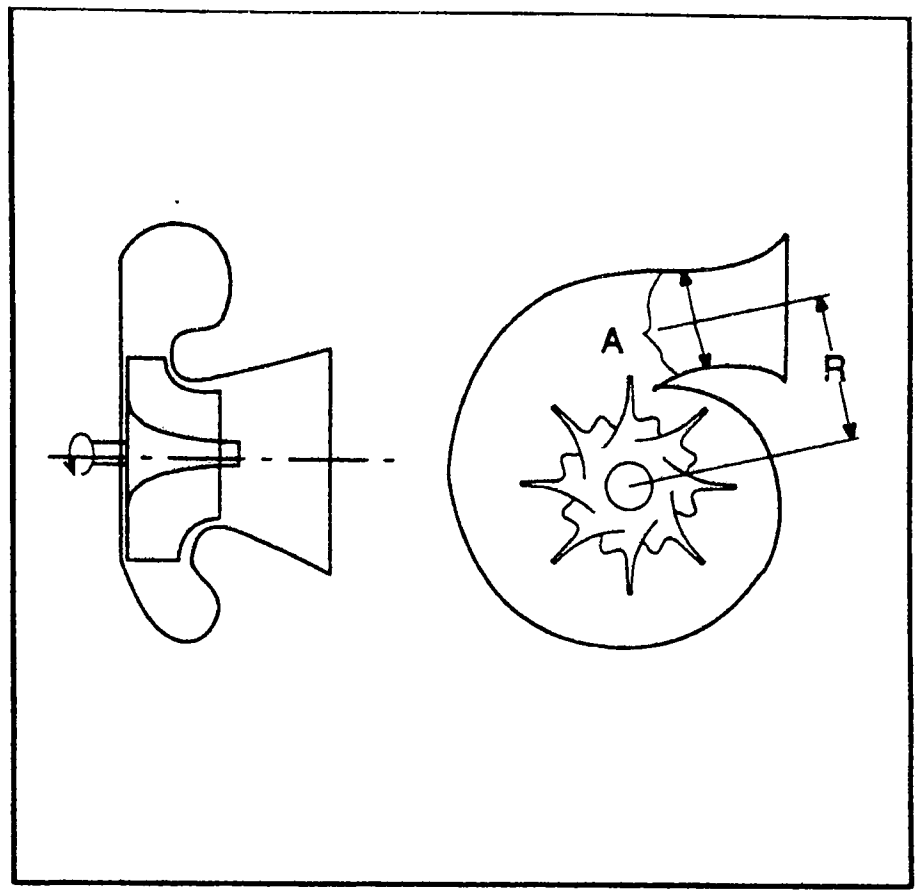

Figure 2.7 Turbocharger A/R Ratio from Merrion in "Diesel Engine Design for the 1990's" (Merrion, 1993).

Decreasing the A/R ratio increases the angular momentum to the turbine. Shaft speed, compression ratio, and engine backpressure are correspondingly increased. The converse also holds. The dimensional data is then expressed in the form of compressor and turbine maps (Merrion 1993).

Figure 2.8 shows an example of a typical compressor map showing the relationship between mass flow rates, compressor pressure ratio, and speed versus efficiency.

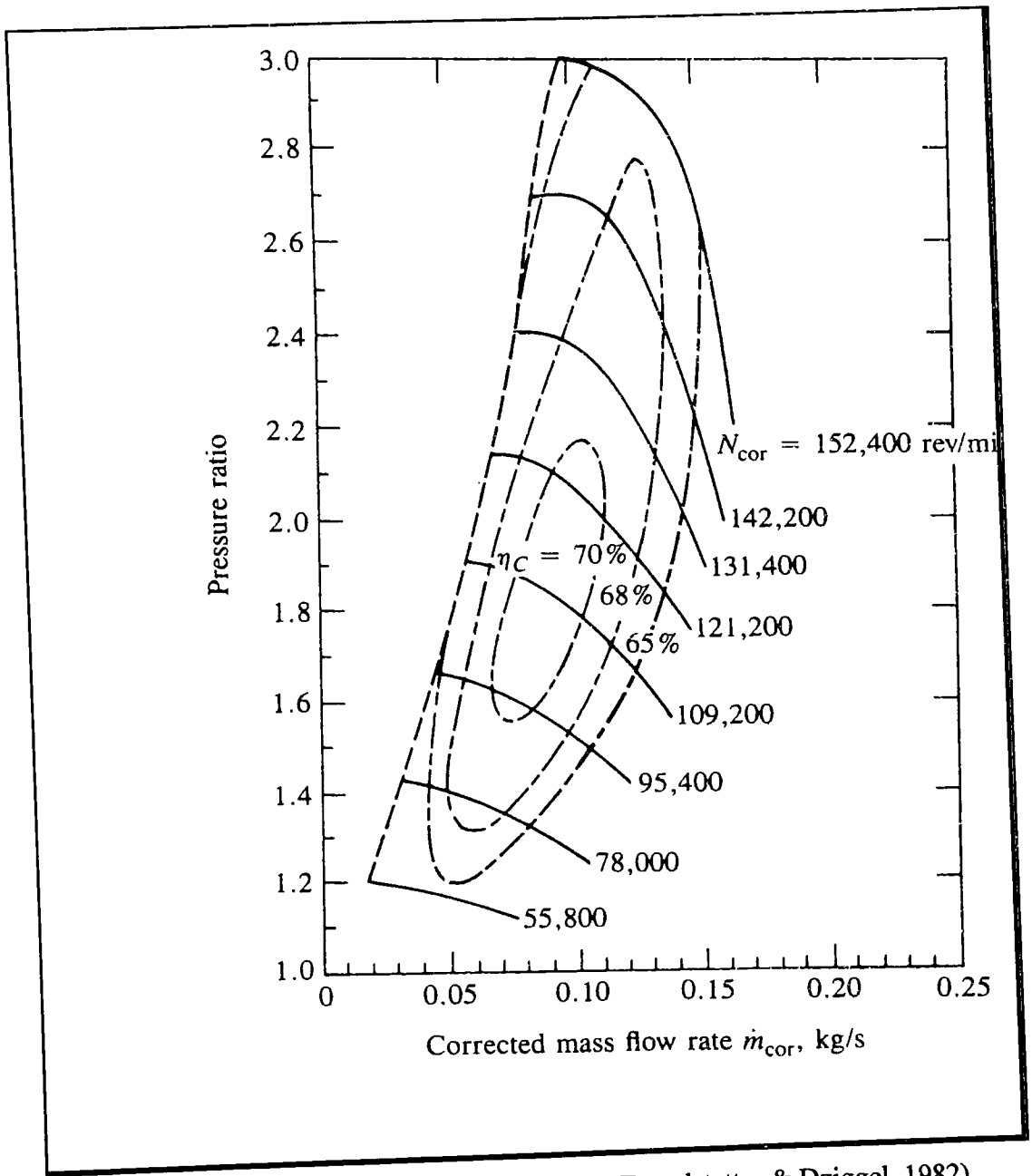

Figure 2.8 Typical Compressor Performance Map (Brandstetter & Dziggel, 1982).

On the compressor performance map, the left edge shows the unstable boundary, where the compressor can cause self-damage. This limit is avoided with proper turbine selection. The right edge is where the sonic velocity is reached, causing choked flow. This capped maximum flow causes the rotational speed lines to be vertical. The upper

edge is the mechanical rotational speed limit that additionally defines the maximum pressure ratio limit. The operating domain of a typical turbine map is shown in Figure 2.9, the operating regime is rather small.

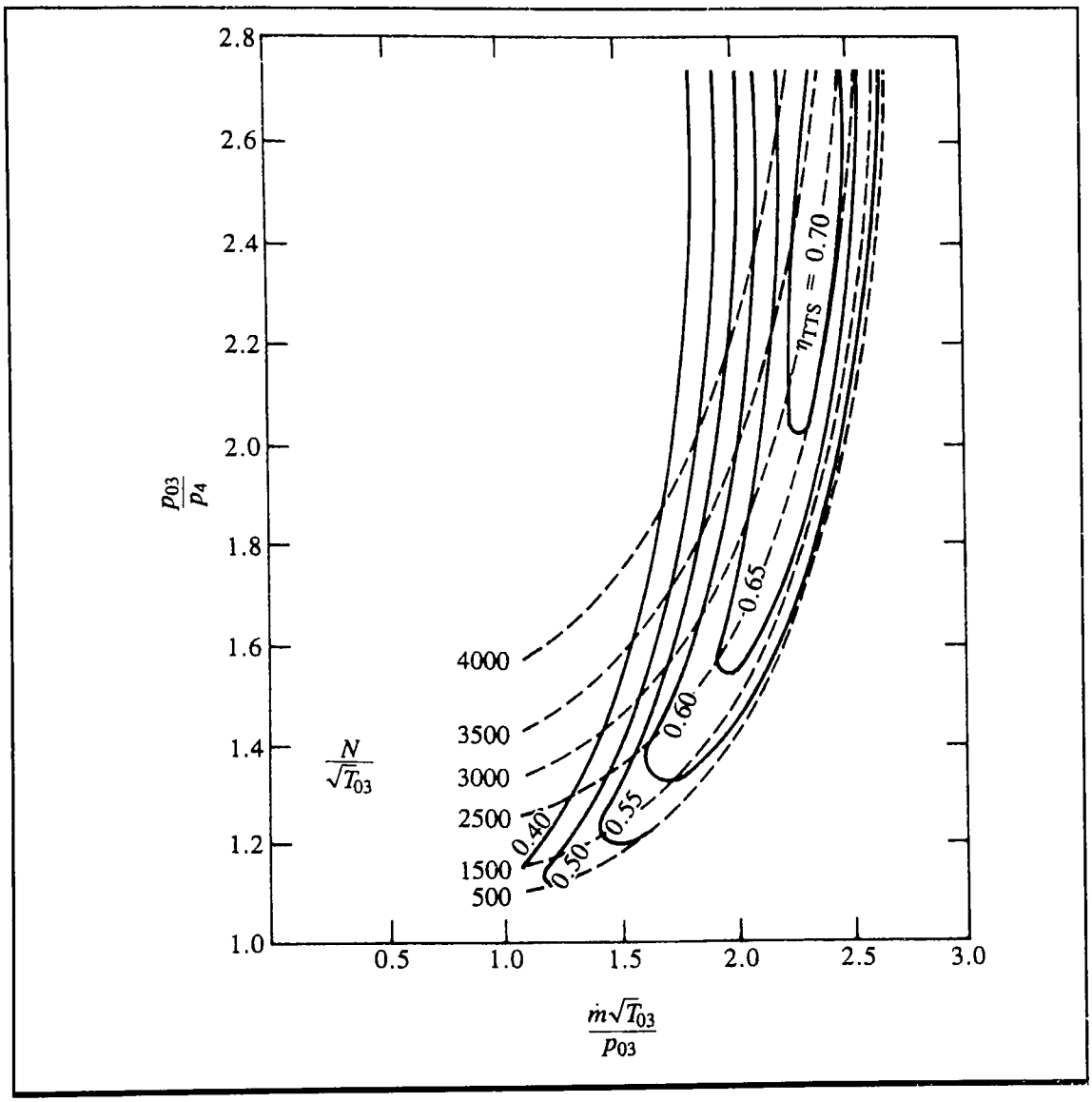

Figure 2.9 Typical Turbine Performance Map (Watson & Janota, 1982).

From Figure 2.9, at higher mass flow rates, the turbine rotational speed lines tend to overlap one another. This overlap causes difficulty working with this type of turbocharger map. As a result, an alternative flow map has been used. A typical alternative turbine map is shown in Figure 2.10.

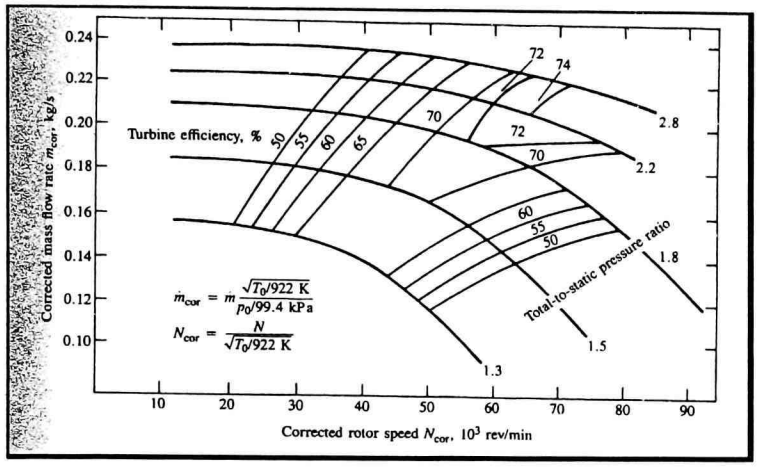

Figure 2.10 Alternative Turbine Map (Flynn, 1979).

Figure 2.10 shows larger performance regimes making it easier to determine the performance of the turbocharger turbine. Typically, turbine efficiency includes the turbine adiabatic efficiency and the turbocharger mechanical efficiency, as they are difficult to measure separately. As efficiency increases, the result is less backpressure on the engine.

The current turbocharger sizing and selection process is a several step process structured as follows:

a. Determine the engine mass flow requirement. This flow rate is found from the engine data and engine volumetric efficiency.
b. Determine the air density and compressor pressure ratio required.
c. Select a suitable compressor. The fact that turbocharger efficiency cannot possibly be simultaneously maximized at all engine-operating requirements is important to recognize. An adequate compressor surge margin must be maintained. Most importantly, adequate boost and air-fuel ratio at the engine

peak torque speed must be balanced while avoiding excessive boost that causes knock and exceeding structural requirements at higher speeds.

d. Select the turbine design that produces the required shaft power (or torque) at each compressor matched airflow condition.

e. Select an over-boost prevention technology, as discussed previously, coupled with the avoidance of turbo lag. Turbo lag is caused by the inability of the rotating inertia in the turbocharger to change instantaneously. As a result, the vehicle has a delayed response, and smoke may dominate the exhaust due to lack of air from the compressor. To avoid turbo lag, it is desirable to reduce turbine A/R. Reducing the turbine A/R ratio increases the airflow and rotational speed at the turbocharger resulting in excessive boost at high speeds. This coupling is the reason that these steps are commonly analyzed together. Turbines with ceramic wheels are increasing in popularity, especially in passenger cars, because of lower inertia and better response.

The compression of any gas in any real process causes a temperature rise in the gas. This increase in temperature decreases the density of the gas entering the engine. Intercooling heat exchangers provides charge air cooling, thereby increasing the density of the air supplied to the engine. As outlined by Merrion (1993), intercooling increases the specific output of the engine, the altitude capability, and the reliability (due to lower engine temperatures). Additionally, it decreases the brake specific fuel consumption. Component material cost is also lowered due to the lower temperatures that occur. Intercooling has a positive effect on exhaust emissions, especially NO_x. There are three types of intercoolers: (1) air-to-engine water exiting from the radiator, (2) air-to-water with separate radiator system, and (3) air-to-air. Option 1 is the easiest to implement, but it is the least effective. Option 2 is desirable, but it requires excessive additional equipment. The air-to-air option provides the best performance and simplicity, but air ducting requires a lot of space. Whichever option is utilized, intercooling is very attractive when turbocharging engines (Merrion, 1993).

Sekar (1982) discussed the evolution of the Diesel engine. There was a significant trend towards higher specific output. Differing approaches have been employed to achieve a higher power-to-weight ratio in Diesel engines. A key parameter was the charge airflow rate. Most of the methods to increase the power output of a given displacement engine concentrated on providing more air for combustion. In the 1960's and 1970's, turbocharging became the standard method utilized for increasing the power output, reducing smoke, and improving fuel consumption. In many applications, compressor pressure ratios greater than 2.5 were common, limited only by turbocharger speeds and materials. As discussed previously, the objective is to increase the intake charge air density, and one way of accomplishing this is to cool the charge air. Sekar reviewed the evolution of air charge cooling and its effects on engine performance. Air charge cooling favorably impacted fuel consumption, emissions (especially NO_x), altitude performance, thermal loading of engine components, and the capability for higher specific output. The exhaust gas turbine inlet temperature generally limited the engine capability. Charge air-cooling helped to increase the rating in two ways: higher charge air density and lower turbine inlet temperature. Vertically integrated companies generally preferred an air-to-air system, while independent engine manufacturers seem to prefer air-to-water systems.

Davidson (1984) additionally discussed the benefits of charge air-cooling. An air charge cooling system was developed to provide the required intake manifold temperatures. This system went further to warm charge air under light engine loads while also providing superior air charge cooling when required. This system improved durability, improved fuel economy, and permitted less restrictive smoke controls.

Wallace et al. (1997) discussed the use of Variable Geometry Turbocharging (VGT). VGT generally adjusts the A/R ratio by changing the turbine nozzle sizes. VGT has found limited applications on heavy-duty "truck-type" engines due to improving torque back-up and transient response. Diesel passenger cars have also begun to incorporate VGT technology. It was recognized that VGT additionally offered the potential to improve the emission characteristics relative to engines equipped with

conventional wastegated fixed geometry turbochargers (FGT). The investigation was to assess the benefits of VGT over conventional turbochargers relative to lower fuel consumption and reduced emissions. It was demonstrated that torque backup was improved by VGT from approximately 25% to 35%, with peak torque occurring at lower speeds than with conventional turbocharging. The passenger car engine under urban drive conditions operates mainly in the low load, low speed regime where emissions of NO_x and hydrocarbons are critical. Wallace et al. investigated the potential of a VGT to reduce and control the emissions from a prototype passenger car direct injection (DI) Diesel engine. The automotive engine was first base-lined for emissions and brake specific fuel consumption with a fixed geometry turbocharger, followed by installation and evaluation of a VGT equipped with swiveling turbine nozzle vanes. An initial investigation of a VGT, in conjunction with a controlled exhaust gas recirculation valve, showed that up to 19% improvement at partial load of NO_x emissions could be made without compromising fuel consumption.

In the following study, Hawley et al. (1988) determined that using a VGT resulted in a 10% torque enhancement over the speed range 1000 to 3500 revolutions per minute without exceeding the limits of maximum cylinder pressure, pre-turbine temperature, and the Bosch smoke test. Hawley et al. used a computer simulation where compressor and turbine performance maps are input as numerical arrays in the usual manner. This method of entering performance maps was standard procedure for fixed gate turbocharging (FGT) with a uniquely defined turbine map. However, the variable gate turbocharging (VGT) used has a different operating map for each vane setting with dramatic enhancement in mass flow and smaller changes in efficiency. The procedure adopted was to use a turbine map for the baseline FGT and employ mass flow and efficiency scale factors. These factors corrected for changes in behavior due to vane angle. The scale factors were calibrated by varying them in small increments for any given operating point.

VGT offered improvements over the baseline FGT performance by lowering brake specific fuel consumption, pre-turbine temperature at higher speeds, smoke

levels over the entire speed range, and by possibly raising the general limiting torque level up to 13 percent without exceeding engine turbocharger limits.

The simulation package ODES (Otto Diesel Engine Simulation) was developed at the University of Bath. The approach was incorporated into this simulation package (Hawley et al., 1998).

Shayler, Baylis, Chick, and Bell (1999) provide an excellent precursor to the research described herein. When comparing Diesel engines to spark ignition gasoline engines, Diesel engines offered superior fuel economy with inferior power to weight ratios in naturally aspired form. The differential in power output is reduced when the engine is turbocharged and/or intercooled. The use of exhaust gas recirculation, EGR, is commonly used to limit NO_x emissions on both and spark ignition engines.

2.3 Turbocharged Compression Ignition Engine

Rudolf Diesel invented the Diesel cycle engine in 1892. Figure 2.11 shows a CAD layout of a modern Diesel Engine.

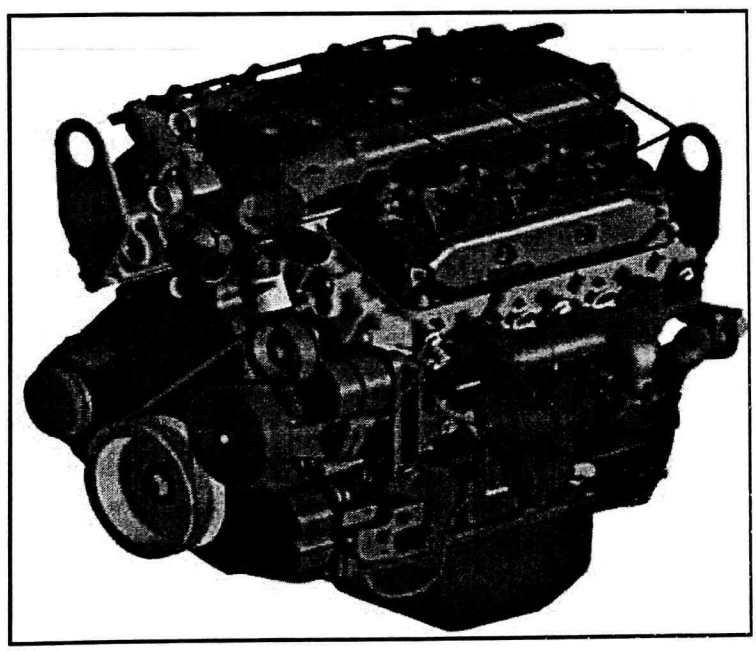

Figure 2.11 Diesel Engine (The new DELTA engine, n.d.).

The Diesel engine is functionally similar to the gasoline engine. The major difference is that a Diesel engine utilizes compression ignition (CI), while a gasoline engine uses a spark ignition (SI). A CI engine does not typically contain spark plugs to ignite the air-fuel mixture in the cylinder. Instead, the heat associated with the compression of the air-fuel mixture causes the mixture to ignite.

The Diesel engine is frequently applied in marine, industrial, and agriculture applications due to its fuel efficiency and relatively small parts count. The disadvantages to the Diesel engine have been weight and increased exhaust pollution compared to the gasoline engine. Both disadvantages are a result of the higher pressures at which a CI engine operates. The higher pressure causes the structure of the engine to be stronger and heavier. The higher pressure also increases the concentration of several pollutants in the exhaust stream. Substantial research in the last 20 years has made the Diesel engine more useful for automotive applications by addressing these shortcomings. The majority of the improvements have resulted from the development of reliable, efficient turbochargers. Because the CI engine process injects the fuel after the air has been compressed, supercharging and turbocharging advantageous. This process avoids premature detonation or "knock" that is an issue with the SI engine.

The definition for the indicated mean effective pressure was given previously as

$$imep = \eta_f Amep = \eta_f \frac{\rho_{amb} Q_{LH} \eta_v}{A/F}. \tag{2.26}$$

For SI engines, the air-fuel ratio is held approximately constant, equal to or slightly less than the stoichiometric value or a slightly rich mixture. Operator regulation of the power output is accomplished through variations of the volumetric efficiency with the throttle plate.

By contrast, for normally aspirated CI engines, the volumetric efficiency is approximately constant at a value determined by the fixed elements in the air induction system. Power regulation is achieved by controlling the cylinder fuel injection rate or the

air-fuel ratio. Values of the air-fuel ratio for CI engines are generally significantly above the stoichiometric value or a lean mixture.

In the case of turbocharged CI engines, the volumetric efficiency varies because of the action of the compressor in the air induction path. The turbocharger pressure ratio and thereby, the volumetric efficiency are not directly controlled by the operator. The pressure ratio is determined by the energy input to the turbine from the exhaust stream and the flow rate, speed, and power matching of the turbine and compressor. The flow rates through the turbine and compressor are approximately equal, the power output from the turbine is equal to the power input requirement of the compressor, and since the turbine and compressor usually share a common shaft, their rotation speeds are equal. As with the normally aspirated CI engine, the operator controls the power output by regulating the fuel injection rate.

The combined influence of the air-fuel ratio and the volumetric efficiency on engine power or imep complicates the problem of determining the engine operational state. It is useful to examine the results of a simple analysis of an ideal CI engine to determine the underlying relationships between volumetric efficiency, air-fuel ratio, turbocharger pressure ratio, and engine speed and power. As will be described in the next chapter, these relationships are used as a guide in the reduction and correlation of actual experimental data. Consider the block diagram for a CI engine with a turbocharger illustrated in Figure 2.12 and the corresponding *Pv* diagram for the CI engine cycle in Figure 2.13.

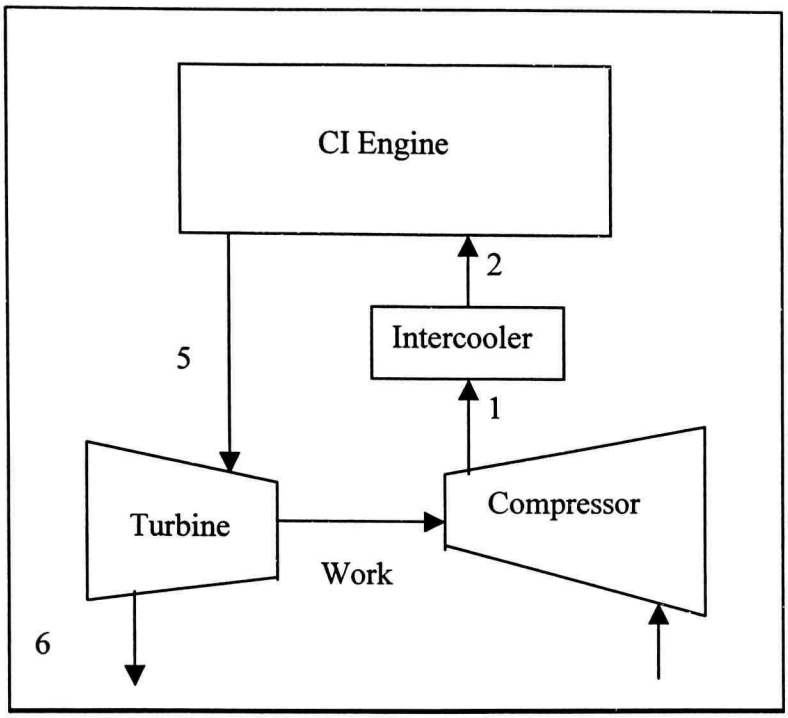

Figure 2.12 Schematic of Ideal Turbocharged CI Engine

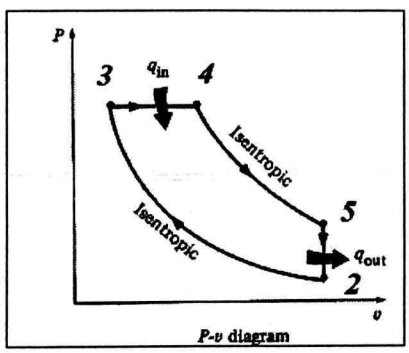

Figure 2.13 State Diagram for Ideal Turbocharged CI Engine

The primary assumptions for the analysis are an ideal gas, constant specific heats, an isentropic compression stroke from state 2 to state 3, constant pressure during the fuel combustion and initial phase of the expansion stroke from state 3 to state 4 with further isentropic expansion after the fuel combustion from state 4 to state 5. The turbine and compressor efficiencies are each approximated with constant or average values. In

addition, the air induction circuit includes an intercooler where the exit temperature is taken as approximately equal to the ambient temperature.

For the process through the compressor,

$$T_i = T_{amb} \qquad p_1 = p_r p_{amb}$$
$$p_i = p_{amb} \qquad T_1 = T_{amb} + \frac{w_c}{c_p} \qquad w_{comp} = \frac{1}{\eta_c} c_p T_{amb} \left(p_r^{\frac{\gamma-1}{\gamma}} - 1 \right) . \tag{2.27}$$
$$v_1 = \frac{RT_1}{p_1}$$

The exit conditions from the intercooler are

$$v_2 = v_1 \qquad T_2 = T_{amb} \qquad p_2 = \frac{RT_2}{v_2} . \tag{2.28}$$

The isentropic compression from state 2 to state 3 yields

$$v_3 = \frac{v_2}{r} \qquad T_3 = T_2 \left(\frac{v_2}{v_3} \right)^{\gamma-1} \qquad p_3 = \left(\frac{v_2}{v_3} \right)^{\gamma} \tag{2.29}$$

and the work input required for the compression is

$$w_C = w_{2-3} = c_v (T_3 - T_2) . \tag{2.30}$$

The initial expansion with fuel combustion from state 3 to state 4 is approximated with a constant pressure process,

$$p_4 = p_3 \qquad T_4 = \frac{T_3}{1 + \frac{1}{A/F}} + \frac{Q_{LH}}{c_p (A/F + 1)} \qquad v_4 = \frac{RT_4}{p_4} \tag{2.31}$$

and the remaining expansion from state 4 to state 5 is an isentropic process,

$$v_5 = \frac{v_1}{1+\frac{1}{A/F}} \qquad T_5 = T_4\left(\frac{v_4}{v_5}\right)^{\gamma-1} \qquad p_5 = \left(\frac{v_4}{v_5}\right)^{\gamma}. \tag{2.32}$$

The work output for the expansion stroke is given by

$$w_E = w_{3-4} + w_{4-5} = p_3\left[\left(1+\frac{1}{A/F}\right)v_4 - v_3\right] + \left(1+\frac{1}{A/F}\right)c_v(T_4 - T_5). \tag{2.33}$$

The exhaust gases expand through the turbine from state 5 to the ambient pressure. The work extraction by the turbine per unit mass of the air and fuel combustion products is given by

$$w_{turb} = \left(1+\frac{1}{A/F}\right)\eta_{turb}c_p T_5\left[1-\left(\frac{p_{amb}}{p_5}\right)^{\frac{\gamma-1}{\gamma}}\right]. \tag{2.34}$$

Equations 2.27 to 2.34 define the properties at each state point through the simplified CI engine and turbocharger. The net work output per unit mass of air through the engine and the overall thermal efficiency are given by

$$w_{net} = w_E - w_C = w_{3-4} + w_{4-5} - w_{w-3} \qquad \eta_{th} = \frac{w_{net}}{Q_{LH}/A/F}. \tag{2.35}$$

The corresponding indicated mean effective pressure is

$$imep = \frac{w_{net}}{v_2\left(1-\frac{1}{r}\right)} = \eta_f Amep = \eta_f \eta_v \frac{\rho_{amb} Q_{LH}}{A/F} \tag{2.36}$$

where

$$\eta_v = \frac{\dot{m}_a}{\frac{n}{2} V_d \rho_{amb}} = \frac{v_{amb}}{v_2}.$$

The volumetric efficiency is a function of the pressure ratio provided by the turbocharger compressor. This dependency, which is illustrated in Figure 2.14, suggests that experimentally determined values of volumetric efficiency should be well correlated to the pressure ratio by a linear curve fit.

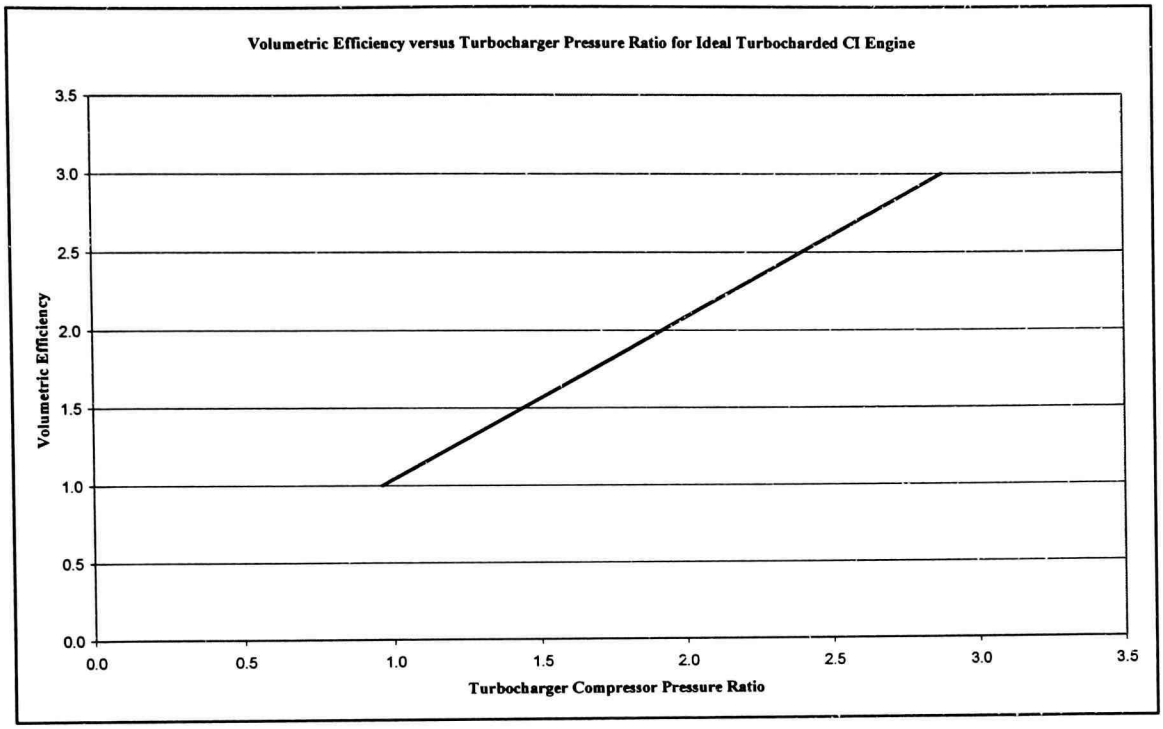

Figure 2.14 Volumetric Efficiency versus Pressure Ratio for Ideal Turbocharged CI Engine

From Equation 2.36, it is apparent that the *imep* is functionally dependent on both the volumetric efficiency and the air-fuel ratio. Taking a representative engine compression ratio of 18, standard air properties, standard atmosphere ambient conditions and taking $Q_{LH} = 4.3 \times 10^4 \frac{kJ}{kg}$, the resulting calculated *imep* is plotted with respect to *Amep* in Figure 2.15 along lines of constant air-fuel ratio for turbocharger pressure ratios of 1 to 3.

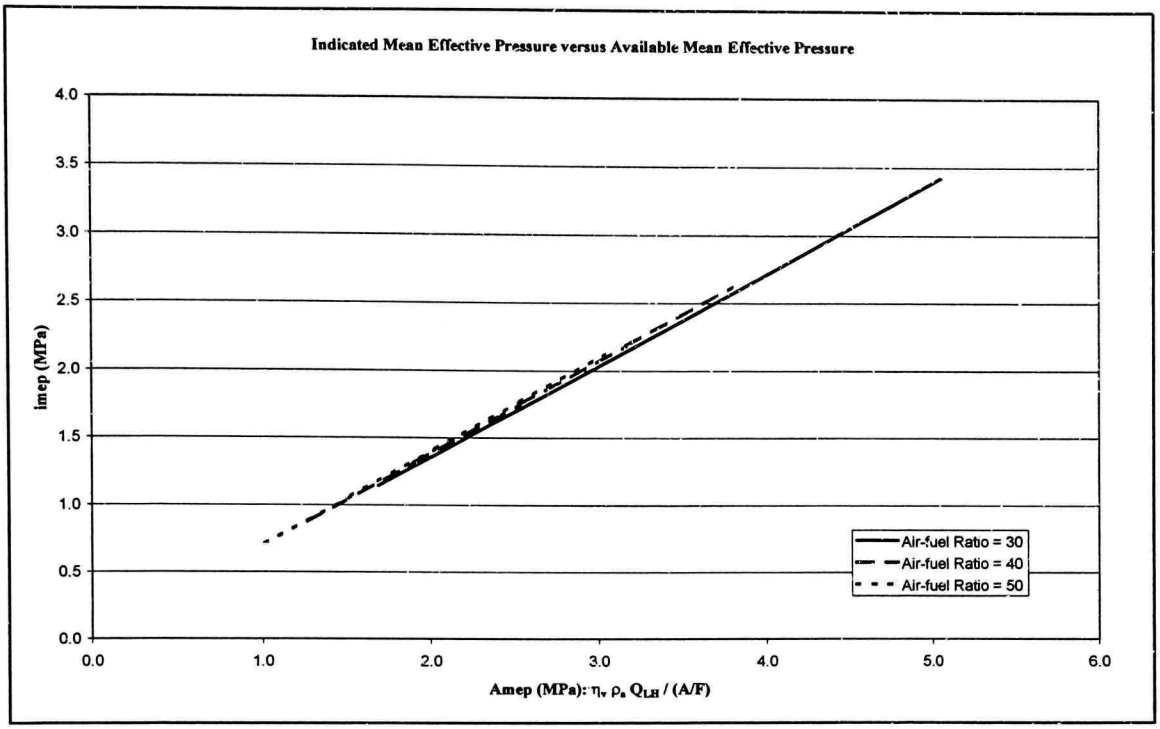

Figure 2.15 Indicated Mean Effective Pressure versus Available Mean Effective Pressure for Ideal Turbocharged CI Engine

This figure illustrates the principal difficulty in analyzing the turbocharged CI engine. Note that based on the CI engine cycle analysis alone, the specification of an engine power and speed requirement or equivalently, the *imep*, does not lead to a unique combination of volumetric efficiency and air-fuel ratio. Determination of the specific values of these parameters requires application of the matched operating conditions for the turbocharger compressor in the engine inlet flow and the turbine in the exhaust flow. Figure 2.16 illustrates the variation of the energy input requirement per unit mass of air for the turbocharger compressor and the energy extraction per unit mass of the air-fuel combustion products for the turbine.

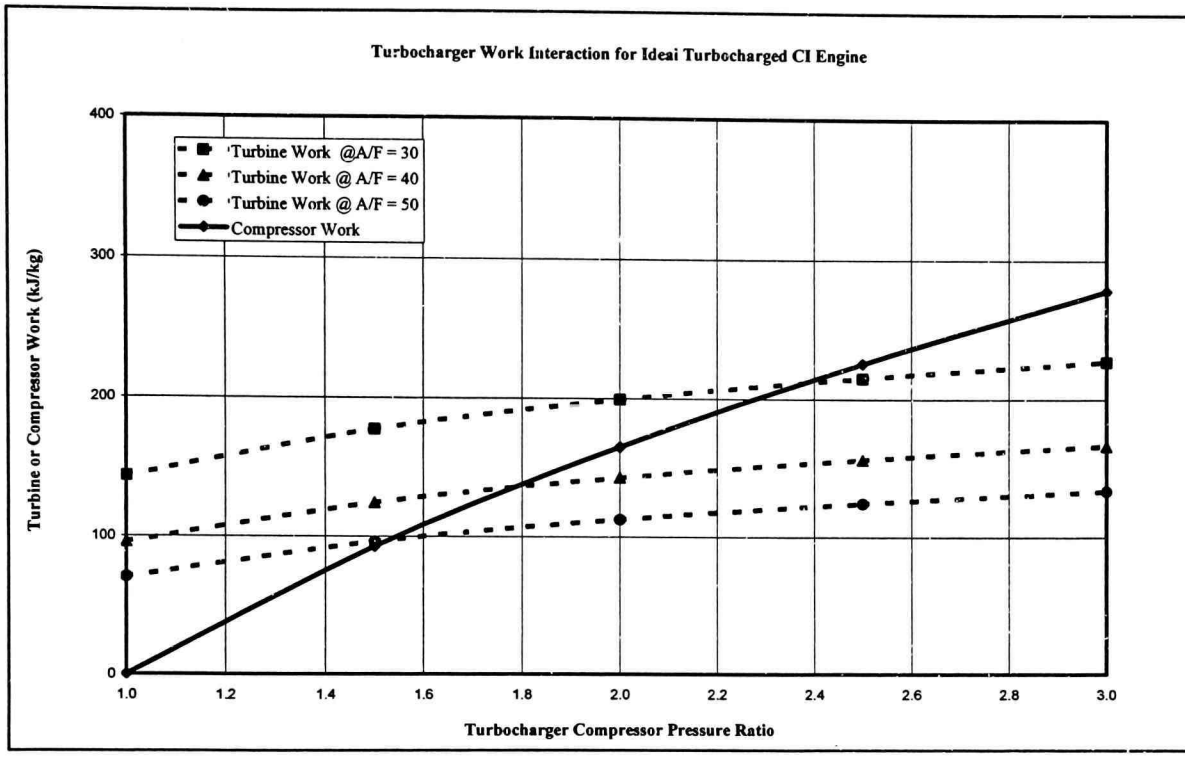

Figure 2.16 Specific Turbocharger Works for Ideal Turbocharged CI Engine

The compressor energy requirement is a function of only the pressure ratio. The turbine energy extraction depends on the exhaust flow pressure and temperature, and is, therefore, dependent on both the pressure ratio and air-fuel ratio. At any actual steady-state engine operating point, the energy extraction from the turbine is equal to the energy requirement for the compressor. These operating points are indicated by the intersections of the compressor energy requirement curve with the lines (for constant air-fuel ratio) of turbine energy extraction. These points of intersection define a unique relationship between the turbocharger pressure ratio and engine air-fuel ratio that is illustrated in Figure 2.17.

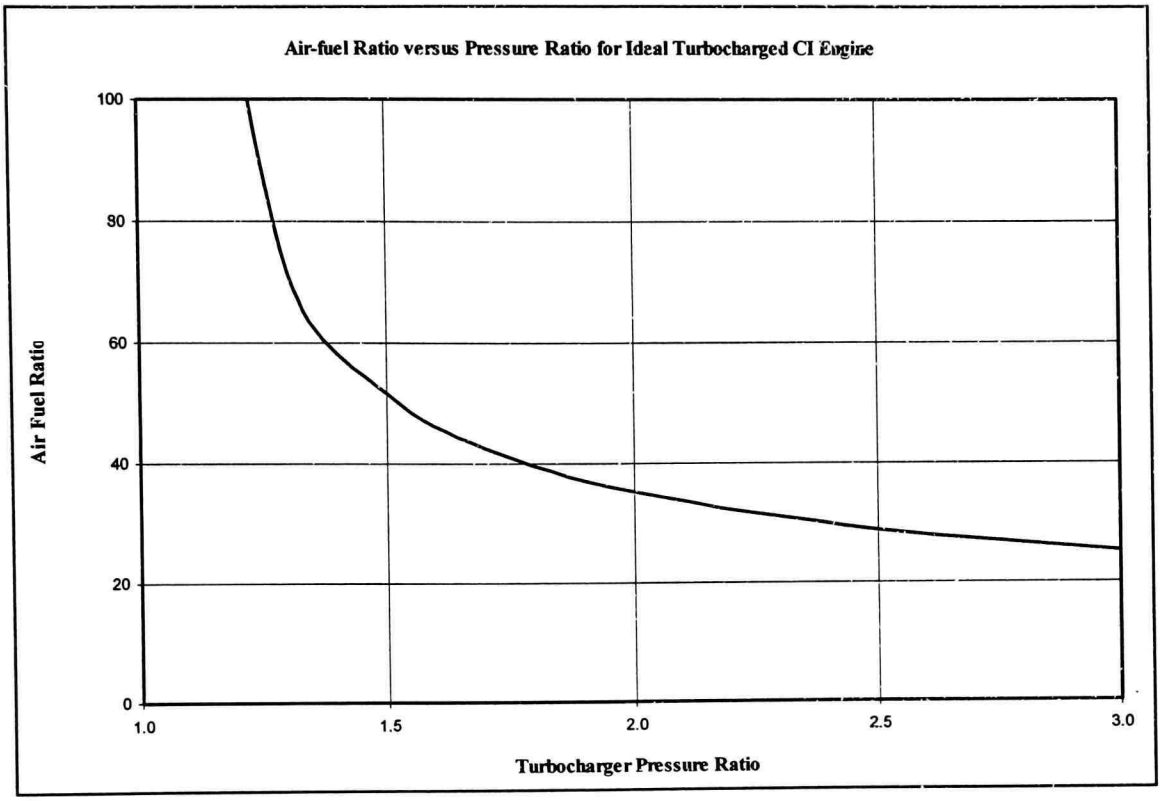

Figure 2.17 Air-fuel Ratio versus Pressure Ratio for Ideal Turbocharged CI Engine

The relationship is more conveniently represented in Figure 2.18 by plotting turbocharger pressure ratio versus $Amep = \eta_v \rho_{amb} Q_{LH} / A/F$, where both the air-fuel ratio (Figure 2.17) and volumetric efficiency (Figure 2.14) are unique functions of the pressure ratio.

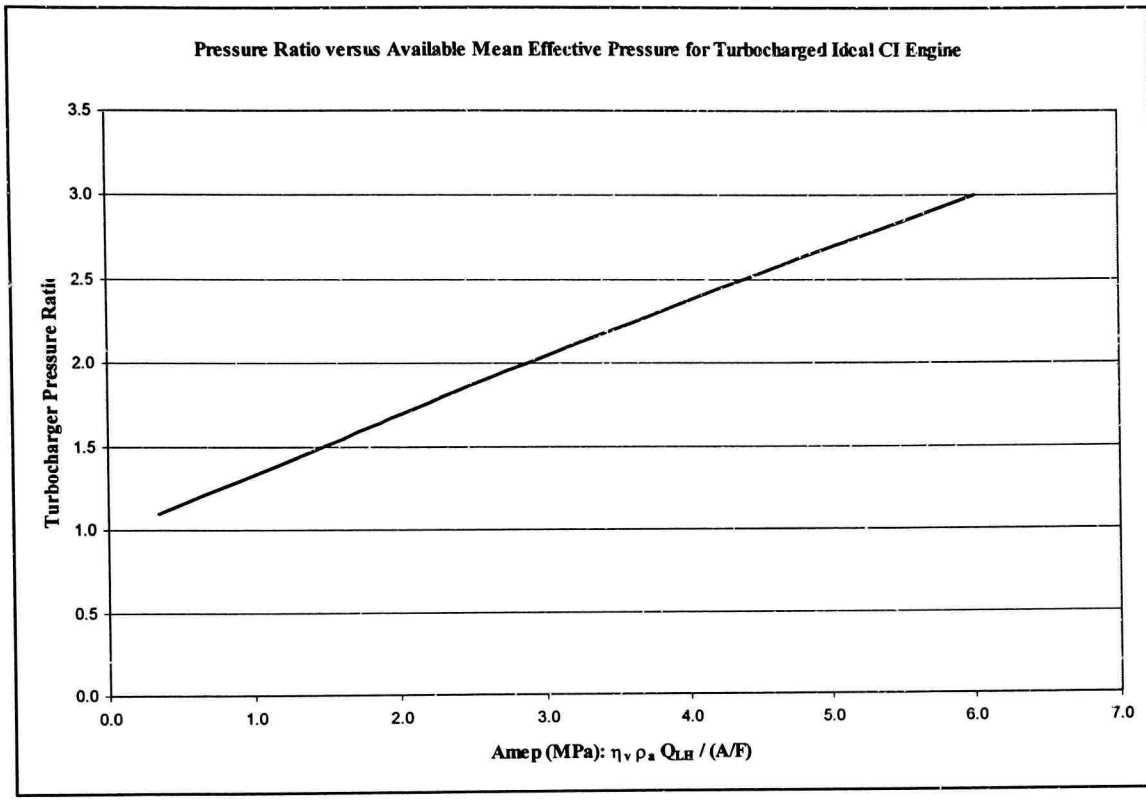

Figure 2.18 Pressure Ratio versus Available Mean Effective Pressure for Turbocharged Ideal CI Engine

Figure 2.18 suggests that experimentally determined values of turbocharger compressor ratio should be approximately linearly related to the corresponding values of *Amep*. With a unique relationship established between turbocharger pressure ratio and engine air-fuel ratio, corresponding values of *imep* and *Amep* may be calculated with the results shown in Figure 2.19.

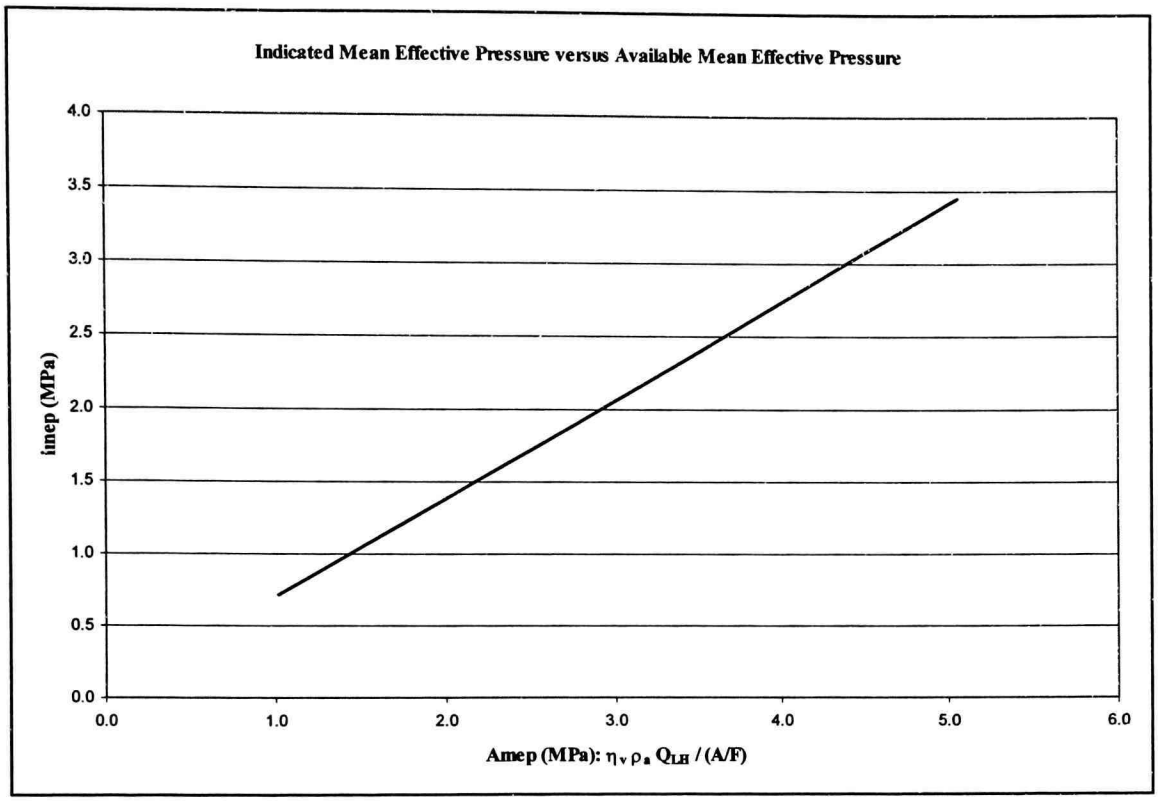

Figure 2.19 Indicated Mean Effective Pressure versus Available Mean Effective Pressure for Matched Ideal Turbocharged CI Engine.

Not surprisingly, the *imep* is linear with respect to *Amep* with the slope equal to the fuel conversion efficiency.

2.4 Heat Transfer

Many researchers currently use some form of the heat transfer analysis outlined by Annand (1963). This is a generalized equation accounting for both the convection and radiation component of the heat transfer in a cylinder of a reciprocating engine.

Gehres (1963) of Union Carbide discussed the interesting phenomena of nucleate boiling that can occur under severe driving conditions. Tests indicate that at these severe driving conditions, up to 60% of the cylinder heat transfer surface is cooled by nucleate boiling. Additionally, these hot spots represent 80% of the heat transferred to the coolant. The coolant boiling point controls the engine hot spot temperatures. Gehres

further correlated the effects of differing cooling media properties to the occurrences of this type of engine cooling. The heat transfer coefficient from the coolant-to-metal is many times greater than the transfer coefficient of metal-to-air. Therefore, at the radiator, the properties of the coolant do not have a major impact on the heat transferred.

Finlay, Harris, Boam, and Parks (1985) discussed the influence of cylinder head material, coolant composition, pressure, temperature, and velocity on cylinder head temperatures. Each of these parameters was varied, and its influence on combustion chamber wall temperature was determined. Agreement was shown between measured values and corresponding predictions from a heat transfer model. Forced convection, sub-cooled, and nucleate boiling were included in the model. The results suggested that nucleate boiling was an integral factor in the transfer of heat from the cylinder head to coolant.

Finlay et al. (1985) reiterated that the reduction of lead levels in petrol, higher compression ratios, and the increasing use of turbocharging is aggravating premature detonation in the automotive spark ignition engines. Knowledge of the local coolant temperatures and velocities, surface heat fluxes, and heat transfer coefficients were necessary to design an effective engine cooling system. In 1985, this information was not available due to the complex geometry of the coolant flow passages in most engines.

An aluminum cylinder head was found to have lower combustion chamber wall temperatures and was able to tolerate more ignition advance than a cast iron cylinder head of similar geometry under conditions of almost equal power generation. Combustion chamber wall temperatures were not sensitive to cooling water pump speed. Therefore, pump speed changes did not increase resistance to low speed knock. Equations developed for forced convective, nucleate boiling heat transfer were used to predict the relationship between heat flux and surface temperature in the cylinder head in the liquid-cooled regions. The theory predicted the measured changes in the wall temperature resulting from changes in coolant velocity, pressure, and composition (Finlay et al., 1985).

Alkidas and Cole (1985) reported that the time histories of the local heat fluxes were significantly different at different locations of measurement. These differences are attributed to the lack of spatial uniformity in the fluid motion and combustion. Because of the extreme difficulties associated with the estimation of errors in the measurement of surface heat flux, an error analysis of the heat flux temperature measurements was not performed.

Lahvic (1986) presented a correlation for the estimating heat rejection to the then engine coolant. This dissertation is the result of updating the prediction methodology for Ford Motor Company. Lahvic regression is the following correlation (Lahvic, 1986):

$$\dot{Q}_{coolant}[Btu/hr] = 8.66V_D[L]n[rpm] + 148T[ft\ lb] + 835P[hp] - 1010V_D + 2890. \quad (2.31)$$

Liu, Xu, and Hou (1993) investigated the heat exchange characteristics of an engine series containing a water-cooled radiating system. The analysis of the radiator indicated that most of the heat transfer resistance comes from the fin to air heat transfer coefficients. Increasing the airflow or the fin surface efficiency could increase the heat transfer coefficient. Liu et al. also proposed to meet differing loads by varying the fan size and speed. From a heat balance, 24% (30% at lower speeds) of the overall heat of combustion is rejected to cooling system. If the intercooler is placed before the radiator, the net impact could be negative. Therefore, airflow path is critical in the design of an intercooler. For the particular engine used in their test, the engine coolant was held to 95°C, corresponding to a 35°C ambient temperature.

Cao and Wang (1995) investigated the use of heat pipes for cooling pistons. Piston cooling is a critical measure for achieving efficient engine performance. A higher working temperature is required to increase engine thermal efficiency and reduce the discharge of soot from the engine. The maximum temperature a piston can sustain is a critical restriction in engine performance. The maximum temperature is even more critical for aluminum alloy-based pistons. These alloys have a pronounced temperature dependence on their mechanical properties. Due to the reciprocating motion of the piston,

cooling is difficult. Commonly, pistons are cooled by the crankcase oil plash/mist under crown cooling method. Additional oil cooling may be necessary for medium- and high-speed engine pistons. An internal cooling gallery in conjunction with an oil jet on the piston crown provided improved cooling. Cao and Wang observed that the reciprocating heat pipe was also feasible for cooling an engine piston. In similar systems, an analysis of the piston cooling system indicated that the reciprocating heat pipe cooling method at the valve stems could sustain much higher engine powers.

Rakopoulos and Mavropoulos (2000) discussed the complexity of heat transfer in an internal combustion engine. This complexity was attributed to the fact that the relevant phenomena are transient, three-dimensional, and subject to rapid swings in cylinder gas pressures and temperatures. The combustion chamber itself with its moving boundaries adds more complexity. Their experimental investigation was an effort to examine the short-term response during an engine cycle. Heat fluxes to the exhaust manifold wall were obtained and analyzed with the corresponding heat losses to the combustion chamber walls under the same engine operating conditions.

Rakopoulos and Mavropoilos (2000) applied the unsteady heat conduction equation to calculate the heat flux with boundary conditions derived from experimental temperature measurements. As expected, increasing the engine speed resulted in increases of the values of the peak heat fluxes in both the cylinder head and exhaust manifold. This increase was due to the increase of the gas side heat transfer coefficients. However, it was shown that as engine speed increases, the increase of cylinder head peak heat flux becomes minimal, whereas the heat losses from the exhaust gases to the manifold increase. As the engine speed increases, there is only a small increase in the cylinder head peak heat flux because the combustion gas peak pressure and temperature decrease with increasing speed under constant load. The decreasing load was attributed to combustion deterioration. The higher gas velocities in the exhaust manifold dominate the heat transfer as the engine speed increases. The heat loss increases are approximately proportional with engine speed. After the inlet valve opens, the warmer combustion chamber walls transfer heat to the fresh air entering the cylinder. Thus, the cylinder heat

flux becomes negative during that period. The cylinder pressure increases after the inlet valve closes. However, the cylinder heat flux remains negative at the beginning then rises slightly during compression. Combustion starts, and the heat flux increases rapidly, reaching a maximum, and then decreases to a small value by 40-60° after top-dead-center.

Hribemik and Moskwa (2000) discussed the effects of cooling the charge air using a heat exchanger between the turbocharger and the engine intake. This additional equipment offset the temperature rise of charge air due to pressure boosting. Air-to-air intercoolers typically have high thermal inertia; therefore, their transient characteristics are normally overlooked. Because of this, the NTU-effectiveness method, which is most appropriate for steady state analysis, is often used in the simulation of transient engine operation. However, during transient operation the intercooler is subjected to a wide range of unsteady operating conditions. Air mass flow rate, boost pressure, and temperature vary during transient operation as functions of engine speed, turbocharger speed, and mass flow rate of cooling air. The cooling air mass flow is a function of engine fan speed, vehicle speed, and obstructions around the intercooler. Recognizing that the NTU-effectiveness method is not accurate under transient conditions, Hribemik and Moskwa proposed a two-dimensional model of a cross-flow heat exchanger to study the intercooler/engine interaction. After the model had been verified against experimental results, it was incorporated into a zero-dimensional simulation model of a turbocharged Diesel engine. Hribemik and Moskwa found that steady state conditions were reached after approximately 12 seconds, while the rated power was reached after approximately 7 seconds. Under most situations, this seems like a short period; however, in heavy urban traffic this could affect engine performance.

The development of an analytical method for predicting engine heat rejection to coolant requires experimental measurement of engine heat rejection. This experimental data is necessary not only to assess the accuracy of the analytical predictions, but also for deriving empirical constants used in the analytical method.

Oler, Parish, Williams, and Burns (2002) provide an excellent discussion of the difficulties associated with engine heat rejection measurements. As they describe, heat rejection testing is typically performed with the engine installed in a dynamometer cell, as it is difficult to properly instrument an engine installed in a vehicle. The engine is usually equipped with a simple cooling system where 100% of the engine coolant circulates through one half of a liquid-to-liquid heat exchanger. Cold water circulated through the other half of the heat exchanger removes heat from the hot engine coolant and thereby simulates the function of a vehicle's radiator. A smaller, separate heat exchanger cools the engine oil at high engine speeds. A highly simplified diagram of a typical heat rejection test setup is shown in Figure 2.20.

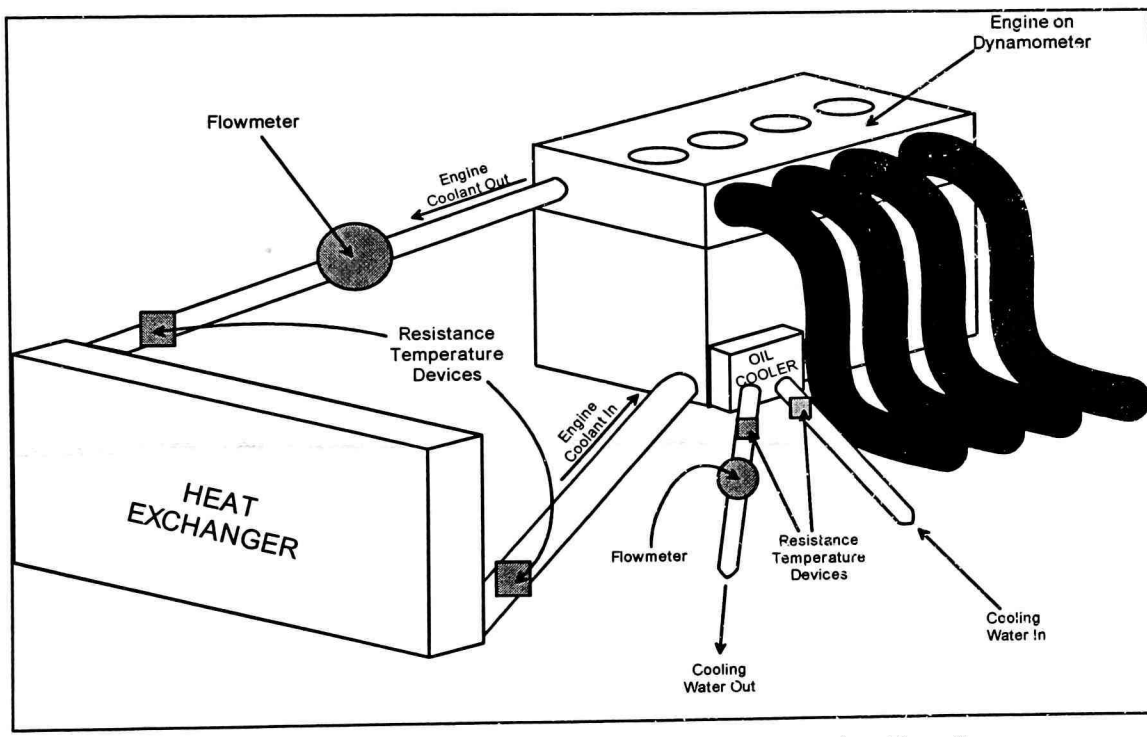

Figure 2.20 Highly Simplified Diagram of a Typical Heat Rejection Test Setup.

Under test conditions, the engine is operated at a constant speed and throttle setting, producing a fixed brake power. The engine operates at this condition until the temperature of the coolant exiting the engine stabilizes at a constant level, indicating the engine has attained steady-state operation. Under steady-state conditions, the two heat

exchangers maintain constant coolant inlet and engine oil temperatures by extracting heat from the coolant and engine oil at a constant rate.

For an engine operating under steady-state conditions, heat rejection to coolant can be calculated from the difference between the inlet and outlet temperatures of the coolant, coolant mass flow rate, and coolant specific heat,

$$\dot{Q}_{coolant} = \dot{m}_c C_p \Delta T_c . \tag{2.31}$$

A matched set of resistance temperature devices (RTDs) is used to measure the difference in coolant inlet and outlet temperatures. The mass flow rate of the coolant is determined using a flow meter installed in the engine cooling circuit. These measurements, used in conjunction with Equation 2.31, allow calculation of the engine heat rejection to coolant. If the engine oil cooler is in operation, the heat rejected to the oil cooler is calculated in a similar manner and included in the total engine heat rejection to coolant.

Oler et al. note that there is a certain amount of error associated with any experimental data, and heat rejection to coolant is no exception. Engine heat rejection to coolant is, in fact, quite difficult to measure accurately and with repeatability. The two primary sources of error in measuring heat rejection to coolant are errors in flow rate measurement and errors in temperature measurement.

Typically, the type of flow meter used in a given experiment drives the accuracy of coolant mass flow rate measurement. Measuring engine heat rejection with the engine installed on a dynamometer stand allows the use of an orifice-type flow meter, which measures the mass flow rate of a liquid based upon the pressure drop the moving liquid experiences as it passes through an orifice. When properly calibrated, this type of device produces measurements that are accurate to within less than three percent. Given the turbulent nature of the flow through an engine cooling system and the frequent presence of vapor bubbles in the coolant, this is a very accurate measurement. These devices, however, are too large to fit under the hood of a typical vehicle, plus they require that the

cooling circuit have relatively few bends to keep flow turbulence to a minimum. These limitations restrict the use of this type of flow meter to the dynamometer stand. Measurement of heat rejection in the vehicle environment requires the use of a smaller, turbine-style flow meter. These flow meters are typically less accurate than the orifice-type flow meter. In addition, the cooling system as installed in a vehicle typically features many bends in the circuit, creating turbulence in the coolant flow that decreases the accuracy of the flow measurement.

An additional cause for inaccuracy in the measurement of engine heat rejection is the relatively small temperature change that takes place across the heat exchanger. Under steady state operation, the engine coolant typically undergoes a temperature change of approximately 10° C as it passes through the heat exchanger, which is relatively small. As a result, the errors inherent in the inlet and exit temperature measurements, while small in the absolute sense, can appear relatively large as a percentage of the total measurement. Thus, a 1° C error in the measurement of the coolant temperature change across the heat exchanger can result in a 10% error in the calculated heat rejection to coolant.

Because of these factors, even under the best circumstances, any measurement of engine heat rejection can be in error by approximately 5% due to measurement error alone. Unfortunately, given the large amount of time required for an engine to reach steady state operation at any given operating condition, it is impractical to take a large number of data samples and determine a mean, which could eliminate at least some of the common cause variability

For a given mass of air and fuel inside an engine cylinder, optimum spark timing exists that produces maximum engine torque. This timing is called maximum brake torque (MBT) spark timing. For a given engine operating condition, firing the spark plug earlier or later than MBT timing produces less than the maximum amount of output torque.

In typical automotive applications, engines usually employ spark timing that is retarded relative to MBT (i.e., the spark plug is fired later in the cycle than the optimum

timing). This is because the use of retarded spark timing reduces the occurrence of engine knock, although retarded spark also causes the engine to produce less than the maximum amount of brake torque for a given operating condition. The amount of spark retard relative to MBT timing varies from one engine operating condition to the next. In addition, the amount of spark retard required for a given engine operating condition may be completely different for two different engine configurations. Thus, when examining a large sample of engine data such as the one used in the current study, the data will contain a tremendous amount of variation in spark timing relative to MBT. It is important, therefore, to understand the impact that this variability may have upon the results of the study.

Operating an engine with retarded spark timing relative to MBT causes the engine to operate less efficiently. The peak pressure attained inside the cylinder is lower than realized with MBT timing, thus leading to a lower power output from the engine. In turn, a lower power output means the engine is extracting less energy from the hot combustion gases. The net effect of this is that retarded spark timing produces higher exhaust gas temperatures than MBT timing for a given engine operating condition. This is an intuitive result. Simply stated, if the engine operates at a less efficient condition, it should waste a greater amount of energy. In this case, potentially useful energy is lost in the form of hotter exhaust gases.

As the hot exhaust gas flows through the engine exhaust ports at high velocity, it transfers a significant amount of heat to the coolant in the engine cylinder head. A higher exhaust gas temperature, therefore, increases the amount of heat rejection to the coolant. Retarding the spark timing from MBT thus increases the amount of engine heat rejection to the coolant. Again this is an intuitive result, given that heat rejected to the coolant is another form of wasted energy.

It is important to note that the preceding analysis assumes that constant output torque was maintained from the engine as the spark timing was retarded. This seems confusing at first, given that the output torque should decrease as the spark timing is retarded. Indeed, if the spark timing was simply retarded at a given operating condition

and the amount of throttle opening was unchanged, the preceding analysis may be invalid. Keep in mind, however, that engines are designed for use in motor vehicles--not on dynamometer stands--and that the operator of a motor vehicle primarily is concerned with maintaining constant torque output, not a constant throttle opening. Motor vehicles require a fixed amount of output power from the engine to maintain a given speed on a particular grade of road, regardless of the engine spark timing or amount of throttle opening. If the engine calibration computer retards the engine spark for a given operating condition, the driver will simply tip-in the accelerator pedal and open the throttle wider to maintain the same amount of output power and, therefore, the same speed. When discussing heat rejection to coolant, which is a parameter applicable to the design of the full vehicle instead of just the engine, it is more useful to think in terms of constant engine output torque or power instead of constant throttle position.

The data used in deriving the analytical method for predicting engine heat rejection comes from a variety of different engines using a wide variety of engine calibration strategies. Some of the dynamometer data, in fact, contains heat rejection measurements for four to five different settings of spark timing at a constant amount of output torque. Given that no data exists on the value of MBT spark timing for the various operating conditions tested, it is impossible to analytically "correct" this data back to MBT timing or even to determine the amount of spark retard relative to MBT for a given operating condition. This wide variation of spark timings, therefore, introduces a certain amount of error into the results of the analytical method, as the analytical method cannot account for the effect of retarded spark timing upon heat rejection. Although it is impossible to accurately quantify the effects of this error, it is known that, for a constant amount of output torque, significant changes in spark timing can produce changes in heat rejection to coolant on the order of 5%.

One significant aspect of automobile emissions is the formation of oxides of nitrogen (NO_x), which can act as a source of urban air pollution. NO_x formation is a complex process that occurs in high temperature regions during in-cylinder combustion events, primarily in the areas immediately behind the flame front. NO_x formation can be

reduced by diluting the air-fuel mixture in the cylinder with recycled exhaust gas, which, among other things, has the net effect of reducing the peak temperature of the combustion products. Dilution of the air-fuel mixture often is accomplished using exhaust gas recirculation (EGR).

A vehicle's EGR system captures a small portion of engine exhaust gas and reroutes this gas into the engine's incoming charge of fresh air, thus diluting the air-fuel mixture and lowering the peak combustion temperature. Since excessive dilution of the air-fuel mixture causes unstable combustion or engine misfires, the amount of exhaust gas recycled must vary with engine operating condition to ensure stable combustion. Typically, no exhaust gas is recycled at high relative power operation since such dilution reduces the engine's peak power output. At partial throttle settings, the amount of recycled exhaust gas may exceed 10% of the amount of incoming fresh air. The amount of EGR that an engine can tolerate at any given operating condition is highly dependent upon unique characteristics of that particular engine; thus, as with spark timing, there is no generic rule as to the proper amount of EGR for a given part-throttle engine operating condition.

EGR rate, therefore, introduces another potential source of error into the comparison of heat rejection predicted analytically to that measured on the dynamometer. Recall that the experimental data used in this study was originally intended for use in designing vehicle-cooling systems, not deriving an analytical method. The data used, therefore, reflects a wide variety of engine calibration strategies. Some, but not all, of the experimental heat rejection data used in this study was measured with the engine's EGR system in operation. Experimental determination of the amount of EGR used at any given engine operating condition is extraordinarily difficult, requiring a detailed analysis of the composition of the engine exhaust gas. For the vast majority of the engines tested, therefore, EGR rate simply was not measured.

The fact that at least some of the engines used to generate the experimental heat rejection data were equipped with functioning EGR systems ensures that the experimental data covers a broad range of combustion gas temperatures. Since no data is

available as to how much EGR was used at individual operating conditions, it is impossible to incorporate a correction for EGR effect upon combustion gas temperature into the analytical method. This difference in assumed, and actual combustion gas temperatures, therefore, account for some of the difference between the predicted and measured engine heat rejection (Oler, 2002).

2.5 Computer Simulation

Computer simulation is the next area where significant research is being conducted. There is obviously a need to accurately model automobile performance before an actual automobile is produced. The shear expense of prototyping activities such as wind tunnel validation is enormous. Additionally, design cycle times may be significantly diminished through the application of computer-aided simulation, design, and manufacturing.

Gerhard (2002) developed an engine simulation from experimental investigations conducted on a high speed Diesel engine. Evaluating heat balances and measuring steady state temperature fields separately determined heat fluxes to the different engine components. A comparison with the results of cycle simulations carried out with correlations for the local mean heat transfer coefficient demonstrated that the heat lost to the cylinder walls and the resulting influence on the process variables could be accurately modeled. The steady state temperature fields occurring in the components during operation could also be accurately predicted. Gerhard noted that the design of supercharged Diesel engines could become a problem of optimization. A compromise must be found between power density, fuel consumption, and construction effort. The numbers of design parameters that can be varied is too large to investigate experimentally. The expense and complexity make it impossible to find the optimum solution by experiments alone. Computer simulations allow designers to solve problems theoretically with many variables. These calculations cannot substitute for experiments, but they could reduce the number of experimental tests necessary. The time, cost, and risks for the development of a new engine are decreased.

Watts and Heywood (1980) give an excellent overview of computer simulation techniques that are still used today. Computer simulations of the complete cycle for a four-stroke, spark-ignition engine can be used to examine the effect of changes in operating and design variables on engine performance, efficiency, and emissions. These types of simulations are "thermodynamic" or "zero-dimensional" in structure. Their formulation is based on the first law of thermodynamics, without including the details of the combustion chamber and the shape of the flame front. The inputs to the calculation are typically basic engine geometry, engine speed, intake mixture fuel-air equivalence ratio, exhaust gas recycle fraction, intake manifold pressure, combustion chamber wall temperatures, and parameters which define the mixture burning rate. One-dimensional, quasi-steady flow equations are used to obtain the mass flow through the valves during the intake and exhaust stroke. The first law of thermodynamics is used to determine the condition in the engine cylinder during each portion of the four-stroke cycle. Empirical correlations are used for heat transfer between the gas in the cylinder and the walls. The cycle simulation then predicts the mass flow rate of fuel and air through the engine, cylinder pressure, unburned and burned mixture temperatures, heat transfer to the combustion chamber walls, and work transfer to the piston. All of these outputs are determined as functions of crank angle during the cycle. The indicated power, specific fuel consumption, efficiency, mean effective pressure, and mean exhaust temperature are then computed for the particular engine operating point. Engine friction is then estimated to obtain brake values of these quantities. The calculated cylinder pressure, burned gas temperature profiles, equivalence ratio, and fuel composition can be used to compute the rate of formation and decomposition of NO_x. This approach permeates the literature.

Additionally, Watts and Heywood (1980) evaluated the wide-open-throttle predictions of a previously developed cycle simulation against experimental data from both a naturally aspirated and a turbocharged production engine. The simulation was then used to compare the fuel consumption, NO_x emissions and performance characteristics of these two engines over the complete load and speed range. This example illustrated the usefulness of a cycle simulation of this type evaluating two

different engine concepts to provide the same performance characteristics. Various aspects of the effect of heat transfer on engine performance, efficiency, and NO_x emissions were compared. These aspects compared the effect of variations and uncertainty in heat transfer predictions with cold combustion chamber walls. The impact of ceramic materials on selected engine components over a range of combustion chamber wall temperatures at engine compression ratios of 8 and 16:1 was also evaluated. The results of the ceramic component simulations were discussed in the previous adiabatic engine section.

A smaller turbocharged engine was determined to be more efficient than the larger engine at the same power level at speeds and loads typical of normal vehicle use. This increase in efficiency is attributed to improved mechanical efficiency. At the maximum brake torque speed, the two engines provided similar brake power. However, the smaller turbocharged engine exhibited higher brake specific NO_x emissions than the larger engine at a given power output due to the higher relative load. Consequently, the smaller engine ran at higher cylinder pressures and temperatures to produce equal power.

Additionally, studies were performed for the large naturally aspirated engine to examine the effect of reduced heat transfer on engine performance, efficiency, and NO_x emissions. Decreasing load and speed increased the heat transfer's impact. Retarded timing reduced heat transfer due to reduced peak burned gas temperatures. Heat transfer peaked at the stoichiometric equivalence ratio and decreased for rich mixtures. Watts and Heywood (1980) found that heat transfer uncertainty did not significantly affect simulation predictions of performance and efficiency. Brake specific NO_x increased as heat transfer was reduced due to the higher burned gas temperatures. Watt and Heywood used a standard heat transfer model that was found throughout the literature with the exception of including a burned and unburned portion to the gas temperatures.

Moeckel (1994) used a commercially available computational fluid dynamics code, Flotran, to identify modifications that improved coolant distribution throughout the engine. A simplified 2-D approach was taken and experimentally verified. The accurate

prediction of three-dimensional heat transfer film coefficients requires extremely large models that were not available at the time of publication.

D'Adda, Lisbona, Occella, and Maiorana (1994) outlined the use of the considerable development of recent analytical methodologies for engine design. The application of these methodologies to the design of the cooling system of a high specific power engine was performed. For the optimization of the coolant flow inside the block and head passages, two different codes have been employed. The complete analysis of the coolant circuit was performed using a one-dimensional code developed at the Fiat Research Center. The results were input as boundary conditions for a detailed three-dimensional simulation of the coolant passages inside the engine with the commercial code STAR-CD. The study focused on an initial engine design with possible design modifications deduced, analytically verified, and then applied to the final engine solution. This new approach for the optimization of the cooling system was considered a useful tool for engine design. D'Adda et al. considered optimization of the coolant system in internal combustion engines, a critical task in the design process. The thermal condition influenced the structural integrity of the engine as well as performance and emissions. The design of high specific power engines has to ensure sufficient cooling velocities to prevent metal temperature reaching excessive levels. It has been demonstrated that the thermal condition of the engine is not very sensitive to the total coolant flow rate, but it is sensitive to local geometrical characteristics of the passages and coolant velocities.

The current need for time reduction in the design process does not allow an experimentally based trial and error approach. The development of analytical methodology helped engine designers in the definition of the cooling system primarily for the coolant passages inside the engine.

The approach outlined by D'Adda et al. (1994) has a common theme throughout engineering: first use a macro approach to find a sound design, and then follow up with a more detailed simulation and/or experimentation. Results using this approach applied to engine cooling passages were promising in reducing design cycle time.

Woodward (1995) offered another thermodynamic approach and improvement to the traditional limited pressure air-cycle that has an unrealistic constant-volume cooling model between the cylinder exhaust and cylinder intake. By substituting isentropic expansion, throttling, and constant-pressure cooling in the place of constant volume cooling, a better ideal cycle for the actual processes is formulated. This model is better equipped to handle the prediction of 30% losses to the engine coolant. This essential heat rejection is predicted from the new model and a second law analysis.

Bulaty, Codan, and Skopil (1996) reiterated the common theme of shrinking design cycle times. Powerful personal computers and technically mature simulation software were driving this new surge for decreased cycle times. Hence, the calculation of engine performance had not only become reliable, but also far more economical than experimentation. The sharp rise in the power density of the modern engine was primarily due to the parallel development of reliable turbochargers. Engine builders have provided increased demand for turbocharged equipment. Thus, these engine systems have become considerably more complex and flexible.

Additionally, to add code to existing simulation software for the future turbocharging demand would have been a costly modification. Clearly, an augmented system that allowed for insertion into existing codes was a necessity. The required turbocharging computer simulation program would need to be user-friendly, reliable, and accurate. Bulaty, Codan, and Skopil (1996) believed that they developed a necessary, useful computer simulation of turbocharging systems. However, the details of the simulator are not presented.

Mohan, Arici, Yang, and Johnson (1997) outlined a similar code, which was an enhancement of the Vehicle Engine Cooling System Simulation (VECSS) developed at Michigan Technological University and modified to include a turbocharged Diesel engine with a charge air cooler model. The radiator and charge air cooler model showed good agreement with experimental data. These models consisted of heat balances and a Colburn or Nusselt type analysis to find the heat transfer coefficients--a typical approach. The code showed that accuracy for the thermal performance was within 1.5% at the

middle to high loads and 5% at low loads. The VECSS code uses a standard convective Nusselt correlation. Additionally, Mohan et al. (1997) pointed out that engines have a significant amount of radiation heat transfer due to the high temperatures of gases as well as carbonaceous particles formed during combustion. Standard forms of radiation heat transfer equations were used with experimentally determined coefficients. Turbocharger performance maps were used in the simulation.

Intercoolers, or charge air coolers, are heat exchangers located between a turbocharger compressor and the engine. These devices cool the air that leaves the compressor, thereby increasing the charge density and performance of the engine. There were few models in the literature that used full gas dynamic, or 'wave-action,' simulation. Furthermore, these models tended to approximate the behavior of the intercooler by assuming constant performance under all operating conditions. A full-wave action intercooler model was developed that predicts intercooler performance at different engine operating conditions. Intercoolers pass hot air to be cooled through a heat exchanger exposed to a coolant. Like all heat exchangers, the design goal was to expose the hot gases to the maximum allowable cooling surface area while minimizing the pressure drop. One approach to quantify the performance of an intercooler is its effectiveness. Heat exchanger effectiveness is defined as the ratio of the actual heat transfer to the theoretical maximum heat transfer. This approach is a standard analysis that can be found in any undergraduate heat transfer text. Intercooler performance varies strongly with the mass flow rates through the heat exchanger. As the mass flow rate of the charge air increases, the effectiveness drops for a given coolant flow rate. Thus, the performance of the intercooler varies over the load and speed range of the engine. Another important characteristic of the intercooler is the pressure drop. This pressure drop impairs engine performance. Therefore, it must be accounted. Computational fluid dynamics (CFD) is beginning to become prevalent in intercooler design. CFD does and will continue to accurately characterize heat transfer versus the required pressure to overcome flow restriction (Bromnick, Pearson, & Winterbone, 1998).

Worden and Zehr (1999) discussed the critical nature of coolant flow velocities to the durability of the engine itself. The geometries of the individual component parts used in the system should be designed to minimize turbulence that affects the type and rate of corrosion. Additionally, flow passages must be "sized" to maintain minimum coolant velocities. In high velocity flow, a combination of the mechanical damage produced by the impingement on a metal surface and the inherent corrodibility of the metal may result. Aluminum alloys are more prone than other alloy metals to corrosion damage because of the low inherent hardness of the material. Coolant velocities for the flow were predicated in the individual cooling system components based on CFD analysis. Erosion-corrosion damage is shown to be a function of the type of coolant and the angle of attack of the fluid stream with the casting wall surface.

2.6 Adiabatic Engine Research

An "adiabatic" engine is a term used to describe any engine where the heat rejected to the coolant is reduced by some means. Techniques include coating the cylinder walls and using emulsified fuel (water added), or oil (instead of water), as the coolant.

Kamo (1977) made a claim of greatly improved thermal efficiency due to turbocharging an engine with thermal insulation.

Wallace, Way, and Vollmert (1979) investigated the constant temperature limiting case. An existing and well-proven Diesel cycle simulation program was applied to the Perkins 6.354 6-cylinder 4-cycle Diesel engine. A relatively thin layer of 2 mm bonded silicon nitride to the cylinder walls was used to reduce heat loss to coolant by approximately 50%. Such materials were associated with "isothermal" operation of the engine. The wall temperature had minimal cyclic fluctuations approaching a temperature of 300°C. Wallace et al. found that isothermal operation of the engine resulted in little improvement of the indicated thermal efficiency. The reduced heat loss to coolant was transferred primarily to the exhaust enthalpy. This conclusion was based on cycle calculations with unlimited maximum cylinder pressure and fixed heat release timing and

duration. The benefit of increased exhaust enthalpy could be realized fully only when a turbocharger was added to the engine. Substantial improvements in Diesel engines indicated thermal efficiency could be achieved only if adiabatic engine operation was approximated with gains of the order of 14% for fully adiabatic operation, or 7% for semi-adiabatic operation. Materials and methods of construction showed that the requirements for true adiabatic operation presented great practical difficulties (Wallace et al., 1979).

Way and Wallace (1979) extended their purely theoretical investigation with the addition of a turbocharger. Turbocharging was frequently suggested as a way of improving the thermal efficiency of engines. However, in the past the gains had not proved sufficient to justify the additional expense. Way and Wallace hypothesized, as discussed in their previous paper, that when an insulated engine was used to reduce heat losses to a minimum the increase in exhaust temperature should make the compounded engine more attractive. The investigation showed the effect of reduced heat loss on the interaction between an engine and the turbocharger. Turbocharging increased the efficiency by a significant margin, while the effect of heat suppression on engine efficiency alone was relatively small. The turbocharger performance did increase due to the increased exhaust temperature. This combination was necessary before the viability for any partially insulated engine scheme to be successful.

Way and Wallace (1979) found that the use of turbo compounding enabled the thermal efficiency and corresponding torque to be raised by 2-3 percentage points. Turbo compounding is accomplished through multiple turbocharger and intercoolers designed for the flows and temperatures that they would see. Turbo compounding significantly improved the matching of the turbocharger, thus enabling a smaller turbine to be fitted. This configuration improved the air-fuel ratio, hence improving efficiency and smoke at low engine speeds. Improvements that are more significant would be achieved at low engine speeds by implementing a variable turbine geometry device. Reduction of heat loss with conventional insulating techniques without turbocharging yields limited improvements in efficiency. Way and Wallace claimed that true adiabatic operation

would result in much more drastic improvements in efficiency of up to 10 percentage points. Alternative forms of compounding, such as the use of variable geometry turbines and split power arrangements, could become more cost attractive as fuel prices increase.

Watts and Heywood (1980) found that using ceramic-coated engine components without thermally isolating the ceramic material from its metal support and coolant system produced modest reductions in heat transfer. However, use of isolated ceramic materials and high wall temperatures substantially reduced heat transfer. This reduced heat transfer and decreased the volumetric efficiency and power. Brake specific fuel consumption remained constant. Exhaust temperature and brake specific NO_x increased substantially. From a computer simulation, the use of ceramic material for the piston crown and cylinder head proved to be the most effective means for reducing heat transfer.

Watson, Kyrtatos, and Holmes (1983) described that from a first law of thermodynamics analysis the limited heat rejection engine had merit and potential.

Tovell (1983) discussed the benefits of applying thermal insulation to the exhaust ports and combustion chamber. The reduction of heat loss to the coolant system has always been of considerable interest, as this would allow a reduction in the cost, size, weight, and power requirements. Traditionally the exhaust port lengths are minimized, and the engine internal coolant circuit is configured to provide high coolant velocities in critical areas while using flood cooling elsewhere. Higher fuel efficiencies and shrinking volumes to accommodate cooling systems of sufficient size in high-powered vehicles have made the reduction of heat loss to the engine coolant increasingly important. Tovell also used a computer simulation of a highly rated turbocharged DI truck engine to determine the effectiveness of reduced heat transfer engines. Comparisons were made between a standard engine and engines with the exhaust port, cylinder head, piston, and cylinder liner insulated. Also examined was the necessity of modifying engine conditions when heat losses through the combustion chamber walls are retarded. Tovell also stressed the difficulties in practically and economically insulating actual engine components. However, the successful testing of a ceramic liner located in the exhaust

duct of an engine during more than 1000 hours of engine operation was deemed significant.

Tovell's (1983) simulation found favorable results to insulating the engine components. By eliminating heat loss to the coolant system, fuel consumption was reduced by approximately 7.5%. The effects of this insulation were high exhaust temperatures and cylinder pressures. The largest reduction in fuel consumption and the associated heat loss to coolant was obtained by insulating the piston crown or cylinder head. Tovell stated that reducing heat losses by partially insulating the piston crown, top of the bore, and exhaust port should be feasible in existing engine designs. The simulation predicted a reduction of full power fuel consumption by about 4.6%. Additionally, higher exhaust temperatures must be tolerated with exhaust manifolds and turbochargers capable of operating at higher temperatures. An increase in power unit efficiency to 50% can be obtained if exhaust energy can be recovered. The IMEP of the reciprocating engine should be monitored to avoid excessive maximum cylinder pressures. The pollution impact was also discussed. An increase in NO_x emissions was expected, but hydrocarbons, particulates, and smoke should be reduced. The simulation also predicted that engine noise would be slightly reduced. Fan noise could also be reduced by 2 to 4 dB (Tovell, 1983). This noise reduction is significant, as 3 dB represents a noise reduction of a half.

Kadoli and Aknamurthy (1984) found that a substantial reduction in the heat loss to the coolant resulted in an increase in cylinder work and exhaust gas energy. They studied the performance of a semi-adiabatic engine through compound cooling, which was defined as a cooling method using external oil cooling and an internal methanol water-fuel mixture. The purpose of the oil cooling is to partially insulate the cylinder head and walls, as the thermal conductivity and specific heat of the oil are lower than water, thereby increasing the engine load. To reduce thermal loading, water/methanol was injected at the intake manifold. Oil cooling and methanol injection lowered the BSEC with energy savings of 4-6%. In addition, NO_x emissions were lowered.

Individually, both oil cooling alone and oil cooling with water injection versions provided lower values of BSEC, with energy savings of 3-5%.

Hashem (1989) presented that the waste energy potential by exhaust gases was 17.8% to 30.3% of the energy input at a temperature range of 170°C to 670°C. The thermal content of cooling water represents 9.2% to 13.2% of the engine energy input. The energy lost to the surrounding by convection in the still air state represents 32% to 57% of the energy input (Hashem, 1989).

Woods, Bryzik, and Swartz (1992) discussed that removing the water-cooling system using strategic oil cooling, and upgrading critical engine component materials, reduced the heat rejection to the radiator of a conventional water-cooled engine. This approach has been identified as the low heat rejection engine (LHRE). Many of these LHRE's do not apply in-cylinder insulation. Downsizing of the cooling system in a non-insulated LHRE resulted in a significant increase in structural temperatures. Reduced component life, increased heat loading, and increased airflow resistance occurred. Volumetric efficiency losses lead to increased intake manifold pressures, which increase after cooling heat rejection, offsetting in-cylinder heat rejection reductions. An advanced LHRE employs the use of in-cylinder insulation. This additional step reduces the heat rejection and structural temperatures. Intake air after cooling is reduced, which is a significant portion of the overall heat rejection.

Adiabatic engine intake boost pressure was predominantly controlled by the need to maintain air density, and not volumetric efficiency factors. Boost pressure was primarily dependent on the airflow requirements and resulting air temperature factors. By reducing the air-fuel ratio requirements, a significant reduction of the intake air temperature and boost pressure would occur, thereby further reducing heat rejection. Woods et al. (1992) reiterated that the future adiabatic engine should use reduced air-fuel ratios, be non after-cooled, and use turbo compounding to utilize the high level of available exhaust energy. Comprehensive combustion optimization was not completed. A single cylinder, non-aftercooled, fully insulated engine produced a 52% reduction in radiator heat rejection but no change in net fuel consumption. Combustion optimization

is hypothesized to significantly enhance the system fuel consumption of the fully non-aftercooled insulated engine and to further reduce heat rejection.

With the exception of Kadoli and Aknamurthy (1992) as discussed above, there was not a successful demonstration of a real low heat rejection system. The most sophisticated approach to date comes from Rakopoulos, Andritsakis, and Kyritsis (1992), who employed the second law of thermodynamics to analyze the LHRE. It is a significant tool for understanding the utilization of the fuel's ability to produce reversible work in the internal combustion engine. The irreversibility from combustion is defined by the subtraction of the system availability increase from the availability transferred into the combustion system. This energy is transferred by work, heat, and fuel flow input. Rakopoulos et al. proved that this subtraction leads to an expression connecting the rate of irreversibility production. This expression is applied in this work for the fuel preparation, reaction, and work and heat transfer rate. The irreversibility balance also provides important information for the combustion analysis that cannot be evaluated with a first law analysis.

From the analysis, it was evident that the sum of useful mechanical work per cycle plus the exhaust gas availability increases as the heat rejection decreases. Thus, the second law analysis showed that the limited heat rejection seems to have an advantage, especially when combined with recovery devices. This result is in full agreement with the results of Watson et al. (1983) that approached the problem with a first law analysis. Rakopoulos et al. (1992) also discussed how the irreversibility must increase as the engine speed increases.

Yoshimoto, Tsukahara, and Kuramoto (1996) discussed using water-emulsified fuel and oil cooling (replacing water/antifreeze mixtures) in engines. This technique reduced NO_x and smoke emissions. Additionally, these techniques lowered combustion temperature, promoted mixing of sprayed fuel with air, and enhanced water gas reactionthat resulted in improvements in the overall combustion process. Yoshimoto et al. discussed that there was little agreement that the improved fuel consumption with emulsified fuel operation was more likely the strong influence of operating conditions,

engine variables, injection characteristics, and emulsion properties. These researchers showed that cycling loss had a strong influence on fuel consumption or thermal efficiency. The cooling loss during the combustion process was determined from the gas pressure in the cylinder. The heat transferred out of the system to the cooling water through the entire cycle was measured by varying the outlet temperature of the cooling water. The indicated thermal efficiency was found to correspond directly to changes in the cooling loss. Lower cooling losses than with water-free gasoline and oil cooling were observed with the emulsified fuel due to the evaporating water and the combustion promotion. Therefore, it was established that the reduced cooling loss improved the indicated thermal efficiency. The cycle-to-cycle variation of maximum combustion pressure was the same as with water-free gasoline and oil cooling, regardless of load and injection timing conditions, when a fuel emulsion with water was used. The NO_x concentration was reduced by about 40%. Additionally, the specific fuel consumption was improved by 5% to 9% at rated output. It was confirmed that the emulsified fuel improved the degree of constant volume of combustion and reduced the cooling loss during combustion. Cooling loss and indicated thermal efficiency were shown to closely correlate (Yoshimoto, 1996).

Taymaz, Gur, and Halici (1998) discussed the effect of insulated heat transfer surfaces on direct injected and turbocharged engine fuel consumption and cooling systems. The results indicated a reduction in fuel consumption and heat losses to the engine cooling system of the ceramic-coated engine. The efficiency of the theoretical engine cycle depends directly upon the temperature difference between the hot and cold portions of the engine cycle. Therefore, there is an advantage in increased combustion chamber temperatures. If combustion gas energy can be contained through the expansion cycle, then the efficiency of internal combustion engines can also be increased. While several researchers have reported improvements in thermal efficiency with a LHR engine, others have noted that it declined. With compound techniques, up to 65% suppression of normal heat loss to the coolant is possible with air-gap wall systems or with very high-grade ceramics. Partially stabilized zirconium is a commonly used ceramic. The effect

of insulated heat transfer surfaces on direct injected and turbocharged engine fuel consumption and cooling system was again analyzed. A standard engine and ceramic-coated engine were examined at different engine speeds, loads, and injection timings. The results showed a reduction in fuel consumption and heat loss in the ceramic-coated engine. Application of ceramic coating provided a 5%-25% decrease in heat flow rate to the coolant.

From the timeline shown above there have been significant steps achieved in placing a ceramic coating on the inside surfaces of Diesel engines. While the process has come a long way in the past several years, it has not yet shown to be an economical proposition. Additionally, NASA has provided several research grants over the years to improve the ceramic coating processes. The improvement of a LHRE to date has most likely been disappointing. From a general concept, the LHRE with turbocharging is a logical improvement, but the performance gains have not been realized (Taymazet al., 1998).

2.7 Other Topics Relating to Diesel Engines and Heat Rejection

The last two articles presented in the literature search reveal an interesting trend in engine cooling research. Engine designers are investigating differing schemes of engine cooling to gain relatively small improvements in performance. The suspected reason would be the governmental regulation that is continually tightening.

Ap and Golm (1997) investigated an approach to engine cooling. The intent of this study was reduced cost of all engine-cooling components, reduced gasoline consumption, reduced weight of the engine cooling system, and improved thermal comfort in the passenger compartment. This basic concept consisted of adding a small electric water pump instead of the larger, conventional engine-driven water pump. This system ensured engine cooling at speeds up to 120 km/h under convective cooling in normal conditions. This condition fulfills 95% of the flow requirements of a vehicle at the same performance level as a conventional cooling system. The remaining 5% of the requirements--at vehicle speeds greater than 120 km/h and hill climbing--have been resolved by the use of nucleate boiling in the cylinder head. The nucleate boiling phenomenon has been discussed previously in the proposal and is consistent with this literature. Engine power and vehicle weight were trending upward, while at the same time the engine cooling specification remained unchanged (i.e., the validation tests of hill climbing 12% or 13% grade with and without trailer and the maximum speed at high outside ambient temperature). The physical parameters of the engine cooling system, such as coolant temperature and flow rate, had been increasing. Water pump power ranged from 1 to 2 kW depending on the engine size. Liquid circuit pressure has been increasing from 1.8 to 2.5 bars causing the cost to increase, particularly the hoses.

Reasonable engine cooling and thermal comfort performance were confirmed except for an over temperature of 10°C to 20°C on the cylinder head at full engine load. This problem was proposed solved by "simple geometric modifications of internal coolant passages of the cylinder head." Heater performance for the passenger compartment was improved during the idle and transient otherwise.

Kern, and Ambros (1997) proposed a new concept in engine cooling. The cooling system was designed based on critical operating conditions as mentioned above. For thermally uncritical partial-load conditions where a vehicle normally operates, thermal-management measures offer considerable potential for reducing the impact of the motor vehicle on the environment. Actuators in conjunction with intelligent control systems could be used to enhance the automobile impact on the environment and passengers. As part of its thermal-management strategy, Behr is developing new kinds of actuators, system configurations, and control algorithms that use demand-responsive control and supply of mass and heat flows. Operation mode-dependent control measures depended on the priority of the control objectives required. The intelligent system could adjust the configuration to reduce fuel consumption, pollutant emissions, the cold-start phase, thermal stress, and mechanical loads to be seen in vehicle components. A theoretical study showed a potential savings of up to 50% of the power demand of fan and coolant pump. Measurements on a truck showed savings of more than 1.8% of fuel consumption (Kern & Ambros, 1997).

CHAPTER III
METHODOLOGY

The general methodology utilizes the results of the ideal cycle models for both the naturally aspired spark ignition (SI) and turbocharged compression ignition (CI) engines. The background and ideal models of the cycles were not provided to obtain quantitative results, but to understand the physics governing the power cycle and to create a concise physics-based heat rejection analysis from actual engine data.

3.1 General Methodology to Approximate Engine Heat Rejection

The origins of the heat rejected to the coolant are the heat transfer between the combustion gases and the cylinder walls and the power dissipation due to rubbing friction between moving engine components,

$$\dot{Q}_{coolant} = \dot{Q}_{cyl} + P_{rf} . \tag{3.1}$$

Predictions of the heat transfer to the cylinder walls are obtained from a Nusselt number correlation, while estimates of the frictional power dissipation are based on the engine power and efficiency.

To quantify the heat transfer from the combustion gases, it is broken into contributions from convection and radiation heat transfer. For both SI and CI engines, convection is the dominant heat transfer mechanism. Convection is especially dominant for the spark ignition engine, where it is assumed that the radiation contribution is negligible. The generalized expression for the heat transfer is:

$$\dot{Q}_{cyl} = hA_{ref}\left(\overline{T}_g - T_c\right) + h_r A_{ref}\sigma\left(\overline{T}_f^4 - T_c^4\right) + P_{rf} . \tag{3.2}$$

In Equation 3.2, the convective heat transfer coefficient, h, is calculated from correlations of the form

$$Nu = f(Re) \tag{3.3}$$

or

$$\frac{h\ell_{ref}}{k_g} = f\left(\frac{\rho V_g \ell_{ref}}{\mu}\right). \tag{3.4}$$

Development of the correlation is based on experimental data from which the convective heat transfer coefficient and characteristic combustion gas velocity are obtained. The radiation heat transfer coefficient is assumed constant throughout the data reduction process for the CI engine.

The presentation of the method for predicting heat rejection to the coolant is broken into three components:

1. development of the engine power correlation from which the frictional power dissipation, air and fuel flow rates, and the corresponding combustion gas velocity are calculated,

2. development of the heat transfer correlations for estimating the rate of heat transfer between the combustion gases and the cylinder walls, and

3. application of the engine power and cylinder heat transfer correlations to calculate the net heat transfer to the coolant due to convection to the cylinder walls and energy dissipation resulting from friction between moving engine components. This application will be applied in the Results and Discussion chapter of this dissertation.

As discussed above, the first step in the derivation is to review the ideal model of the process as previously outlined in Chapter II. These guides provide insight to the underlying relationships and guide the reduction of the actual engine data.

The indicated power, P_i, is the engine power output based on the integral, $\oint P dV$, for the compression and expansion strokes in a single cylinder, the number of cylinders, and the rate of work producing cycles (half of the engine speed for four-cycle engines). The indicated engine power output is reflected in two components: the brake power output from the engine, and the friction power dissipation,

$$P_i = P_b + P_f . \tag{3.5}$$

Following Heywood (1988), the friction power is defined to include rubbing friction between moving engine components, pumping work during the intake and exhaust strokes, and the accessory power requirements.

The efficiency of the engine in converting the energy available through fuel combustion into indicated power is defined as the fuel conversion efficiency,

$$\eta_f = \frac{P_i}{\dot{m}_f Q_H} . \tag{3.6}$$

The fuel flow rate is expressed in terms of the airflow rate and the air-to-fuel mixture ratio,

$$\dot{m}_f = \frac{\dot{m}_a}{A/F} . \tag{3.7}$$

The air induction rate for a particular engine is determined by the engine displacement, engine speed, and the fixed and variable elements of the air intake system. Specifically, the fixed elements include the air filter, carburetor body, intake manifold, and the intake ports and valves. The SI engine has an additional principle variable element--the throttle plate. The air induction rate is quantified in terms of the volumetric efficiency, which is the ratio of the airflow rate to the engine volume displacement rate,

$$\eta_V = \frac{\dot{m}_a}{\rho_a \, n/2 \, V_D}. \tag{3.8}$$

The volumetric efficiency is a non-dimensional expression of the mass flow rate through the engine and is directly dependent on throttle position. For normally aspirated engines, the volumetric efficiency typically varies between approximately 0.25 with the throttle closed and 0.85 with the throttle wide open. For turbocharged engines the volumetric efficiency is typically between 0.8 and 3.0.

Combining Equations 3.7 and 3.8 and substituting into Equation 3.5 yields

$$\eta_V \eta_f \, n/2 \, V_D \frac{\rho_a Q_{LH}}{A/F} = P_b + P_f. \tag{3.9}$$

Rearranging and dividing through by the volume displacement rate results in

$$\frac{P_b}{V_D \, n/2} = \eta_V \eta_f \frac{\rho_a Q_{LH}}{A/F} - \frac{P_f}{V_D \, n/2} \tag{3.10}$$

or

$$bmep = \eta_V \eta_f \frac{\rho_a Q_{LH}}{A/F} - fmep, \tag{3.11}$$

where

$$bmep = \frac{P_b}{V_D \, n/2} = \text{brake mean effective pressure,} \tag{3.12}$$

$$fmep = \frac{P_f}{V_D \, n/2} = \text{friction mean effective pressure.} \tag{3.13}$$

Dividing the brake and friction power by the volume displacement rate has the effect of normalizing the influences of engine speed and displacement. The resulting ratios have the units of pressure, which is the basis for the term "mean effective pressure." The indicated mean effective pressure is, by definition, the brake mean effective pressure plus the friction mean effective pressure.

The operation of normally aspired SI engines and turbocharged CI engines is fundamentally different. In SI engines, the fuel is injected with the cylinder charge either at the throttle body or near the cylinder intake ports. Due to emission and ignition knock limitations, the air-fuel ratio is held approximately constant at the ideal stoichiometric ratio. In CI engines, the fuel injection occurs directly into the cylinder at approximately the end of the compression stroke. With the higher compression ratios and cylinder charge temperatures of CI engines, the fuel immediately combusts. Throttling of CI engines is accomplished by regulating the injected fuel flow, thereby changing the air-fuel ratio. In contrast to SI engines, the air-fuel ratio varies widely with values between 15 and 65.

From Chapter II, the fundamental expression defined was the indicated mean effective pressure as a function of the available mean effective pressure. Equation 2.30 is repeated here for clarity:

$$imep = \frac{P_{net}}{\frac{n}{2}V_d} = \eta_f \eta_v \frac{\rho_a Q_{LH}}{A/F}$$

By examination of this equation, the only variable from the SI engine operation that is not constant is the volumetric efficiency. Compared to the CI engine operation, two parameters are not constant. Those two parameters are the volumetric efficiency, like the SI engine, and the air-fuel ratio.

3.2 Naturally Aspired Spark Ignition Engine Power Methology

For the spark ignition engine, the fuel conversion efficiency is functionally dependent on the air-fuel ratio. Experimental data presented by Edson and Taylor (1964) suggests that for slightly rich mixtures the relationship is linear such that

$$\eta_f = \eta_f^* \frac{A/F}{A/F^*}, \tag{3.14}$$

where A/F^* is the ideal stoichiometric value of 14.6, and η_f^* is the corresponding fuel conversion efficiency. Substitution of Equation 3.14 into Equation 3.11 yields the final expression for *bmep*,

$$bmep = \eta_v \eta_f^* \frac{\rho Q_{LH}}{A/F^*} - fmep\,. \tag{3.15}$$

A plot of the brake mean effective pressure versus the available mean effective pressure for the entire data sets from the eleven normally aspired SI engines is shown in Figure 3.1. A legend for this figure, indicating the plot symbols used for each engine, is presented in Table 3.1.

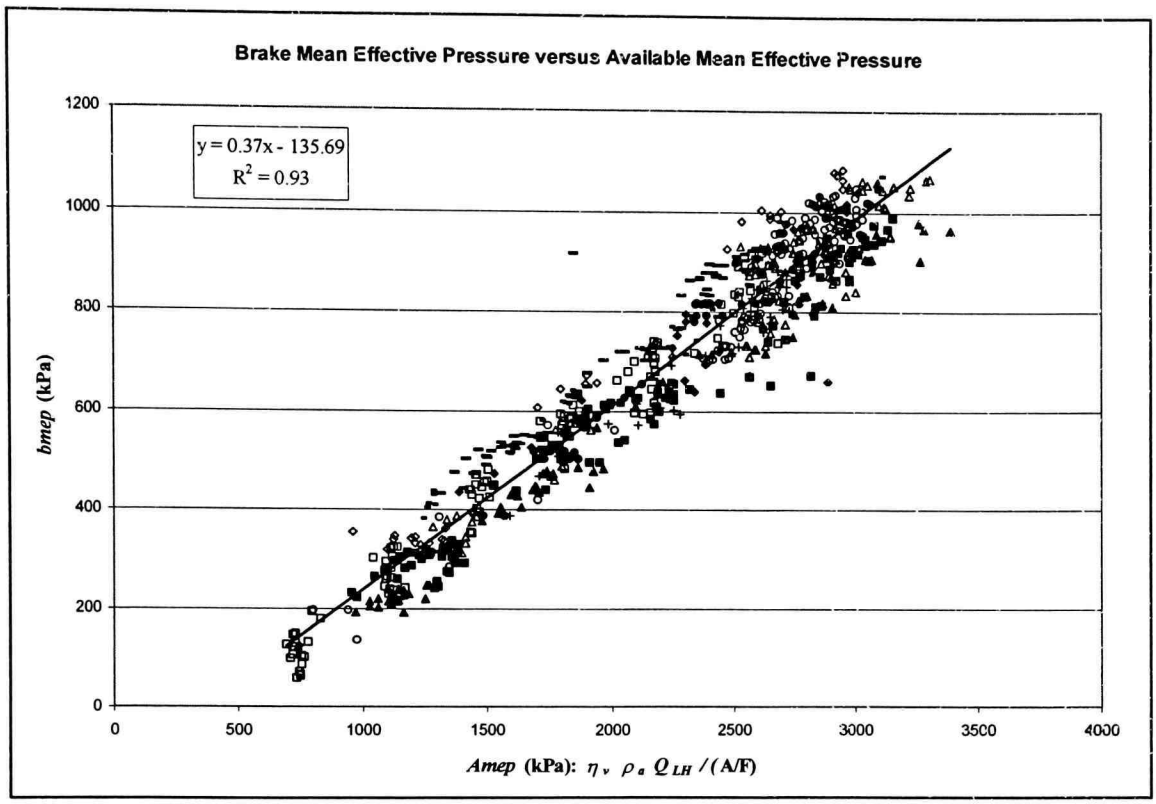

Figure 3.1 Brake Mean Effective Pressure versus Available Mean Effective Pressure for SI Engines.

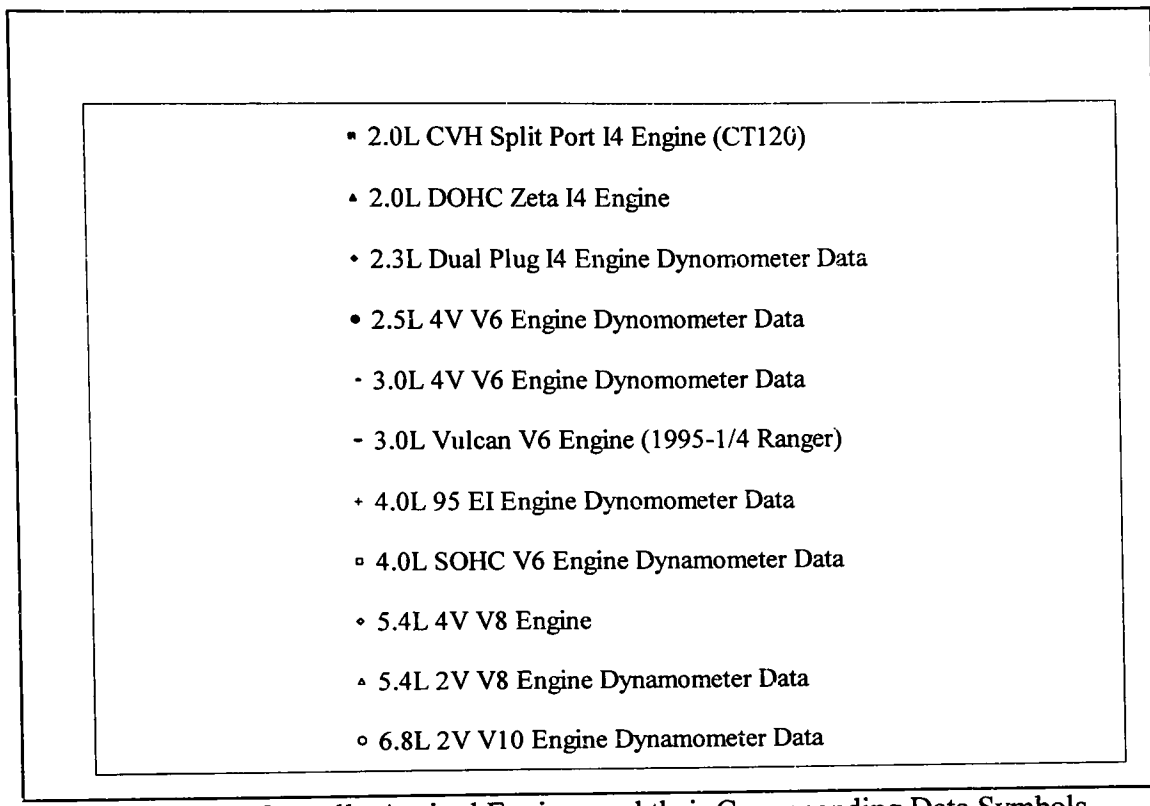

Table 3.1 Eleven Naturally Aspired Engines and their Corresponding Data Symbols.

From the figure, it is noted that the relationship between *bmep* and *Amep* is reasonably consistent and, as expected, may be approximated with a linear least squares curve fit. Based on Equations 3.16 and 3.17 the slope and intercept from the curve fit may be equated to the fuel conversion efficiency and friction mean effective pressure, respectively,

$$\eta_f^* = 37\% \tag{3.16}$$

and

$$fmep = 136\,(\text{kPa})\,. \tag{3.17}$$

The *Amep* calculated from the experimental engine data utilized the stoichiometric air-fuel rather than the actual experimental value. Consequently, the fuel conversion efficiency obtained from the curve fit is a stoichiometric value. The actual values of fuel conversion efficiency at the respective experimental air-fuel ratios varied between 28% and 40%. As shown in Figure 3.1, there is a high coefficient of determination of 0.93. Recalling that

$$imep = bmep + fmep, \tag{3.18}$$

the actual engine data is very similar to the ideal SI engine model shown in Figure 2.4.

When the process is reversed in the Results and Discussion chapter, Equation 3.15 can be rearranged and combined with Equation 3.16 and 3.17 to yield the volumetric efficiency

$$\eta_V = \frac{A/F^*(bmep + 136)}{0.37\rho_a Q_{LH}}.$$

In application to the heat transfer predictions, the engine speed and power are specified from knowledge of the road load, and power train ratios and efficiencies. This allows direct calculation of the *bmep*. With the *bmep* known, Equation 3.19 can be used to calculate the volumetric efficiency and, thereby, the air mass flow rate through the engine, which is the desired result of the engine power correlation for SI engines. This flow rate is applied to the heat transfer correlation to determine a characteristic Reynolds number for flow through the cylinder

3.3 Naturally Aspired Spark Ignition Engine Heat Transfer Methodology

The convective heat transfer to the cylinder walls is characterized in terms of a convective heat transfer coefficient,

$$h = \frac{\dot{q}_{cyl}}{\left(\overline{T}_g - T_w\right)}, \tag{3.20}$$

where

$$\dot{q}_{cyl} \propto \frac{4\dot{Q}_{cyl}}{N_c \pi B^2} = \text{cylinder heat flux,} \tag{3.21}$$

$$B \propto \left[\frac{4V_D}{\pi N_c}\right]^{1/3} = \text{cylinder bore.} \tag{3.22}$$

Assuming a cycle-averaged combustion gas temperature, $\overline{T}_g$, of 447°C (Heywood, 1988) and wall temperature, T_w, of 110°C based on constant coolant temperature results in a temperature differential, $\left(\overline{T}_g - T_w\right)$, of 337°C. This temperature differential of 337°C has been used for all SI engine experimental data reduction in the current investigation.

Direct measurements of the cylinder heat transfer rate, $\dot{Q}_{cyl}$, are difficult to accomplish and are not generally available. Instead, the cylinder heat transfer rate must be deduced from the overall heat rejection to the coolant, which also includes the effect of rubbing friction,

$$\dot{Q}_{cyl} = \dot{Q}_{coolant} - P_{rf}\,. \tag{3.23}$$

The friction power dissipation, P_f, and the corresponding friction mean effective pressure, *fmep*, include contributions associated with rubbing friction between moving components, pumping work during the intake and exhaust strokes, and accessory power requirements,

$$fmep = rfmep + pmep + amep\,. \tag{3.24}$$

For analysis of experimental engine heat rejection data, the fraction of the friction power dissipation due to rubbing friction is taken as a constant,

$$\frac{rfmep}{fmep} = 0.6\,. \tag{3.25}$$

Recall that the friction mean effective pressure was determined as part of the power correlation of the previous section. The value is consistent with recommendations from the literature and is chosen to yield the best collapse of the experimental data. It should be noted that the rubbing friction is a relatively small contribution to the total heat rejected to the coolant. Consequently, the overall accuracy of the heat transfer correlation is relatively insensitive to the choice for the *rfmep/fmep* ratio.

With Equation 3.25, the cylinder heat transfer rate may be found from experimental heat rejection to coolant data using

$$\dot{Q}_{cyl} = \dot{Q}_{coolant} - 0.6\,fmep\,V_D\,n/2 \tag{3.26}$$

and, with application of Equation 3.20, the corresponding convection heat transfer coefficients can be determined.

Variations of the convective heat transfer coefficient are correlated in terms of a general Nusselt number versus Reynolds number relationship. The Nusselt number is defined as

$$Nu = \frac{hB}{k_g}, \tag{3.27}$$

and for application to an engine, the Reynolds number is defined as

$$Re = \frac{\rho V_g B}{\mu}. \tag{3.28}$$

The characteristic gas velocity is

$$V_g \propto \frac{4\dot{m}}{\rho\pi B^2 N_c}, \tag{3.29}$$

giving

$$Re = \frac{4\dot{m}}{\pi B N_c \mu}.$$

For Equation 3.30, the mass flow rate is found from

$$\dot{m} = \dot{m}_a + \dot{m}_f = \dot{m}_a\left(1 + \frac{1}{A/F}\right). \tag{3.31}$$

With Equations 3.27 and 3.28, the Nusselt number versus Reynolds number can be determined from the data for eleven normally aspired SI engines and are presented in Figure 3.2.

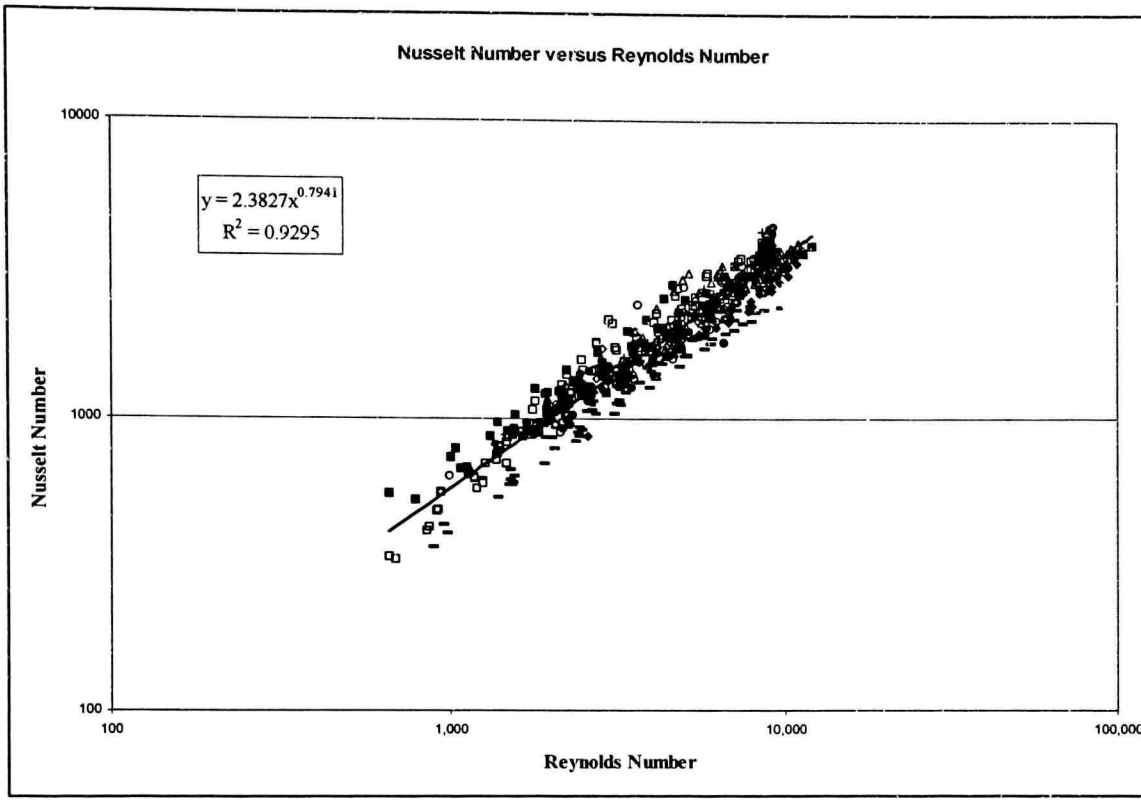

Figure 3.2 Nusselt Number versus Reynolds Numbers for Eleven Normally Aspirated SI Engines.

These data are well correlated by

$$Nu = 2.38\, Re^{0.794}\,. \tag{3.33}$$

These data follow the conventional form of a power law relation with a high coefficient of determination, 0.93.

The power and heat transfer correlations can be applied to predict the heat rejection from an arbitrary SI engine by applying the following procedure.

Specification of the engine speed and brake power requirement, with Equation 3.19 allows calculation of the volumetric efficiency and corresponding mass flow rate.

With mass flow rate determined, a corresponding Reynolds number is obtained from Equation 3.30.

Equation 3.33 is applied to determine the Nusselt number and Equation 3.27 is used to calculate the corresponding heat transfer coefficient.

The rate of convected heat transfer from the cylinder walls and to the coolant is obtained from Equation 3.20.

The additional heat to the coolant from rubbing friction is calculated as prescribed by Equation 3.25.

3.4 Turbocharged Compression Ignition Engine Power Correlation

As previously discussed, there are two additional complications in the analysis to the turbocharged CI engine heat rejection. These differences are the stronger presence of the radiation heat transfer mode and the coupled variations in air flow and air-fuel ratio that are dependent on the turbocharger operation. For convenience, Equation 3.15 and the definition of available mean effective pressure are restated as

$$bmep = \eta_f Amep = \eta_f \eta_V \frac{\rho Q_{LH}}{A/F} - fmep \,.$$

This relation is used to compare the experiment data for the CI engines. The results are presented in Figure 3.3 showing the brake mean effective pressure versus the available mean effective pressure with the resulting linear regression.

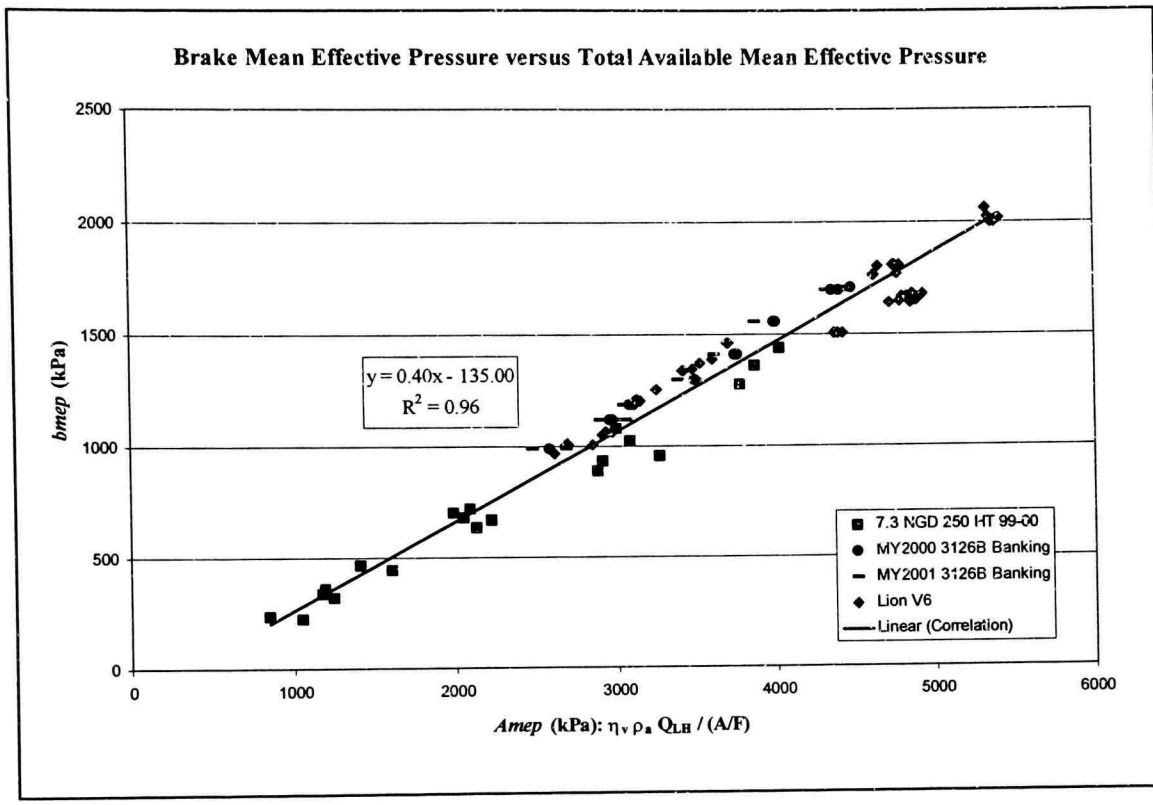

Figure 3.3 Brake Mean Effective Pressure versus Available Mean Effective Pressure for Turbocharged CI Engines.

The slope of the line again directly determines the fuel conversion efficiency and the intercept determines the friction mean effective pressure.

$$\eta_f = 40\% \tag{3.34}$$

$$fmep = 135 \text{ (kPa)}. \tag{3.35}$$

The coefficient of determination is very strong at 0.96. Figure 3.3 was anticipated from the ideal model predictions shown in Figure 2.13.

All of the turbocharged CI engines analyzed were run very lean. Air-fuel ratios as high as 55, compared to the stoichiometric value of 14.5, where typical. The lean operation of the CI engine dictates that the fuel conversion efficiency is essentially

constant. For the turbocharged CI engines, the fuel conversion efficiency is constant at 40%. In comparison, SI engines have a constant stoichiometric fuel conversion efficiency of 37%, but the actual fuel conversion efficiency ranged from 28% to 40% depending on how rich to lean, respectively.

In the experimental data, the airflow rate and air-fuel ratio are known. However, the underlying relationship between the volumetric efficiency and A/F ratio must be determined. From the ideal turbocharged CI model, the volumetric efficiency is determined by the interaction with the turbocharger. The turbocharger pressure ratio or corresponding rate of energy supplied to the induction airflow is, in turn, dependent on the inlet conditions to the turbine and turbine power extraction. The general approach to handle the coupling between the engine and turbocharger will be to correlate the turbocharger pressure ratio to the available mean effective pressure. The volumetric efficiency can then be correlated to the turbocharger pressure ratio. With the volumetric efficiency known, the heat transfer correlation will then be developed.

A plot of volumetric efficiency versus turbocharger pressure ratio for the four collections of CI engine data is presented in Figure 3.4. As expected, this data is well correlated by a linear curve fit.

$$\eta_v = 0.8031\, P_r \tag{3.36}$$

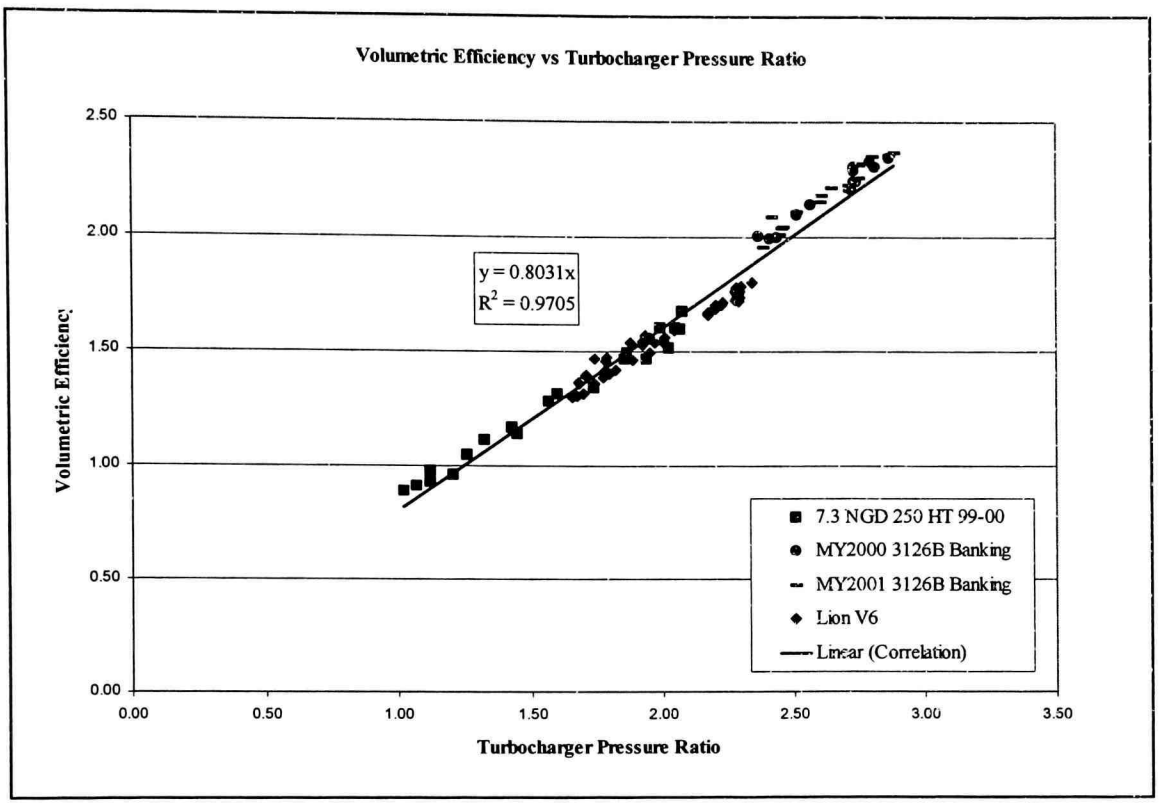

Figure 3.4 Turbocharger Pressure Ratio versus Volumetric Efficiency for CI Engines.

Figure 3.5 contains a plot of turbocharger pressure ratio versus available mean effective pressure for the four collections of turbocharged CI engine data. From the ideal CI engine analysis, it is expected that this data may be well correlated by a relation of the form

$$P_r = 1 + C\ Amep \tag{3.37}$$

From the figure, it is noted that data from the 7.3 L NGD and Lion V6 engines are reasonably consistent and may be represented by

$$P_r = 1 + 0.25\left[\frac{1}{MPa}\right] Amep \tag{3.38}$$

The 3126 B Engine, however, does not exhibit the expected linear variation as all data points were obtained near the wastegate limited maximum pressure ratio of approximately 2.5. It is presumed that data taken at lower *Amep* values would yield lower pressure ratios that would follow the expected linear relationship with a significantly higher slope than that noted for the 7.3 NGD and Lion V6 engines.

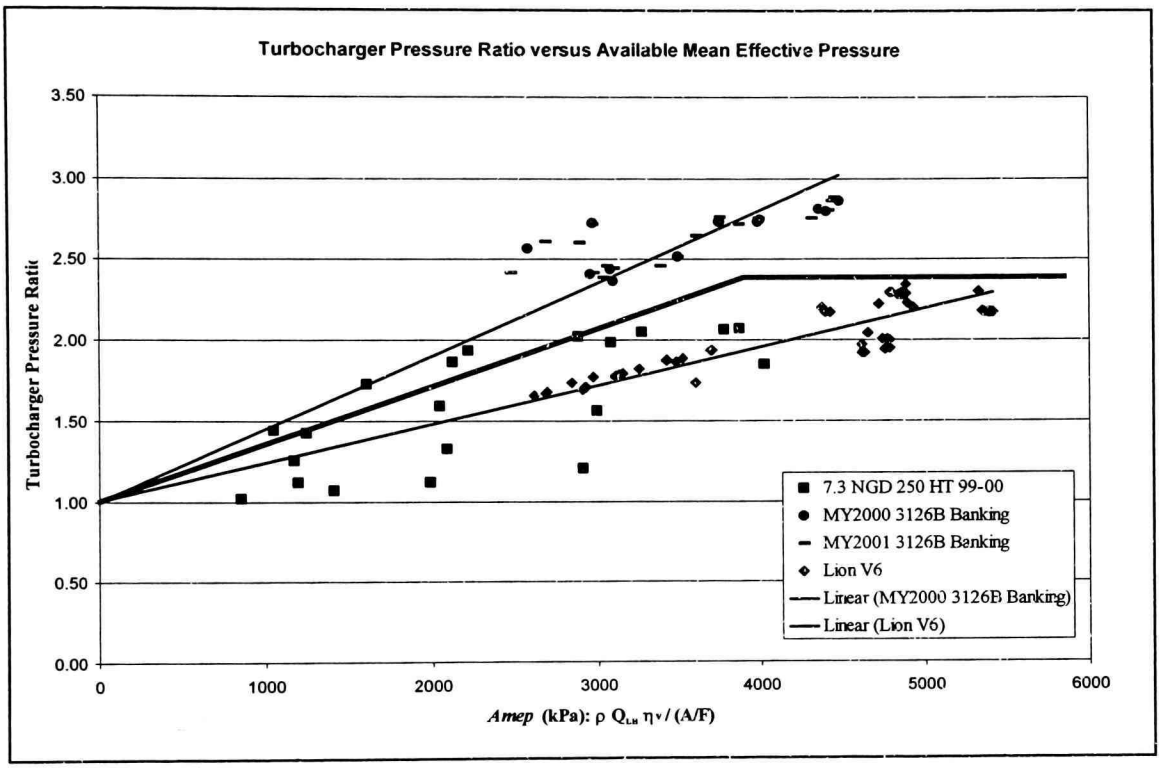

Figure 3.5 Turbocharger Pressure Ratio versus Available Mean Effective Pressure for CI Engines.

The difference between the pressure ratio characteristics of the 3126 B engine data and the 7.3 NGD and Lion V6 engine data are a consequence of the matching of the engines with turbochargers for their expected applications. With additional specifications for the engines and the turbochargers, this dependency could be incorporated into the overall heat rejection model for turbocharged CI engines. However, it is a major objective for the current investigation to limit the engine specific data for use in the heat rejection model to simplify the engine displacement and number of cylinders. The

motivation for this objective is additional engine data is often simply not available early in a vehicle design cycle.

With this limitation in mind, it was determined that a satisfactory representation of the pressure ratio versus available mean effective pressure relationship for all four engines is

$$P_r = \begin{cases} 1 + 0.35\left[\dfrac{1}{\text{MPa}}\right] Amep & Amep < 4.0 \text{ MPa} \\ 2.4 & Amep \geq 4.0 \text{ MPa} \end{cases} \tag{3.39}$$

3.5 Turbocharged Compression Ignition Engine Heat Transfer Methodology

The heat transferred to the coolant for a turbocharged CI engine can be determined by

$$\dot{Q}_{cool} = \dot{Q}_{conv} + \dot{Q}_{rad} + P_{rf} . \tag{3.40}$$

Using standard correlations for the convection and radiation heat transfer, Equation 3.40 can be expanded to yield

$$\dot{Q}_{cool} = hA_B\left(\overline{T}_g - T_w\right) + h_r \sigma A_B(\overline{T}_f^4 - T_w^4) + P_{rf} ,$$

as was indicated for the SI engine correlation, the heat transfer reference area is defined to be the cylinder area

$$A_B = \frac{\pi B^2}{4} , \tag{3.42}$$

and

$$B \propto \left[\frac{4V_D}{\pi N_c}\right]^{1/3} = \text{cylinder bore.}$$

From the data analysis, it became evident that the normalized form of Equation 3.41 provided a better analysis of the heat transfer to the coolant for the CI engine. This normalized form is shown in Equation 3.44:

$$q_c mep = \frac{hA_B}{V_D n/2}\left(\overline{T}_g - T_w\right) + \frac{h_r \sigma A_B}{V_D n/2}\left(\overline{T}_f^4 - T_w^4\right) + rfmep. \tag{3.44}$$

For SI engines, the air-fuel ratio is approximately constant so that a constant cycle averaged temperature and corresponding combustion gas properties could be assumed. For the CI engines, wide variations of lean air-fuel ratios and gas temperatures are expected and must be incorporated in the heat rejection model. The cycle-averaged temperature for the turbocharged engines will be approximated as the average temperature between the wall and potential heat release of the fuel:

$$\overline{T}_g = \frac{\Delta T_c}{2} + T_w. \tag{3.45}$$

The change in combustion temperature due to the potential heat released from combustion found in Equation 3.46 is calculated by:

$$\Delta T_c = \frac{Q_{LH}}{\dot{m} C_P}.$$

The specific heat of the combusted gas can be calculated from an approximation from data found in Heywood, 1988.

$$C_{p,g} = 1 + 1.42x10^{-4}T + 2.47x10^{-4}\phi T$$

As was done for the SI engines, the coolant and wall temperatures are assumed constant at 110°C.

Where the convection heat transfer is proportional to the difference in the gas and wall temperatures, the radiation heat transfer is expected to be proportional to the difference in the temperatures raised to the fourth power. Consequently, a simple average of the expected minimum and maximum temperatures is not appropriate for radiation heat transfer calculations. Applying the simple average temperature to the correlations was found to yield radiant emissivity time view factor greater than one. This result is clearly unrealistic and dictates that the gas temperature has been underestimated.

A more appropriate choice for a cycle averaged gas temperature for the radiation heat transfer correlation is

$$\overline{T}_f = \Delta T_c + 288.16 \tag{3.48}$$

The choices for average gas temperatures in the convection and radiation heat transfer calculation is essentially arbitrary. The expressions given by Equations 3.45 and 3.48 can be expected to yield temperature estimates that are at least proportional to the actual temperatures over the expected range of air-fuel ratios. Any discrepancy that results from the temperature approximations will be folded into the correlation coefficients and will not cause a problem so long as the temperatures used in the heat transfer predictions are obtained in the same way. Furthermore, the temperature approximations that have been chosen yield intuitive satisfactory values for the convection and radiative heat transfer coefficients.

The convective heat transfer coefficient is correlated in terms of a general Nusselt number versus Reynolds number relationship. The Nusselt number is defined as

$$Nu = \frac{hB}{k_g} = a\mathrm{Re}^b\ \mathrm{Pr}^{0.3} \tag{3.49}$$

where

$$Re = \frac{\rho V_g B}{\mu} \tag{3.50}$$

and

$$\mathrm{Pr} = \frac{\mu C_p}{k_g}. \tag{3.51}$$

For the turbocharged CI engines, the thermal conductivity of the gas is not constant due to variations of the air-fuel ratio, and thus the cycle averaged temperature. Equation 3.52 approximates Combusted gas thermal conductivity:

$$k_g = 8.82e^{-4}\overline{T}_g^{0.75} \quad \left(\frac{W}{mK}\right). \tag{3.52}$$

Equation 3.52 is derived from extrapolated thermal conductivity information found in Heywood (1988).

The gas viscosity variation with cycle averaged temperature is taken as

$$\mu_g = \frac{3.3e^{-7}\overline{T}_g^{0.7}}{1+0.027\phi}, \tag{3.53}$$

where ϕ is the fuel equivalence ratio

$$\phi = \left(\frac{A/F}{(A/F)^*}\right)^{-1}. \tag{3.54}$$

The characteristic gas velocity is

$$V_g \propto \frac{4\dot{m}}{\rho\pi B^2 N_c}, \tag{3.55}$$

giving

$$Re = \frac{4\dot{m}}{\pi B N_c \mu_g}. \tag{3.56}$$

The air mass flow rate for Equation 3.57 is found from

$$\dot{m} = \dot{m}_a + \dot{m}_f = \dot{m}_a\left(1 + \frac{1}{A/F}\right),$$

thus completing the required variables for the convection heat transfer. Radiation from the gas to the walls must now be outlined.

Heywood (1988) detailed that *fmep* can be approximated as follows:

$$fmep = C_1 + C_2\frac{n}{120} + C_3\left(\frac{n}{120}\right)^2, \tag{3.58}$$

where, C_1 term represents the boundary loss, C_2 term represents the hydrodynamic or rubbing loss, and C_3 term is the turbulent loss. Therefore, the hydrodynamic term was used to determine the *rfmep* through the coefficient C_2. This approach is different from the approach used on the SI engine. The rfmep is determined from the heat transfer correlation instead of the power correlation.

A multiple linear regression of Equation 3.44 can be analyzed to determine the heat transfer coefficients. No plots are available due to the multivariable output requirements. From the regression, the heat transfer coefficients and rubbing friction coefficient were determined:

$$h = 2.495\,\mathrm{Re}^{0.7}\,\mathrm{Pr}^{0.3},$$

$$h_r = 0.341,$$

$$C_2 = 5.98\,\frac{s}{kPa}, \tag{3.59}$$

or

$$q_c mep = \frac{2.50\,k_g\,\mathrm{Re}^{0.7}\,\mathrm{Pr}^{0.3}\,\pi B}{4V_D\,n/2}\left(\overline{T}_g - T_w\right) + \frac{0.3410\sigma\pi B^2}{4V_D\,n/2}\left(\overline{T}_f^4 - T_w^4\right) + 5.98\left[\frac{s}{kPa}\right]\frac{n}{2}. \tag{3.60}$$

The coefficient of determination was 0.97, yielding evidence of a satisfactory correlation. Additionally, the radiation contributed between 2% to 30%.

These correlations can be applied to predict the heat rejection from an arbitrary CI engine by applying the following procedure.

Given brake power and engine speed, calculate *bmep*.

The *bmep* and Equation 3.15 are used to find the *Amep*.

The *Amep* and Equation 3.39 are used to find the turbocharger pressure ratio that with Equation 3.36 yields the volumetric efficiency.

The volumetric efficiency and *Amep* are combined to find the air-fuel ratio.

The air-fuel ratio and volumetric efficiency yield the fuel and airflow rates and allows calculation of the cycle averaged temperatures and gas properties.

Reynolds number and Prandtl number can be calculated and used to obtain Nusselt number and corresponding convection heat transfer coefficient.

Equation 3.60 is used to obtain the heat transferred to the coolant.

This completes the process to determine the heat rejection to the coolant for the CI engine. Applying the correlation data back to the original dataset is discussed in the

Results and Discussion section of the dissertation. The results are used to help quantify the success of the correlation.

CHAPTER IV
RESULTS AND DISCUSSION

Correlations have been developed for the naturally aspired SI engines and turbocharged CI engines. The new correlations will be applied to the original sets of engines to determine the accuracy of the method. The scope of this investigation is to determine the heat rejection based on minimal initial data. The input parameter requirements for the heat rejection calculations are the engine speed, brake power requirement, engine displacement, and number of cylinders. With the engine power correlation and the cylinder heat transfer correlation known, the heat rejection to the coolant may be predicted for any arbitrary combination of normally aspirated gasoline or turbocharged Diesel engine, power requirement, and engine speed.

The experimental data used in the development of this analytical method represent eleven different naturally aspirated gasoline engines ranging from 2.0 liters to 6.8 liters in displacement, and three different turbocharged Diesel engines ranging from 2.7 liters to 7.3 liters. This sample of engines covers a very broad spectrum of vehicle applications, ranging from small economy cars to commercial trucks. In addition, the experimental data covers a wide range of engine geometries, ranging from inline four cylinder engines to ten cylinder engines in a "V" configuration. Both two and four valve per cylinder designs is included.

It is important to note that, although all of the heat rejection data used in this experiment was obtained using the same overall method of measurement, this data was not gathered expressly for use in developing this analytical method. On the contrary, this analytical method was developed from existing data as a potential means of reducing the reliance of vehicle design upon experimental data, particularly early in the design of a new vehicle when experimental data may be unavailable. The experimental data used here originally was gathered for use in the design of cooling systems for a variety of vehicles. The experimental data, therefore, represents a wide range of engine calibration strategies. Although this is not an ideal scenario for the development of an analytical

tool, recreating the amount of data used in this study with consistent engine calibration strategies would require such a tremendous investment of time and money as to make the project impractical.

The analytical method presented here produces predictions that, in general, correlate well with measured experimental data. There are, however, some discrepancies between the predicted heat rejection to coolant and the heat to coolant measured experimentally. This fact is not surprising, given that the analytical method uses several approximations and assumptions in its derivation. Many factors may account for the discrepancies between the predicted engine heat rejection and that measured experimentally.

Heat transfer is dependent upon temperature differential, and thus heat rejection to coolant is dependent upon the difference between the temperature of the hot engine cylinder liner and the coolant. The heat rejection to coolant predicted using the analytical method assumes a constant coolant inlet temperature of 110° C. On the other hand, a variety of different coolant inlet temperatures was used in the development of the experimental heat rejection data. No single coolant inlet temperature is applicable to all of the experimental data. The resulting differences between assumed and actual coolant inlet temperature will account for some of the disparities between the predicted and measured heat rejection to coolant.

Accurate prediction of engine heat rejection depends upon accurate prediction of engine friction, as the heat generated by rubbing friction is a significant contributor to heat rejection to coolant. The relationship given in the new correlations was used in conjunction with the experimental data to derive an *fmep* of 136 kPa for the SI engines. In reality, *fmep* varies significantly with engine speed. In a typical four-cylinder engine, for example, it is typical for *fmep* to vary from approximately 100 kPa at low engine speeds to 300 kPa at very high speeds; this variation is not linear (Patton, 1989; Thring, 1992. The value of 135 kPa, therefore, represents a best-fit value of *fmep* for all of the experimental data and not necessarily a precise prediction of *fmep* at any particular engine operating condition.

Comparison of the analytically predicted value of *fmep* to measurements found in the literature (Patton, Nitschke, & Heywood, 1989; Thring, 1992) indicates that the *fmep* assumed in the analytical heat rejection predictions is probably smaller than the actual *fmep* at moderate to high engine speeds. If this is the case, at high engine speeds the analytical model is under-predicting the contribution of rubbing friction to the total amount of engine heat rejection to coolant. The effect of this under-prediction would be most significant at part-throttle operation at high engine speeds. At part-throttle operation, the amount of heat rejection from the hot combustion gases is lower than at full-throttle operation, yet the amount of heat rejection from rubbing friction is effectively the same as at full-throttle operation since rubbing friction is primarily a function of engine rotational speed. Thus, the contribution of rubbing friction to overall engine heat rejection is greater at part-throttle operation. Any negative effects due to under-predicting the rubbing friction would therefore be most apparent at part-throttle operation at high engine speeds. For the turbocharged compression ignition heat rejection correlation, the variable rubbing friction was included.

This behavior seems to support the theory that the analytical model under-estimates the contribution due to rubbing friction at moderate to high engine speeds for the SI engine series. Analytical methods do exist for predicting engine *fmep* due to rubbing components (Patton et al., 1989; Thring, 1992), although these methods are somewhat complex. It is possible that, as a future improvement, one of these methods to derive *fmep* could enhance the analytical method. It is possible, however, that the inclusion of one of these methods could introduce a level of complexity into the analytical method far exceeding the intended scope of the analytical method (Oler, 2002).

4.1 Naturally Aspired Spark Ignition Engine Results and Discussion

For the SI engine, the only limitation on the calculation is that the power specification be within the capabilities of the given engine. Testing for this limitation is easily incorporated into the calculations, as described below.

The first step in the calculation is the application of the engine power correlation to determine the mass flow rate through the engine,

$$bmep = \frac{P_b}{V_D n/2} = \eta_v \eta_f \frac{\rho_a Q_{LH}}{A/F} - fmep. \tag{4.1}$$

The general SI engine power correlation is rearranged to obtain the corresponding volumetric efficiency:

$$\eta_V = (bmep + 135)\frac{A/F^*}{0.373 \rho Q_{LH}}. \tag{4.2}$$

As previously stated, the volumetric efficiency is a non-dimensional expression of the mass flow rate through the engine. It is also a direct indication of the throttle position, with a volumetric efficiency of approximately 0.25 at the throttle closed or idle position and 0.85 at wide-open throttle. An engine speed and power requirement leading to a *bmep* and corresponding volumetric efficiency significantly outside of that range is not within the capabilities of the specified engine, and a meaningful heat rejection calculation cannot be accomplished.

With the volumetric efficiency known, the heat transfer correlation may be evaluated. This begins by rearranging Equation 3.30 and substituting in Equation 3.31; thus, calculating the cylinder Reynolds number,

$$\mathrm{Re} = 2\frac{\rho n V_D}{\pi B \mu}\eta_V\left(1 + \frac{1}{A/F^*}\right). \tag{4.3}$$

The Reynolds number is applied to find the Nusselt number and the corresponding convection heat transfer coefficient,

$$Nu = 2.38\,\mathrm{Re}^{0.794}, \tag{4.4}$$

and

$$h = \frac{k_g Nu}{B}. \tag{4.5}$$

The cylinder heat rejection is obtained from

$$\dot{Q}_{cyl} = N_c \frac{\pi B^2}{4} h\left(\overline{T}_g - T_c\right). \tag{4.6}$$

The total heat rejection to the coolant is the combination of the cylinder heat transfer and the rubbing friction energy dissipation,

$$\dot{Q}_{coolant} = \dot{Q}_{cyl} + P_{rf}. \tag{4.7}$$

The additional heat rejection associated with the rubbing friction energy dissipation is obtained as a fraction of the overall friction power,

$$P_{rf} = 0.6 fmep V_D \frac{n}{2}. \tag{4.8}$$

Although heat transfer from the engine block is partially accomplished through convection to the surrounding air, radiation to the engine bay, and conduction through engine attachments, the heat transfer rates associated with these mechanisms should be small relative to the heat transfer rate to the coolant.

The heat rejection maps for the eleven SI engines are presented in Figures 4.1 through 4.11. The envelope represents the heat rejection predictions bounded by speeds of 1000 rpm and 6000 rpm and volumetric efficiencies of 0.2 and 0.85. Note that individual engines are keyed per Table 3.1. The overall envelope and corresponding test data points are shown in Figure 4.12.

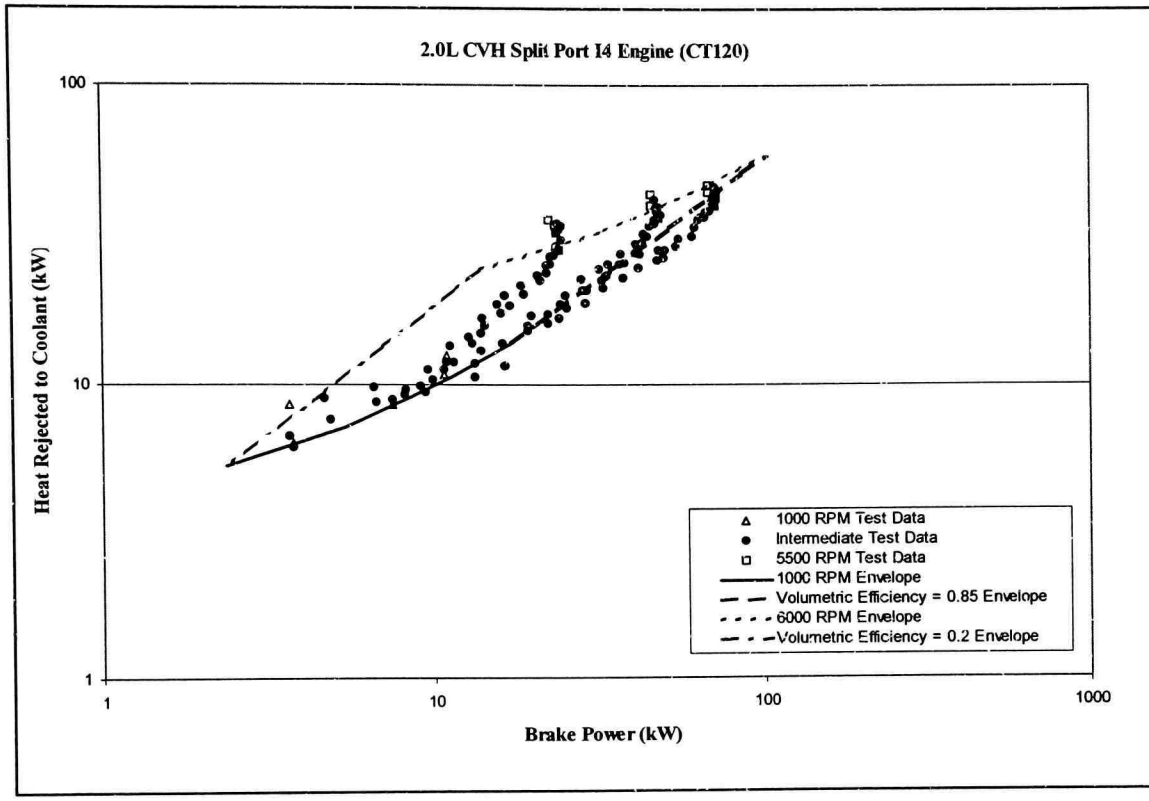

Figure 4.1 2.0L I4 SI Engine Heat Rejection Map.

Figure 4.1 provides the first opportunity to reiterate that the engine tests from which the data were collected were not designed to yield data covering the entire operating envelope of each engine. On the contrary, these tests were run for varying reasons ranging from heat rejection to spark timing evaluation. Therefore, complete datasets over the operating envelope were not available or required to successfully complete the test goals.

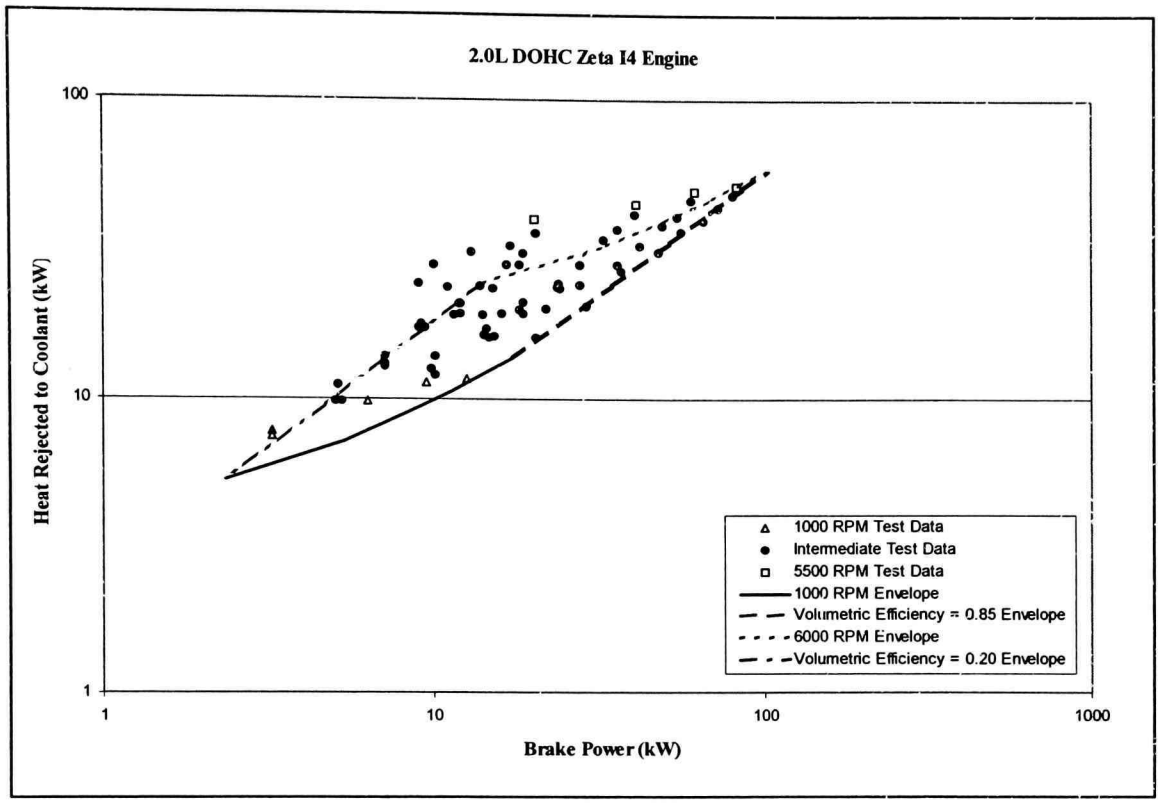

Figure 4.2 2.0L I4 Zeta SI Engine Heat Rejection Map.

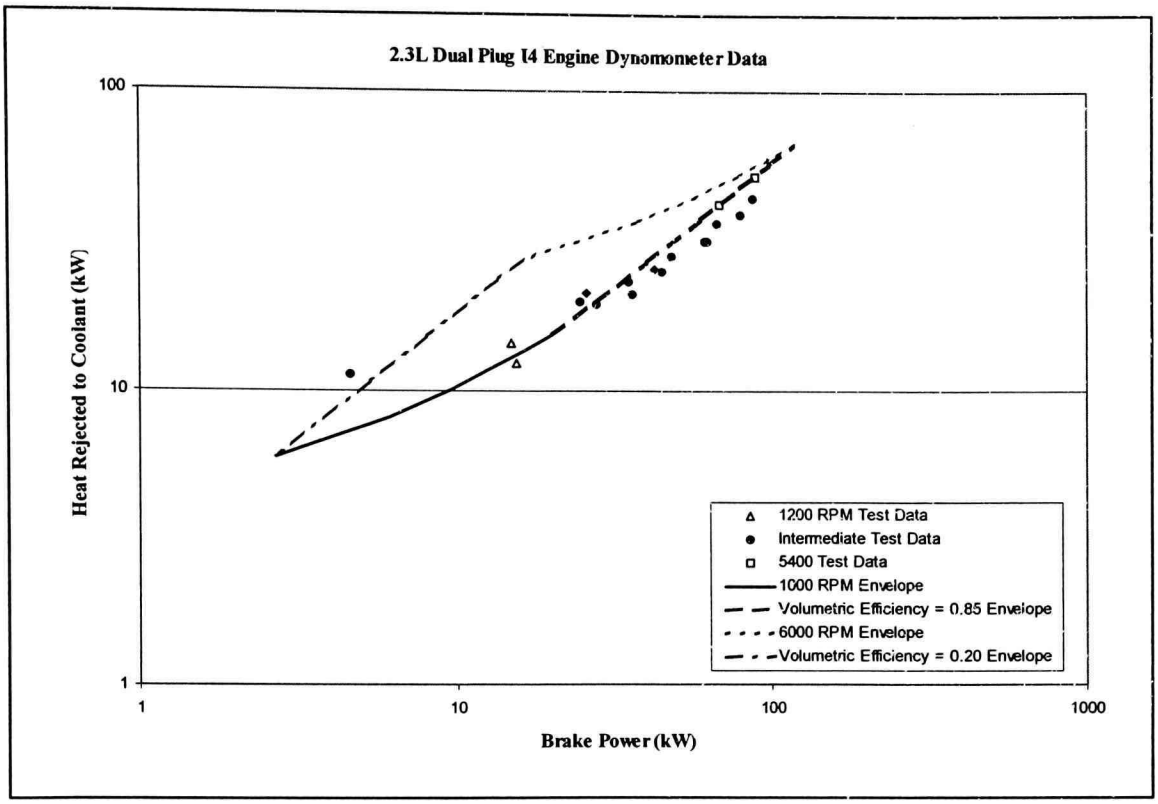

Figure 4.3 2.3L I4 Dual Plug SI Engine Heat Rejection Map.

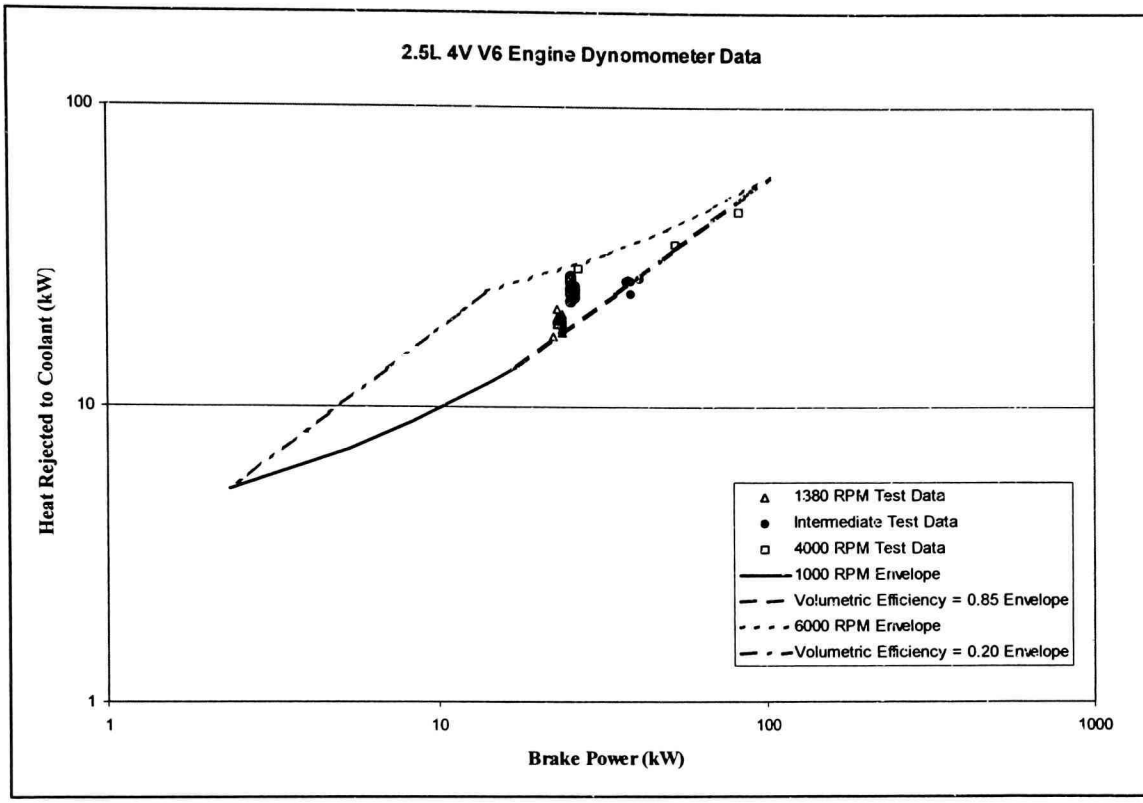

Figure 4.4 2.5L V6 4V SI Engine Heat Rejection Map.

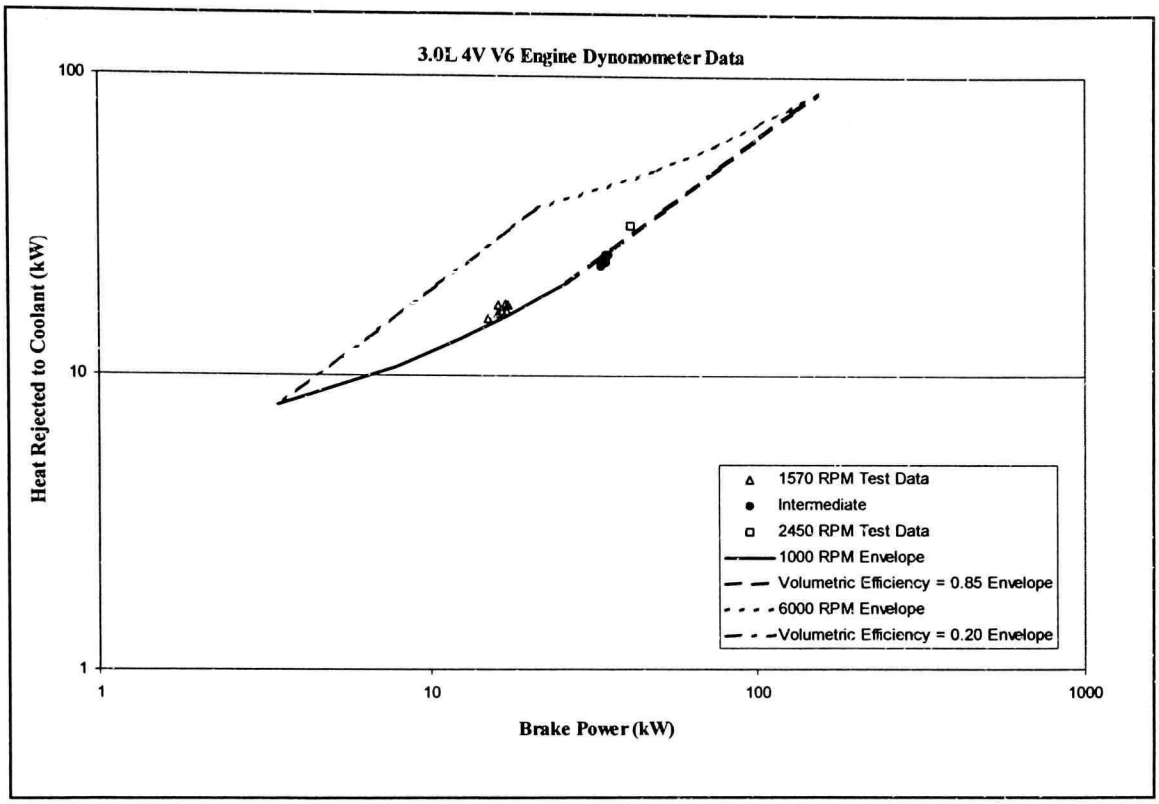

Figure 4.5 3.0L V6 4V SI Engine Heat Rejection Map.

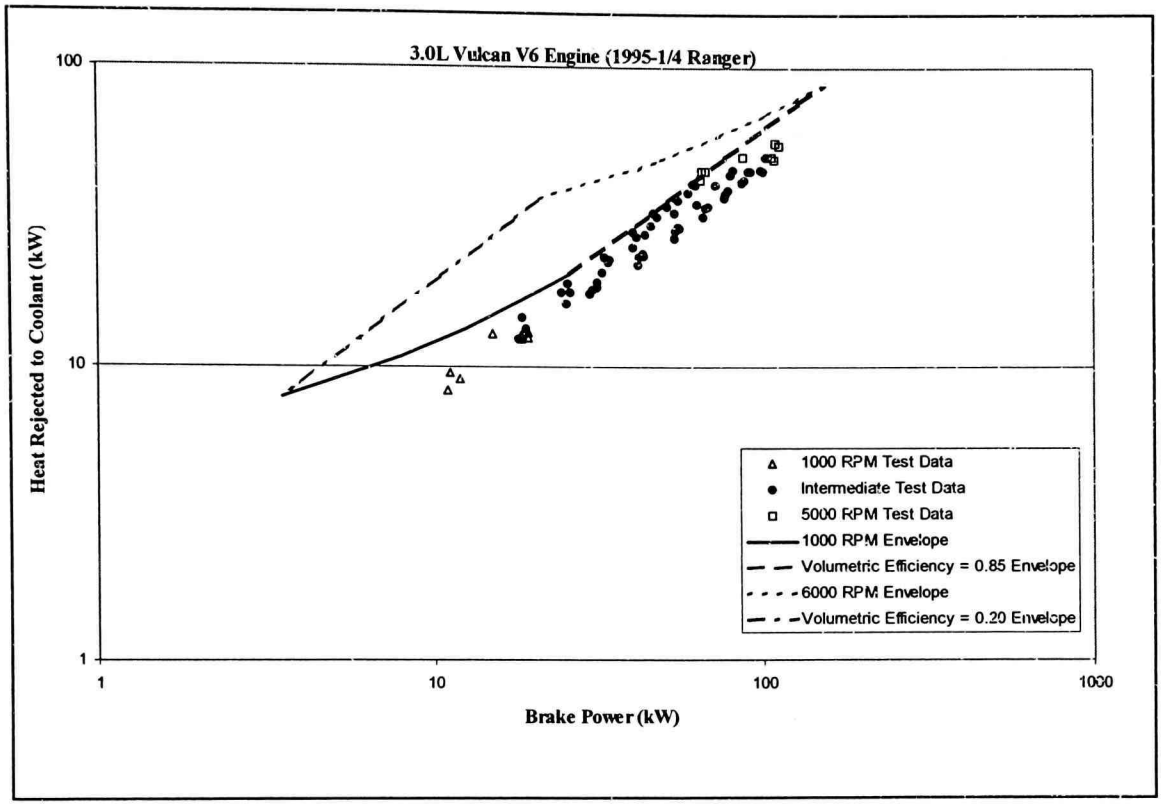

Figure 4.6 3.0L V6 Vulcan SI Engine Heat Rejection Map.

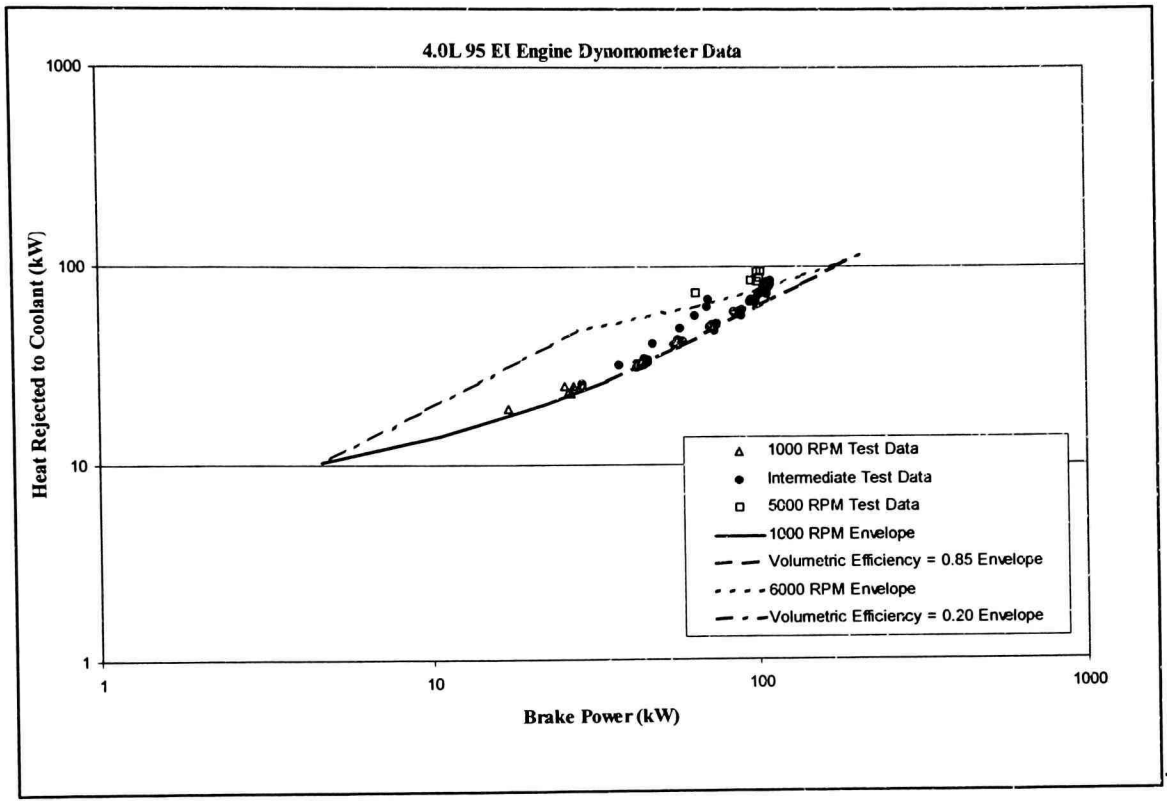

Figure 4.7 4.0L EI '95 SI Engine Heat Rejection Map.

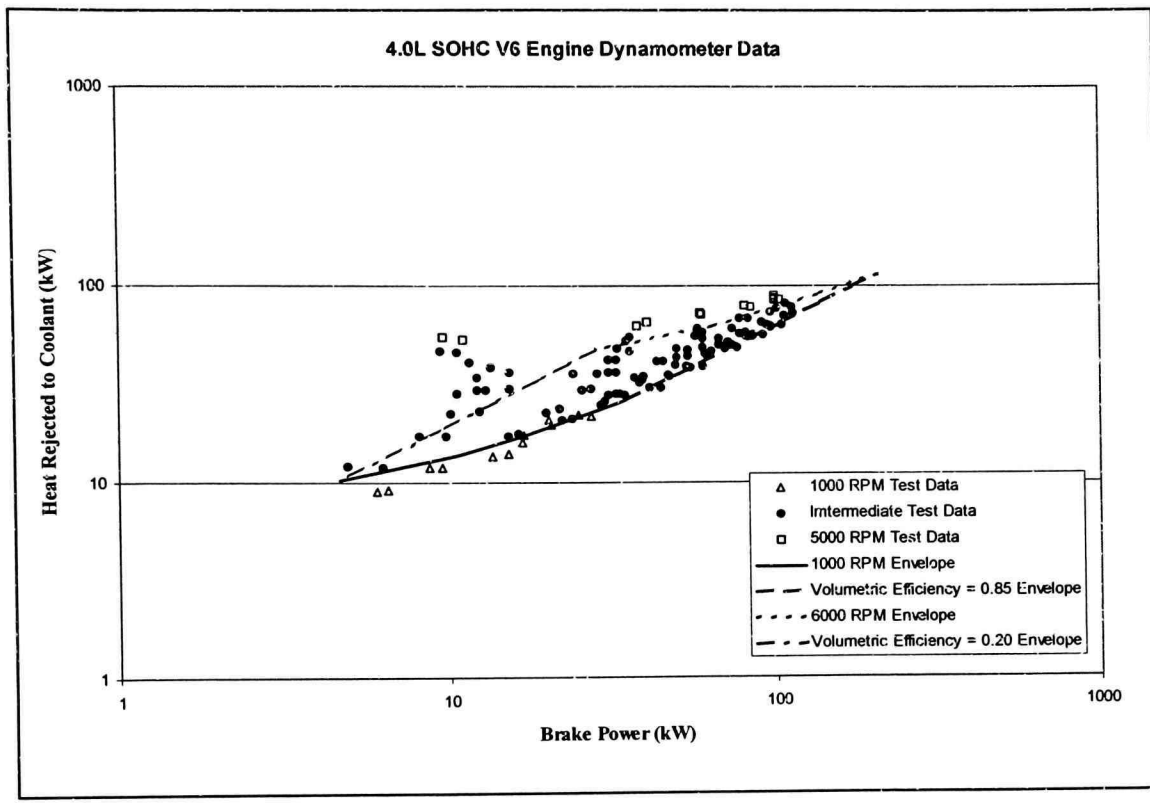

Figure 4.8 4.0L V6 SOHC SI Engine Heat Rejection Map.

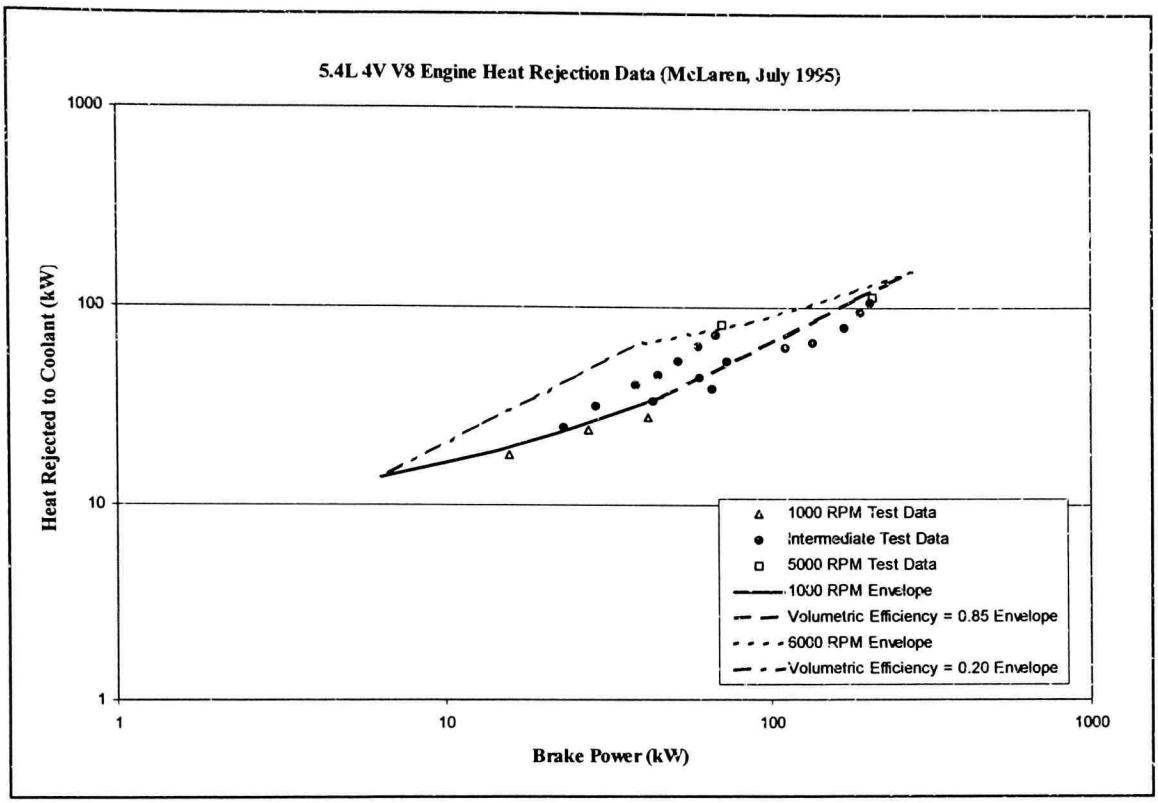

Figure 4.9 5.4L V8 4V SI Engine Heat Rejection Map.

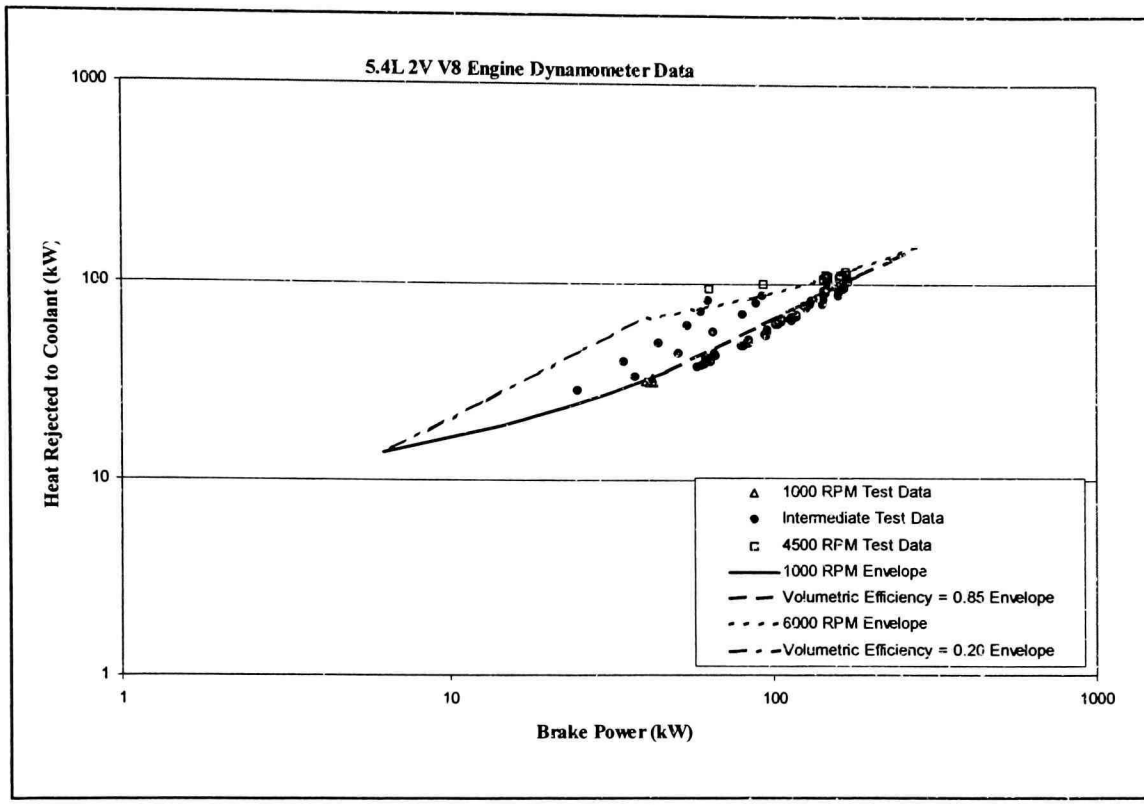

Figure 4.10 5.4L V8 2V SI Engine Heat Rejection Map.

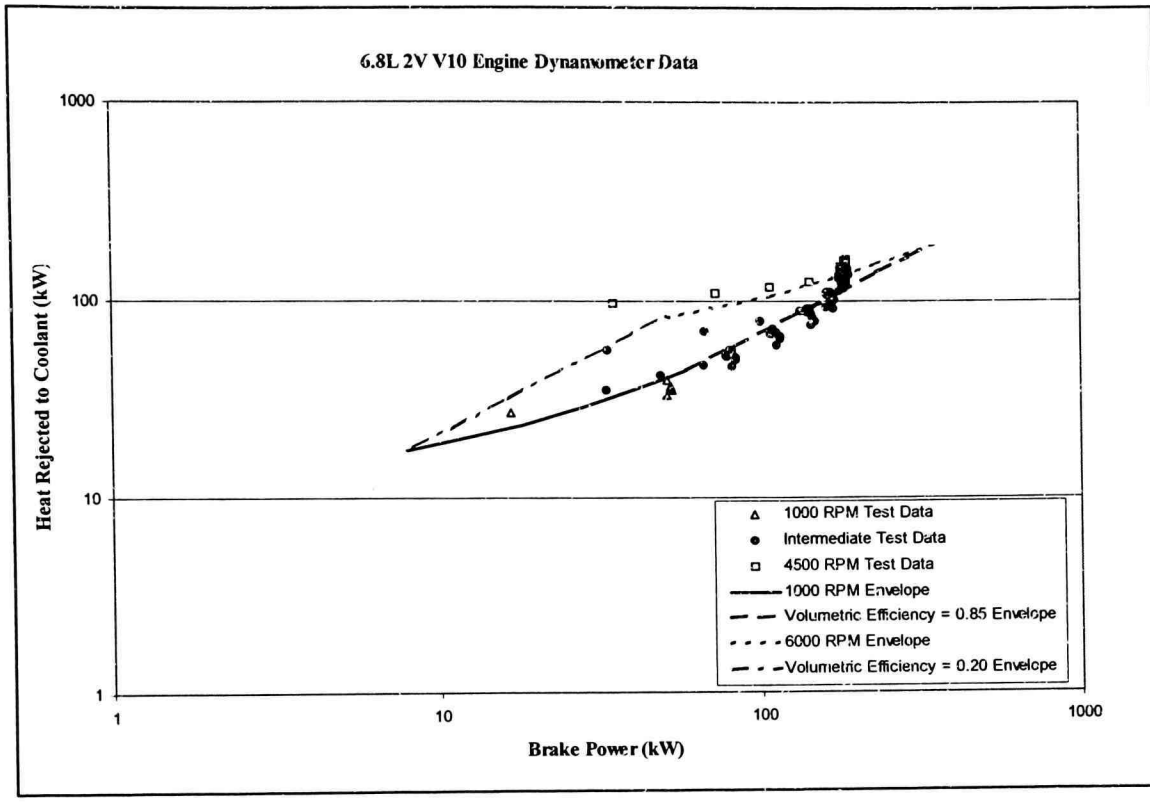

Figure 4.11 6.8L V10 2V SI Engine Heat Rejection Map.

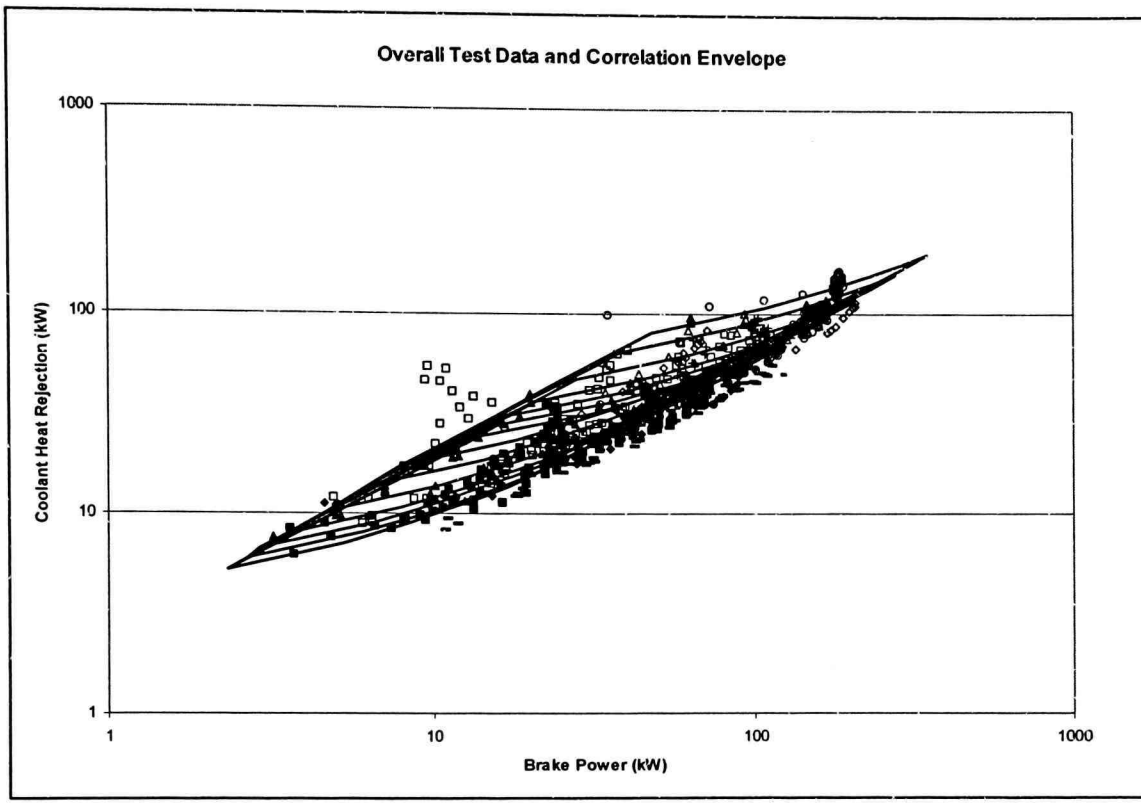

Figure 4.12 Overall Correlation Envelope and Test Data for SI Engines.

The experimental data and predicted heat rejection envelopes from the eleven engines have been combined in Figure 4.12. The remarkable flexibility of the correlation is apparent. It is obvious that a majority of the test data were recorded at high volumetric efficiencies as this operation is shown in the lower right of the envelope. The 4.0L V6 SOHC SI engine was the only engine that was significantly outside the correlation envelops and other test data cluster. Perhaps there is error in the data or other significant operational differences (i.e., supercharging, turbocharging, etc.) not described in the test data sheet.

The results of a comparison of the new correlation and Lahvic calculations with the experimental engine data on a point-by-point basis are shown in Figure 4.13.

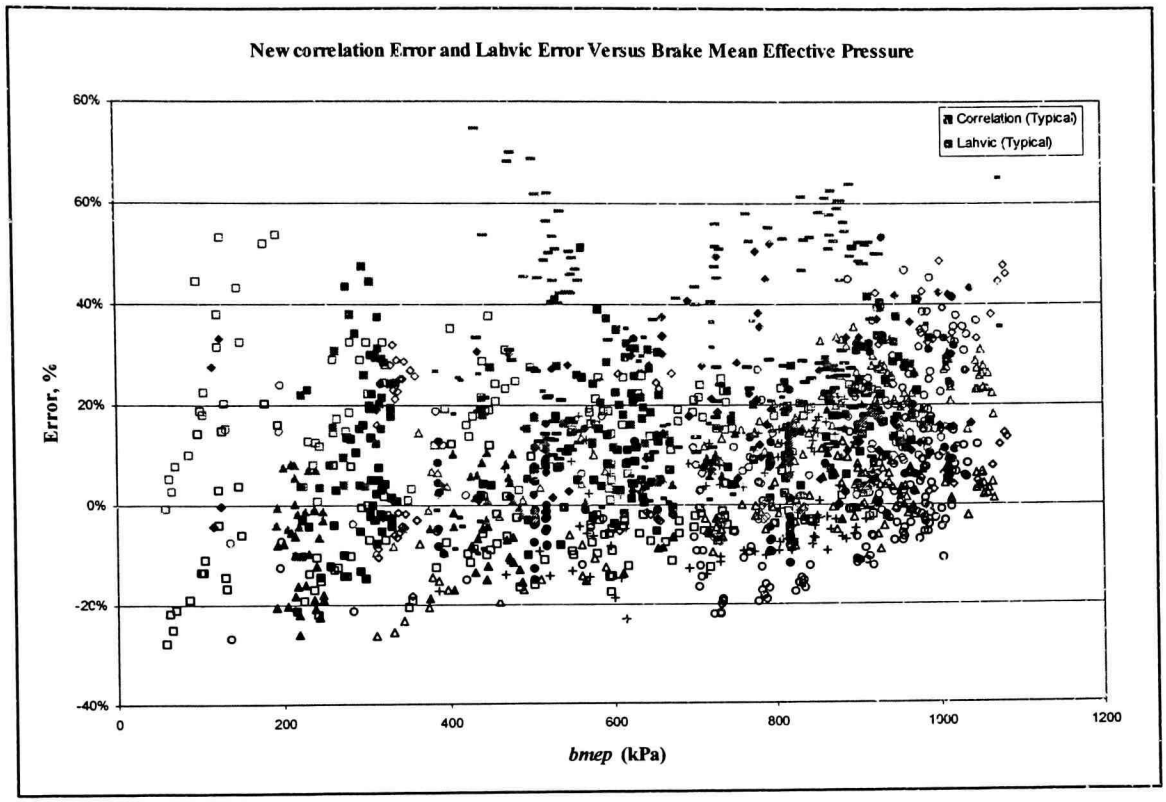

Figure 4.13 New Correlation and Lahvic Error for Naturally Aspired SI Engines.

Each data point represents the percent deviation between the engine data and the predicted result at the same engine speed and brake power. Although the deviation results are plotted versus *bmep*, there is no apparent dependency of the deviations on that parameter.

For the entire collection of data, the mean error deviation is zero and the standard deviation of the error is 11%. For comparison, the results from the Lahvic correlation are 22% for the mean deviation and 15% for the standard deviation of the error. This completes the successful demonstration of a correlation that can predict SI engine heat reject based on minimal initial engine data.

4.2 Turbocharged Compression Ignition Engine Results and Discussion

With the engine power correlation and the cylinder heat transfer correlation known, the heat rejection to the coolant may be predicted for any arbitrary combination of turbocharged CI engine, power requirement, and engine speed. The only limitation on the calculation is that the power specification be within the capabilities of the given engine. The input parameter requirements for the heat rejection calculations are the engine speed, brake power requirement, engine displacement, and number of cylinders. Additionally, if known, the turbocharger wastegate pressure ratio can increase the accuracy of the prediction, although using a typical value for the pressure ratio will yield satisfactory results.

The first step in the calculation is to determine the air mass flow rate though the engine. The bmep and corresponding Amep are calculated Equation 4.1 with a fuel conversion efficiency of 0.40 and an fmep of 136 kPa. From the turbocharged CI engine analysis, the turbocharger pressure ratio was a function of the available mean effective pressure and wastegate pressure ratio. As discussed in the previous chapter, an approximation for the turbocharger characteristics is

$$r_p = Minimum\left(1 + 0.35\left[\frac{1}{MPa}\right]Amep, 2.4\right). \tag{4.10}$$

These two generic parameters are needed to represent the turbocharger sufficiently to obtain the airflow through the CI engines.

With the turbocharger pressure ratio known based on the generic representation from discussions on Figure 3.6, the volumetric efficiency can be found from the correlated values found in Figure 3.5 and Equation 4.11.

$$\eta_v = 0.8031 P_r$$

The airflow rate is determined by definition as shown in Equation 4.12.

$$\dot{m}_a = \eta_v \rho_a \frac{n}{2} V_d \tag{4.12}$$

The next step in the calculation is the application of the engine power correlation to determine the fuel mass flow rate through the engine, where Equation 4.1 finds the brake mean effective pressure:

$$bmep = \frac{P_b}{V_D n/2} = \eta_v \eta_f \frac{\rho_a Q_{LH}}{A/F} - fmep\,. \tag{4.1}$$

The general turbocharged CI engine power correlation is then applied to obtain the corresponding air-fuel ratio

$$A/F = \frac{\eta_V 0.40 \rho_a Q_{LH}}{(bmep + 135)}\,. \tag{4.11}$$

With the airflow rate and air-fuel ratio known, the fuel mass flow rate is also known. The heat transfer correlation for CI engines from Equation 3.57 may be evaluated:

$$q_c mep = \frac{2.50\, k_g\, \mathrm{Re}^{0.7}\, \mathrm{Pr}^{0.3}\, \pi B}{4V_D n/2}\left(\overline{T}_g - T_w\right) + \frac{0.341 \sigma \pi B^2}{4V_D n/2}\left(\overline{T}_f^4 - T_w^4\right) + 5.98\left[\frac{s}{kPa}\right]\frac{n}{2}\,. \tag{3.57}$$

Figures 4.14 to 4.17 contain the heat rejection maps for the turbocharged CI engines. The correlation envelopes are bounded by speeds of 1000 rpm and 4000 rpm and pressure ratios of 1.2 and 3.2.

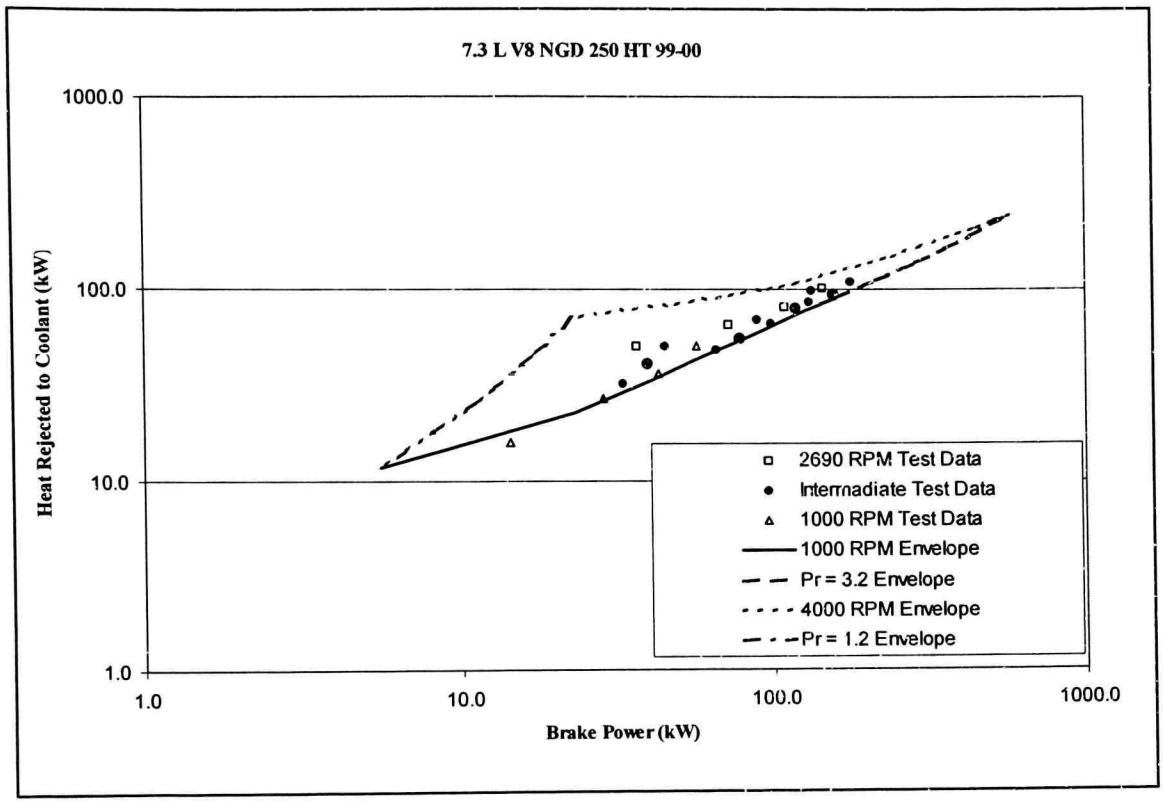

Figure 4.14 7.3 L 250 HT Turbocharged CI Engine Heat Rejection Map.

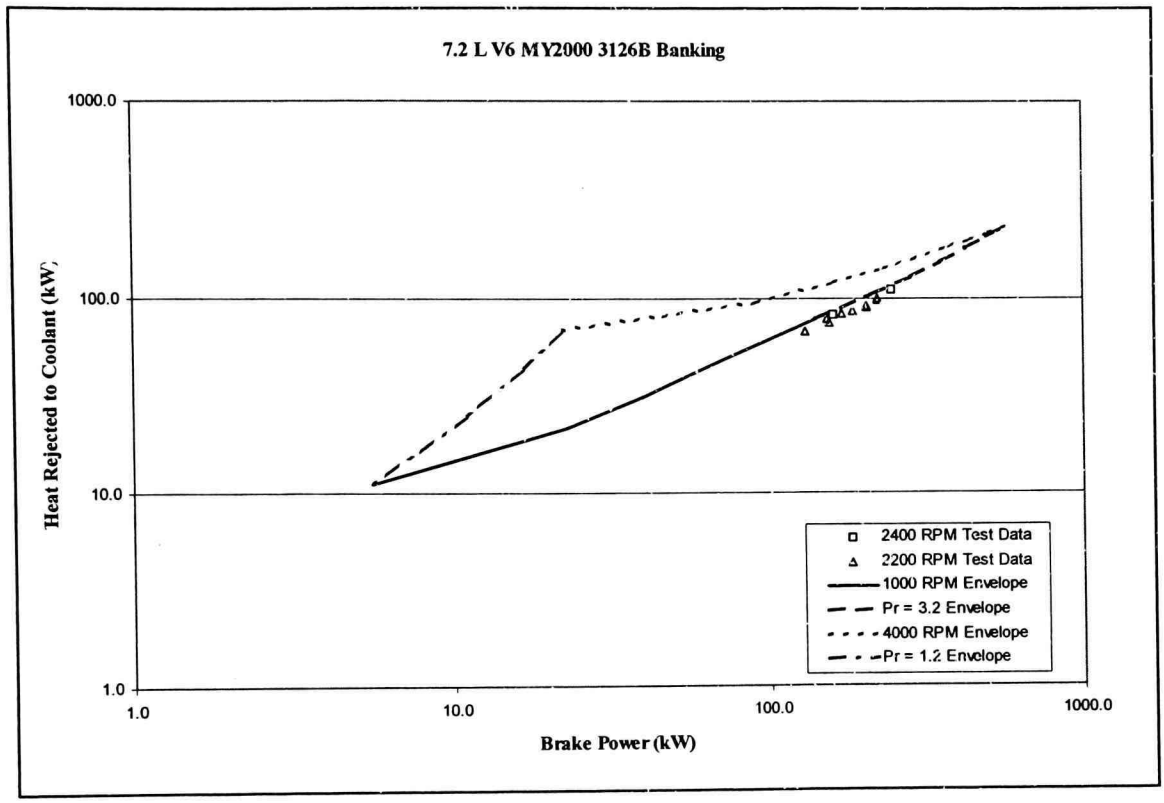

Figure 4.15 7.2 L V6 3126B 2000 Turbocharged CI Engine Heat Rejection Map.

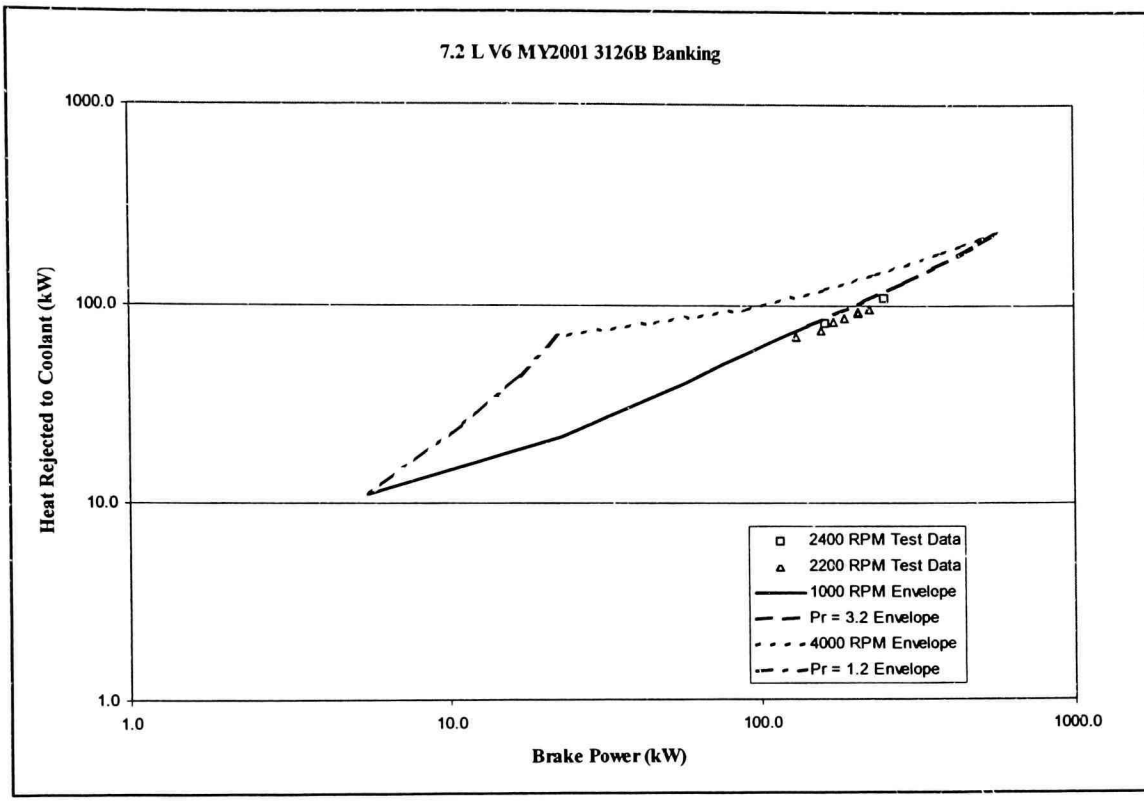

Figure 4.16 7.2 L V6 3126B 2001 Turbocharged CI Engine Heat Rejection Map.

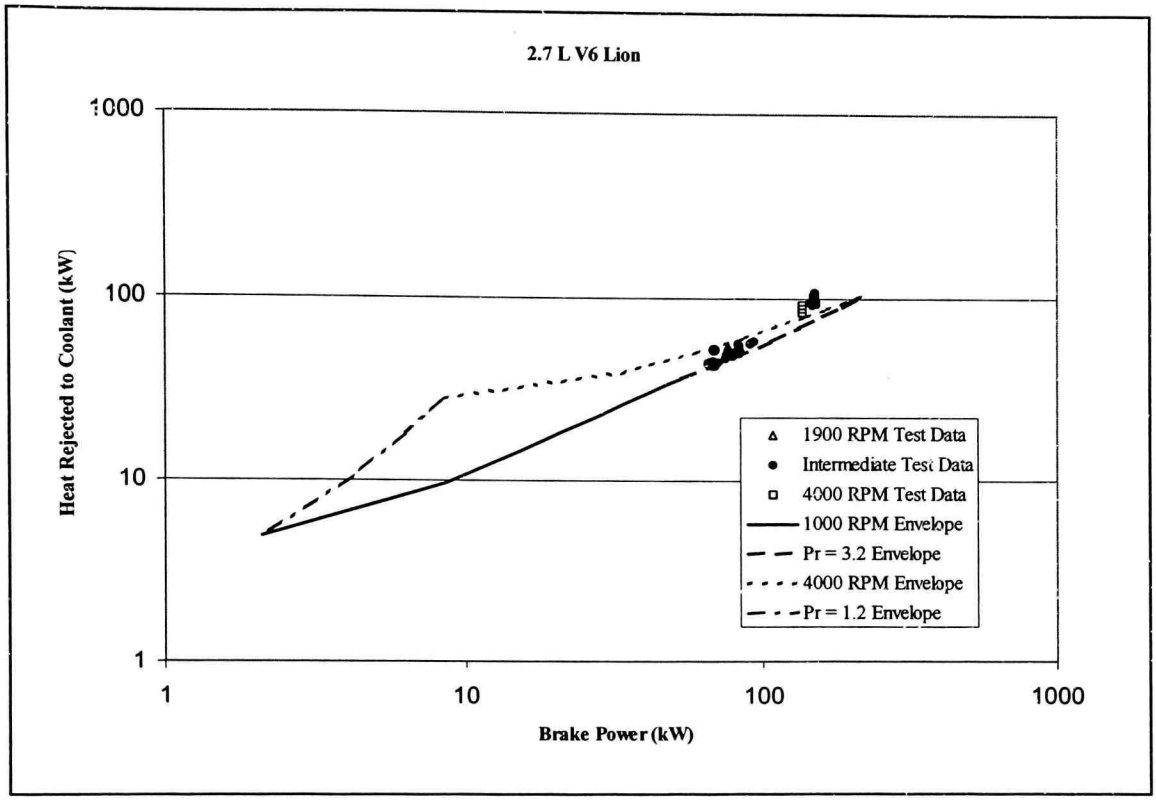

Figure 4.17 2.7 L V6 Lion Turbocharged CI Engine Heat Rejection Map.

These figures demonstrate good agreement in the heat rejection predictions and actual heat rejection data for turbocharged CI engines. Note that in all of these figures the heat rejection data vary approximately linearly with the brake power. This trend is probably a result of the weak dependence of airflow with engine speed due to turbocharging. Additionally, the overall envelope and test data for the CI engines are shown in Figure 4.18.

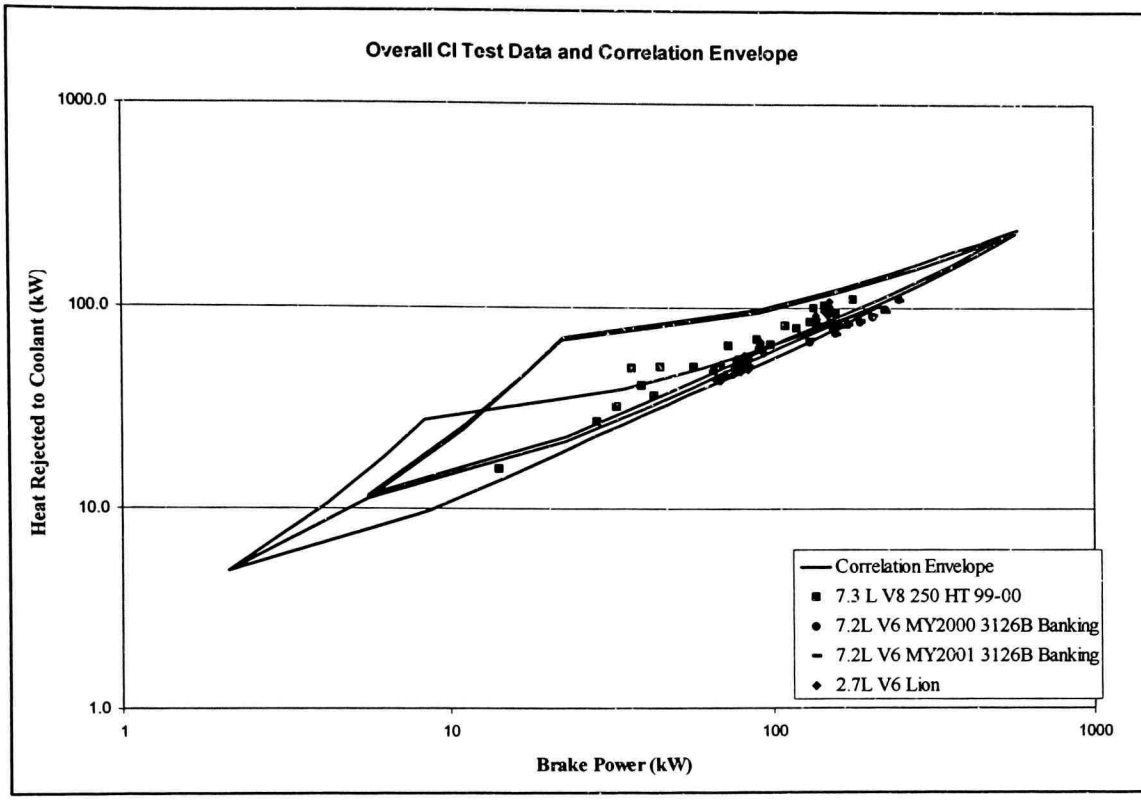

Figure 4.18 Overall CI Test Data and Correlation Envelope.

Again, Figure 4.18 shows the remarkable flexibility of the correlation. The error in the new correlation with a generic turbocharger and the existing Lahvic correlation are presented versus *bmep* in Figure 4.19

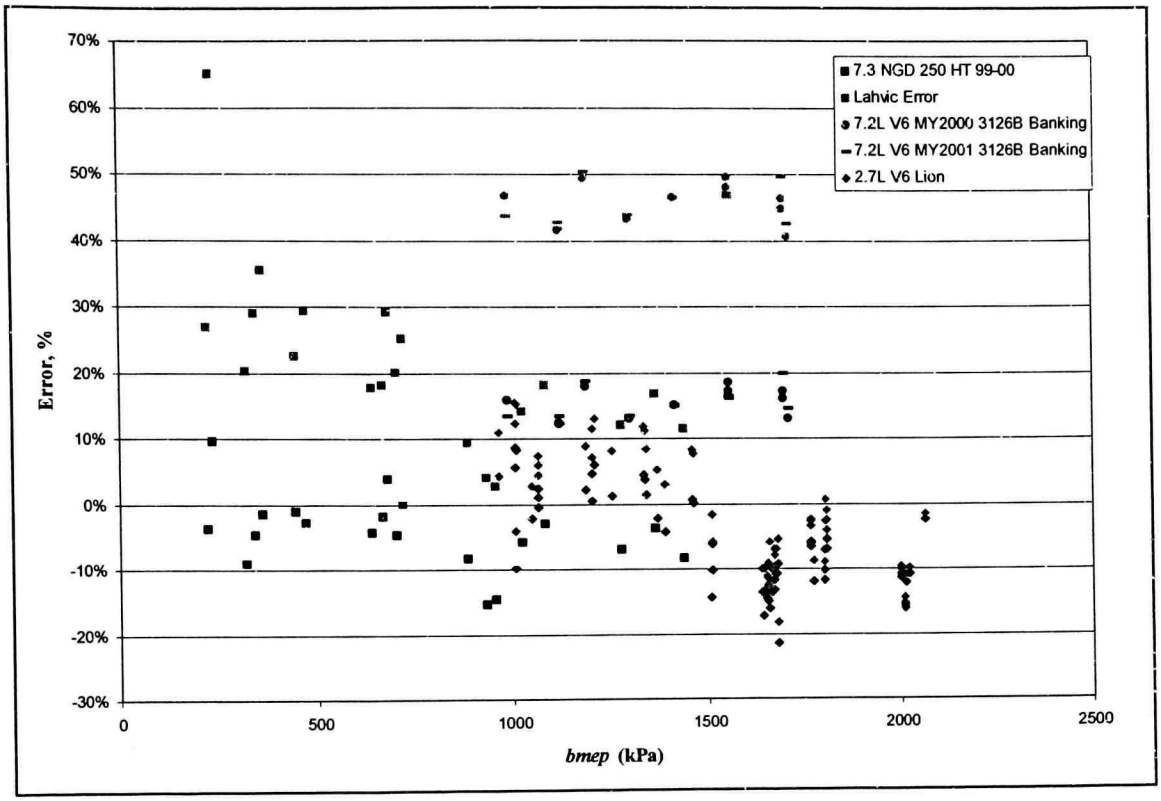

Figure 4.19 New Correlation and Lahvic Error for Turbocharged CI Engines.

Each data point represents the percent deviation between the engine data and the estimation result at the same engine speed and brake power. Although the deviation results are plotted versus *bmep*, there is no apparent dependency of the deviations on that parameter.

For the entire collection of data, the mean error deviation is zero and the standard deviation of the error is 11%. For comparison, the results from the Lahvic correlation are 16% for the mean deviation and 22% for the standard deviation of the error. This completes the successful demonstration of a correlation that can predict CI engine heat reject based on minimal initial engine data. Again, there is a marked improvement over the currently used Lahvic regression, even with a generic wastegate pressure ratio. When the wastegate pressure ratio is known, the accuracy of the new correlation improves over the generic scenario. Obviously, the further the assumed wastegate pressure ratio is away

from the true wastegate pressure ratio, the further the correlation is from predicting an accurate heat rejection.

CHAPTER V
CONCLUSIONS

General methods for estimating the heat rejection to the coolant of a normally aspirated spark ignition (SI) engine and a turbocharged compression ignition (CI) engine have been given. The vehicle parameters or input required for the calculations are the engine displacement, number of cylinders, engine speed, and brake power requirement. For the entire collection of SI engine data, the mean error deviation is zero and the standard deviation of the error is 11%. For the collection of CI engine data, the mean error deviation is zero and the standard deviation of the error is 11%. The CI error is no larger than the SI heat rejection error. In addition, with its direct dependence on volumetric efficiency, the engine power correlation makes it readily apparent if a given speed and power requirement are within the capabilities of a given naturally aspired SI engine.

The primary objective for the calculation method that has been presented is to predict coolant heat load for an arbitrary engine with reasonable accuracy. If, however, data is available for a particular engine, unique values for the friction mean effective pressure, fuel conversion efficiency, and Nusselt number correlation coefficients can be obtained. The resulting coolant heat load calculations can be accomplished with an accuracy that appears to only be limited by the original data. This approach would provide an efficient means of compressing extensive sets of experimental data into an engine database.

The method for naturally aspired SI engines is available in an Excel workbook called ttu_Heat. Heat rejection predictions are based on the standard correlation coefficients from data from eleven engines. Optionally, the user can generate a unique correlation for a specific engine. A heat rejection map, power and heat transfer correlation results, and a correlation error summary support the calculations. The computer program ttu_Heat also includes a worksheet to facilitate unit conversions from dynamometer data files to the SI data needed for the correlation. All of the calculation

worksheets are protected except for the user data entry areas. The workbook as a whole is not protected, which allows users to collect calculation results and build additional worksheets and plots to meet the users needs. Modifications to these correlations were successful at predicting heat rejection from turbocharged diesel engines. Additionally, a theoretical basis for extending the spark ignition engine to include turbocharging has been introduced.

REFERENCES

Alkidas, A. C., & Cole, R. M. (1985). Transient heat flux measurements in a divided-chamber Diesel engine. *Journal of Heat Transfer, 107,* 439-444.

Annand, W. J. (1963). Heat transfer in the cylinders of reciprocating internal combustion engines. *Proceedings of the Institution Mechanical Engineers, 177,* 973-990.

Ap, N. S., & Golm, N. C. (1997). New concept of engine cooling system (Newcool). *SAE 971775.*

Brandstetter, W., & Dziggel, R. (1982). The 4- and 5-cylinder turbocharged Diesel engines for Volkswagen and Audi. Society of Automotive Engineers, *SAE Transactions, 91,* SAE Paper 82044, 1982.

Bromnick, P. A., Pearson, R. J., & Winterbone, D. E. (1998). Intercooler model for unsteady flows in engine manifolds. *Proceedings of the Institution Mechanical Engineers, 212,* Part D, 119-132.

Bulaty, T., Codan, E., & Skopil, M. (1996). A flexible system for the simulation of turbocharged Diesel engines and turbocharging systems. *Proceedings of the ICE-Spring Technical Conference, Youngstown, Ohio, 26-3,* 57-63.

Cao, Y., & Wang, Q. (1995). Thermal analysis of a piston cooling system with reciprocating heat pipes. *Heat Transfer Engineering, 16*(2).

Cengel, Y. A., Boles, M. A., (1989). *Thermodynamics An Engineering Approach,* New York, New York: McGraw-Hill.

Chick, J. P. (1998). The modeling of engine thermal systems. Unpublished doctoral dissertation, University of Nottingham.

D'Adda, C., Lisbona, M. G., Occella, S., & Maiorana, G. (1994). Optimization of the cooling system of a high specific power Diesel engine with analytical methodologies. SAE Conference Proceedings, 4th International Conference—1994 Mar, 1209-1220.

Davidson, S. D. (1984, August). On-highway performance evaluation of a Cummins Diesel engine featuring optimized charge air cooling. Paper presented at West Coast International Meeting & Exposition, San Diego.

Edson, M. H., & Taylor, C. F. (1964). The limits of engine performance – comparison of actual and theoretical cycles. *Digital Calculations of Engine Cycles, 7,* 65-81.

Finlay, I. C., Harris, D., Boam, D. J., & Parks, B. I. (1985). Factors influencing combustion chamber wall temperatures in a liquid-cooled, automotive, spark-Gerhard, W. (1979). Prediction of thermal loading of supercharged Diesel engines. Proceedings from the Institution of Mechanical Engineers, 199,207-214.

Flynn, P. (1979). Turbocharging four cycle Diesel engines. Society of Automotive Engineers,*SAE Transactions, 88,* SAE Paper 790314, 1979.

Ford Power Products (n.d.) Retrieved March 23, 2003, from http://www.fordpowerproducts.com/engine2.jpeg

Gehres, E. (1963, March). *An analysis of engine cooling in modern passenger cars.* Paper presented at National Automobile Meeting, Detroit.

GT15-25. (n.d.) Retrieved August 15, 2002, from http://www.egarrett.com/products/gt_15_25.jsp

Hashem, H. H. (1989, 9th). *Waste energy potential of Diesel engine (experimental evaluation).* Paper presented at 9th Miami International Congress on Energy & Environment, Miami Beach.

Hawley, I. G., Wallace, F. J., Cox, A., Pease, A.C., Bird, G.L., & Horrocks, R. W. (1998). Use of a VGT to improve the limiting torque characteristics of a DI automotive Diesel engine. Institution of Mechanical Engineers Conference Transactions, 11, 347-357.

Heywood, J. (1988). *Internal combustion engine fundamentals*, New York, New York: McGraw-Hill.

Hribemik, A., & Moskwa, J. J. (2000). Transient response of a cross-flow charge air intercooler and its influence on engine operation. *Journal of Dynamic Systems, Measurement, & Control,* 122, 483-489.

Kadoli, F. G., & Aknamurthy. (1984). Performance of Diesel engine with compound cooling. *Proceedings of the XIII National Conference on IC Engines and Combustion, Bangaloro,* 241-246.

Kamo, R. (1977, March). *Cycles and performance studies for advanced Diesel engines.* Paper presented at the Conference on Ceramics for High Performance Applications Newport, RI.

Kern, J., & Ambros P. (1997). Concepts for a controlled optimized vehicle engine cooling system. Society of Automotive Engineers Publication, 971816, 357-362.

Kunitomo, T., Matsuoka, K., & Oguri, T. (1975). Prediction of radiative heat flux in a Diesel engine. Society of Automotive Engineers Transaction, 750786.

Liu, D., Xu, X., & Hou, J. (1993). Analysis and computation of characteristic of the water cooling and radiating system for a heavy duty truck Diesel engine. SAE 939160. Seventh International Pacific Conference and Exposition on Automotive Engineering, Pheonix, Arizona, Nov.15th-19th, 1993, 53-62.

Lahvic, T. R., "Investigation of Engine Heat Rejection", August 1986, Ford Motor Co.

Lundun, B., Povolny, J., & Chelko, L. (1949). Correlation of cylinder head temperatures and coolant heat rejections of a multi-cylinder, liquid cooled engine of 1710 cubic-inch displacement (NACA Report No. 931).

Merrion, D., Diesel engine design for the 1990's. *SAE Special Presentation, 1011, 1993.*

Moeckel, M. D. (1994). Computational fluid dynamic (CFD) analysis of a six cylinder Diesel engine cooling system with experimental correlations. SAE 941081. 45th Annual Earthmoving Industry Conference, Pioria, Illinois, April 12 &13th, 1994, 1-9.

Mohan, K. V., Arici, O., Yang, S., & Johnson, J. H. (1997). A computer simulation of the turbocharged Diesel engine as an enhancement of the vehicle engine cooling system simulation. SAE No. 971804. 237-253.

Oler, W., Parish, O., Williams, J., Burns, M. (2002). *Heat rejection from naturally aspired gasoline automobile engines,* Journal of Ford Engineering.

Patton, K., Nitschke, R.G., & Heywood, J. B. (1989). Development and evaluation of a friction model for spark-ignition engines. SAE Paper 890836.

Povolny, J., Bogdan, initial, & Chelco, L. (1950). Cylinder head temperatures and coolant heat rejection of a multi-cylinder liquid cooled engine of a 1650 cubic inch displacement. (NACA TN 2069).

Rakopoulos, C. D., Andritsakis, E. C., & Kyritsis, D. K. (1992). *Availability, accumulation and destruction in a DI Diesel engine with special reference to the limited cooled case* (Tech. Rep. No. 3). Athens, Greece: National Technical University of Athens, Mechanical Engineering Department, Thermal Engineering Section.

Rakopoulos, C. D., & Mavropoulos, G. C. (2000). Experimental instantaneous heat flux in the cylinder head and exhaust manifold of an air-cooled Diesel engine. *Energy Conversion & Management, 41,* 1265-1281.

Sekar, R. R. (1982, February). *Trends in Diesel engine charge air cooling.* Paper presented at International Congress & Exposition, Detroit.

Shayler, P. J., Baylis, W. S., Chick, J. P., & Bell, P. (1999). The effects of EGR and turbocharging on engine heat rejection rates. Institution of Mechanical Engineers, 4th Vehicle Thermal Management Systems Conference, London, United Kingdom, 1999. 679-693.

Shayler, P., Chick, J., Hayden, D., Yuen, H., & Ma, T. (1997). Progress on modeling engine thermal behavior for VTMS applications. Society of Mechanical Engineers, SAE Paper 971852, 1997.

Shayler, P., Chick, J., & Ma, T. (1996). Effect of coolant mixture composition on heat rejection rate. Society of Automotive Engineers, SAE Paper 960275, 1996.

Shayler, P., Chick, J., Ma, T. (1997). Correlation of engine heat transfer for heat rejection and warm-up modeling. Society of Automotive Engineers, SAE Paper 971851, 1997.

Taylor, C. (1985). The internal combustion engine in theory and practice (Vol. 1). (2nd ed.). MIT.

Taylor, C. F., & Toong, T. Y. (1957). Heat transfer in internal combustion engines. American Society of Mechanical Engineers, ASME Paper 57-HT-17, 1957.

Taymaz, I., Gur, M., & Halici, F. (1998, June). The effect of insulated heat transfer surfaces on direct injected and turbocharged Diesel engine fuel consumption and cooling system. Paper presented at 2nd Trabzon International Energy & Environment Symposium, Trabzon, Turkey.

The new DELTA engine: There are common engines and there are extraordinary engines. (n.d.) Retrieved August 17, 2002, from http://www.detroitdiesel.com/Public/Markets/automotive/adelta1.asp

Thring, R.H. (1992). Engine friction modeling. Society of Automotive Engineers, SAE Paper 920482, 1982.

Tovell, J. F. (1983, February). *The reduction of heat losses to the Diesel engine cooling system.* Paper presented at International Congress & Exposition, Detroit.

Wallace, F. J., Hawley, J. G., Cox, A., Pease, A. C., Horrocks, R. W., & Bird, G.L. (1997). Variable geometry turbocharging of a 1.8 DI automotive Diesel engine. Paper presented at 30th International Symposium on Automotive Technology & Automation, Florence, Italy.

Wallace, F. J., Way, R. J. B, & Vollmert, H. (1979). Effect of partial suppression of heat loss to coolant on the high output Diesel engine cycle. Society of Automotive Engineers, SAE Paper 79082, 1979.

Watson, N., & Janota, M. (1982). *Turbocharging the internal combustion engine*. New York: Wiley-Interscience.

Watson, N., Kyrtatos, K., & Holmes, K. (1983). The performance potential of limited cooled Diesel engines. Proceedings from the Institution of Mechanical Engineers, *197A,* 197-207.

Watts, P. A., & Heywood J. B. (1980, February). Simulation studies of the effects of turbocharging and reduced heat transfer on spark-ignition engine operation. Paper presented at Congress & Exposition, Detroit.

Way, R. J. B., & Wallace, F. J. (1979). Results of matching calculations for turbocharged and compound engines with reduced heat loss. Society of Automotive Engineers, SAE Number 790824, 1979.

Woods, M., Bryzik, W., & Schwarz, E. (1992, February). *Heat rejection from high output adiabatic Diesel engine.* Paper presented at International Congress & Exposition, Detroit.

Woodward, J. B. (1995). Air-standard modeling for closed cycle Diesel engines. Proceedings of the Institution of Mechanical Engineers, 209, 115-123.

Worden, J. A., & Zehr, R. L. (1999, March). Consideration of fluid velocity effects in the design and development of aluminum cooling system components for heavy duty Diesel engines. Paper presented at Heavy Duty Coolants and Cooling Systems International Congress and Exposition, Detroit.

Yoshimoto, Y., Tsukahara, M., & Kuramoto, T. (1996, October). *Improvement of BSFC by reducing Diesel engine cooling losses with emulsified fuel.* Paper presented at International Fall Fuels & Lubricants Meeting & Exposition, San Antonio.